INSTABILITIES AND SUBHARMONIC RESONANCES OF SUBSONIC HEATED ROUND JETS

by

Lian Lai Ng

A Dissertation Submitted to the Faculty of the

DEPARTMENT OF AEROSPACE AND MECHANICAL ENGINNERING

In Partial Fulfillment of the Requirements

For the Degree of

DOCTOR OF PHILOSOPHY

WITH A MAJOR IN AEROSPACE ENGINEERING

In the Graduate College

THE UNIVERSITY OF ARIZONA

1990

INSTABILITIES AND SUBHARMONIC RESONANCES OF SUBSONIC HEATED ROUND JETS

by

Lian Lai Ng

A Dissertation Submitted to the Faculty of the

DEPARTMENT OF AEROSPACE AND MECHANICAL ENGINNERING

In Partial Fulfillment of the Requirements

For the Degree of

DOCTOR OF PHILOSOPHY

WITH A MAJOR IN AEROSPACE ENGINEERING

In the Graduate College

THE UNIVERSITY OF ARIZONA

1990

THE UNIVERSITY OF ARIZONA
GRADUATE COLLEGE

As members of the Final Examination Committee, we certify that we have read the dissertation prepared by Lian Lai Ng

entitled INSTABILITIES AND SUBHARMONIC RESONANCES IN SUBSONIC HEATED ROUND JETS

and recommend that it be accepted as fulfilling the dissertation requirement for the Degree of Doctor of Philosophy.

Thomas F. Balsa	April 18, 90 Date
Chuan F. Chen	Aug 29, 1989 Date
Edward Kerschen	Aug 29, 1989 Date
Henry Perkins	Aug 29 '89 Date
	Date

Final approval and acceptance of this dissertation is contingent upon the candidate's submission of the final copy of the dissertation to the Graduate College.

I hereby certify that I have read this dissertation prepared under my direction and recommend that it be accepted as fulfilling the dissertation requirement.

Dissertation Director Thomas F. Balsa — April 18/90 Date

STATEMENT BY AUTHOR

This dissertation has been submitted in partial fulfillment of requirements for an advanced degree at The University of Arizona and is deposited in the University Library to be made available to borrowers under rules of the library.

Brief quotations from this dissertation are allowable without special permission, provided that accurate acknowledgement of source is made. Requests for permission for extended quotation from or reproduction of this manuscript in whole or in part may be granted by the head of the major department or the Dean of the Graduate College when in his or her judgement of the proposed use of the material is in the interests of scholarship. In all other instances, however, permission must be obtained from the author.

SIGNED: Li Caifang

ACKNOWLEDGMENTS

I would like to acknowledge my advisor, Professor Thomas Balsa, for his invaluable guidance, assistance and support throughout my research. The author also wishes to express his sincere appreciation to other members of the committee, Professors C. F. Chen, Edward Kerschen, Henry Perkins, and Arne Pearsltein, for their availability and constructive comments.

Special thanks must go to the stability and transition team (A. J. Kumar, Gordon Erlebacher, Michele Macaraeg, Bart Singer, Craig Streett, and Tom Zang) at NASA Langley who constantly encouraged me to finish writing my dissertation while I was working at NASA Langley. I have also benefited greatly from the many discussions with Eckart Laurien and fellow researchers Bart Singer and Gordon Erlebacher. The support and friendship of Sylvain Yapo, Xasan Ayanle, Yen-Ming Chen and Y. Jarrah are also appreciated.

Finally, I would like to thank my wife, Wendy Weiner, for her infinite patience, endless love and encouragement. This work is also dedicated to my family in Malaysia and Singapore.

This work was principally supported by NASA Lewis Grant NAG3-485, and partially by NASA Langley Grant NASI-18599.

TABLE OF CONTENTS

LIST OF FIGURES

ABSTRACT

When a jet is perturbed by a periodic excitation of suitable frequency, a large-scale coherent structure develops and grows in amplitude as it propagates downstream. The structure eventually rolls up into vortices at some downstream location. We approximate the "wavy flow" associated with the roll-up of a coherent structure by a parallel mean flow and a small, spatially periodic, axisymmetric wave whose phase velocity and mode shape are given by classical (primary) stability theory. The periodic wave acts as a parametric excitation in the differential equations governing the secondary instability of a subharmonic disturbance.

The (resonant) conditions for which the periodic flow can strongly destabilize a subharmonic disturbance are derived. When the resonant conditions are met, the periodic wave plays a catalytic role to enhance the growth rate of the subharmonic. The stability characteristics of the subharmonic disturbance, as a function of jet Mach number, jet heating, mode number and the amplitude of the periodic wave, are studied via a secondary instability analysis using two independent but complementary methods : (i) method of multiple scales and (ii) normal mode analysis. We found that the growth rates of the subharmonic waves with azimuthal numbers $\beta = 0$ and $\beta = 1$ are enhanced strongly, but comparably, when the amplitude of the periodic wave is increased. Furthermore, compressibility at subsonic Mach numbers has a moderate stabilizing influence on the subharmonic instability modes. Heating suppresses moderately the subharmonic growth rate of an axisymmetric mode, and it reduces more significantly the corresponding growth rate for the first spinning mode (i.e, $\beta = 1$). Our calculations also indicate that while the

presence of a finite-amplitude periodic wave enhances the growth rates of subharmonic instability modes, it minimally distorts the mode shapes of the subharmonic waves.

Chapter 1

INTRODUCTION

1.1 Motivation & Technical Importance

It is now generally accepted that large-scale coherent structures, in addition to fine-scale chaotic motions, exist within all turbulent free shear flows. Free shear flows — such as mixing layers, wakes and jets — are a class of flows characterized by the existence of an inflection point in the streamwise base velocity profile. For compressible flows, the classical inflection point is replaced by a generalized inflection point which is determined by the cross-space derivatives of the base velocity and density. These free shear flows are highly unstable. Small perturbations of suitable frequencies (or wavenumbers) in the flow will grow rapidly through the so-called Kelvin-Helmholtz instability mechanism. The instability waves will evolve into a finite amplitude disturbance which is characterized by streamwise-periodic regions of concentrated vorticity — the so called Kelvin cat's eyes. Although the precise mechanisms of the spreading of turbulent flows are presently still under study, it is generally accepted that the coherent structures play a considerable role in the dynamics of turbulent flows; the relative importance of the large and fine scale structures is still not understood all that well and the effect of the latter on the former has not been quantified experimentally with any degree of precision.

Distinguishable evidence of these wave-like coherent structures in fully turbulent subsonic (unheated) round jets is convincingly displayed in the schlieren photographs of Ahuja

et al. (1982). They concluded that these large-scale structures, whose dimension is comparable to the shear layer thickness, play an important role in controlling the dynamics of turbulent flows. For example, when they excited a jet by an upstream acoustic signal at a strouhal number, $S_e = F_e^* D_j^* / U_j^* = 0.5$ (F_e^* is the excitation frequency, D_j^* is the jet diameter, and U_j^* is the jet velocity), the jet plume was widened considerably. By using a photographic enhancement process, the large-scale vortices were clearly identified at some distance downstream. Further, they found that if the excitation frequency was doubled, a different instability mode was excited, the size of the coherent structure was reduced and the spacing between successive structures was halved. These results confirmed the sensitivity of the naturally existing large-scale turbulence structure to the frequency of the imposed disturbance. The adjacent vortical structures may amalgamate at various degrees of regularity as they convect downstream, thereby generating larger vortices. This pairing of vortices can be seen from Figure 1 of Wille's (1963) work. When he injected smoke into the wall boundary layer of a circular jet nozzle, the smoke rolled up into rings of vortices and proceeded to pair with their neighbors farther downstream. The coalescence of the large scale structures was also demonstrated by Winant and Browand (1974). By injecting a filament of dye into a shear layer, they found that the dye rolled up into discrete two-dimensional (vortical) structures; farther downstream, they observed that two adjoining structures interact to form a single, larger vortex. Together with Laufer, Kaplan & Chu (1973), they conjectured that the sequential mergings of these structures is a possible mechanism for the mixing and spreading of all free shear flows.

Over the years, experiments have established that external excitations can produce changes in large scale and small scale motions in jet flows, although the effect of these on the the radiated noise field is not entirely clear. Ffowcs Williams and Kempton (1978) found that the *increase* in jet noise, due to excitation, is a direct consequence of the

amplified large-scale structures, while the fine-scale chaotic turbulence plays a relatively minor role in the noise generation mechanism. On the other hand, Morris and Tam (1977) argued that, although the large-scale structures are responsible for producing considerable changes in the fine-scale turbulence, the actual noise generation mechanism is a result of the latter. They provided two explanations. First, since the phase speed of an excited large-scale instability wave is subsonic relative to the ambient fluid, the large scale structures are inefficient in directly generating the sound waves. Secondly, if the noise increase is directly caused by the large-scale structures, there would be a distinct frequency band centered around the frequency of an excited, most amplified, instability wave. Instead, jet-noise is broad-band. Nevertheless, irrespective of the mechanism through which noise is produced, the large-scale structures play an important part in the noise generation and the dynamics of turbulent shear flows.

A distinguishing feature of coherent structures is that they are relatively permanent entities — in the sense that they persist for long times and distances — which co-exist with the seemingly completely random turbulent scales. This is in contrast to the completely chaotic small-scale motions which quickly lose their identities. This perseverance of the large scale structures offers a hope that one can manipulate the development of turbulent flows by modifying the evolution of the large scale structures, especially in the initial region of jets and mixing layers. There is now considerable experimental evidence that the large-scale structures, and hence, the global features of turbulent flows can be organized by artificial excitation such as oscillating flaps, vibrating ribbons and acoustic devices (Wygnanski and Petersen 1987). By externally exciting a jet with a loud speaker upstream of the jet nozzle, Ahuja et al. found that not only did the radiated sound increase, but the strength and regularity of the coherent structures were augmented. Ahuja et al. (1982) presented a series of measurements for subsonic jets excited at different frequencies. They

have concluded that higher Mach number unheated jets require higher excitation levels to produce noticeable changes in both large-scale turbulence and small-scale turbulence intensities. One of the objectives of this research is to investigate one mechanism (i.e., a secondary instability theory) that might explain this experimental observation.

The effect of excitation levels on jet mean flow velocity and turbulence intensities were demonstrated by Ahuja et al.. They found that when the excitation level was increased, there was a rapid decay of the mean-velocity with downstream distance. Petersen has shown that the mean velocity profile and the spreading rate of a turbulent, axisymmetric, unheated low speed jet can be altered by introducing a controlled acoustic excitation. This observation is important because the increase of jet spreading and the decrease of the mean velocity impinging on the flaps of a short takeoff and landing aircraft with an under-the-wing or over-the-wing externally blown flap system can lead to a reduction of flap loads and, therefore, a decrease in structural fatigue problems. By decreasing the aerodynamic and thermal loads impinging on the ground through increased mixing and spreading rates, the ground effects for vertical and short takeoff and landing aircraft can similarly be reduced.

Stone & Mckinzie (1984) concluded that "control of flows by intentional excitation of natural flow instabilities involves new and largely unexplored phenomena and offers considerable potential for improving component performance." They stressed that deliberate acoustic excitation — which circumvents the use of intrusive methods such as suction and blowing — of these coherent structures offers a promising new means of controlling turbulent shear flows. Most importantly, they (see also, Ahuja et al. 1986) have also emphasized the fact that, to date, most research work has been centered around unheated jet flows, usually at low speed. Therefore, future research work should be directed towards

the understanding and control of coherent structures in *heated high speed* jets.

Control of turbulent flows via coherent structures has obvious technological significance for application to a considerable number of engineering devices that depend on mixing such as ejectors, internal mixers, combustors, jets engines and high lift devices, to name a few. One of the main culprits of poor ejector performance is an incomplete mixing; therefore, ejector performance may be improved by enhanced mixing. Enhanced mixing in internal mixer nozzles can increase thrust, improve fuel economy, and reduce engine noise. An increase in fuel/air mixing in combustors can lead not only to shorter combustors, but also to improved pollution control. In supersonic jet engines, the interaction of large scale structures with shocks is the source of shock noise (Tam & Jackson 1983); by exciting the jet shear layer with a high frequency, the formation of coherent structures will occur at a smaller scale, thereby reducing the intensity of the radiated jet noise.

Having established the practical importance of manipulating the downstream development of a jet shear layer via controlling the evolution of large-scale structures, we theorize that the effect of manipulating these large-scale structures (or synonymously, instability waves) may be predicted and understood without resorting to the usual empirical requirement for the description of the fine-scale turbulence (see also, Gaster, Kit & Wygnanski 1983). To reinforce this point, the traditional approach to turbulent flows has been known to be more successful in describing existing data rather than predicting new insights. Therefore, the goal of this research is to understand, at least in qualitative terms, how certain characteristics of heated and compressible jets — such as spreading rate — can be altered by external excitation without relying on the empirical modeling of the fine-grain turbulence. We will do this by a systematic examination of the stability and resonances of the coherent structures (assuming that they are instability waves) of subsonic heated

jets.

1.2 Historical Background

When a flow passes through a nozzle, the boundary-layer near the inlet duct at the jet exit quickly evolves into a free shear layer (see Figure 1) which separates the potential core from the unperturbed ambient. When this shear layer is excited by a wave-like disturbance of suitable frequency, an instability wave develops in the flow. In the initial stages of development, where the disturbance amplitude is still small compared to the jet exit velocity, this wave grows in amplitude as it propagates downstream. The characteristics of this instability mode is described well by linear stability theory (Michalke & Hermann 1982, Petersen & Samet 1988). Farther downstream, where the amplitude of the disturbance is of appreciable size, say a small percentage of the mean flow, nonlinear effects become important, and the wave (or coherent structure) reaches a finite-amplitude saturation. An important objective of this work to understand and to promote the (resonance) conditions under which this instability wave can destabilize a subharmonic mode. Physically, this is important since a subharmonic disturbance can generate vortex pairing; this pairing is, at least partially, responsible for jet spreading and mixing.

The existence of large-scale instability waves has now been acknowledged by an overwhelming number of observations; an extensive review of coherent structures in excited shear flows is given by Wygnanski & Petersen (1987). Crow and Champagne (1971) provided the first comprehensive work on the response of a circular incompressible unheated jet to a controlled axisymmetric excitation of a certain amplitude and frequency. By measuring the velocity fluctuations along the jet axis, they found a "preferred" mode at which an excited instability wave reached a maximum amplitude. This preferred mode

has a frequency of $f_p = 0.3U_j^*/D^*$ where U_j^* is the jet exit speed, and D^* is the diameter. They concluded that this mode is an instability wave most capable of reaching a large amplitude before saturating. The significance of this preferred mode lies in the fact that it is the most dominant and frequently occurring of all large scale structures at the end of the potential core. Michalke (1971) determined that the measured phase velocity of the coherent structure, found by Crow & Champagne, agreed reasonably well with that obtained from a linear stability theory based on a turbulent mean flow. By using phase locked measurements of controlled excitations in an axisymmetric cold jet, Petersen & Samet (1988) concluded that the preferred mode is, in fact, a Rayleigh instability mode, provided that the stability analysis is based on the local shear layer thickness and the measured mean velocity profiles. As a result of this finding, they concluded that the preferred mode in, both excited and naturally occurring, jets is a shear layer instability mode rather than a global instability mode involving the entire jet column. This lends considerable credibility to the use of stability theory to understand the nature and the evolution of the quasi-deterministic large scale motions associated with the appearance of coherent structures in both unexcited and excited jets (see also Gaster, Kit & Wygnanski 1985).

There have recently been a number of theoretical works on the inviscid stability characteristics of axisymmetric jets, although studies of either compressible or heated jets remain scarce. Batchelor & Gill (1962) pioneered a theoretical analysis on the inviscid stability characteristics of a top hat velocity profile which characterizes the mean flow close to the jet exit. They found that the top hat velocity profile is unstable to a small disturbance for all axial and azimuthal wavenumbers. Their analysis is supported by Plaschko (1979) and Cohen (1986). Stability theory has now been successfully extended in various ways and applied for jets at near ambient temperatures and at low jet Mach numbers (for example,

Cohen 1986).

The stability characteristics for hot jets, which are of technological interest, have received relatively little attention. Michalke (1971) and Michalke & Hermann (1982) are among the few who investigated the stability characteristics of subsonic heated jets by the linear, inviscid and parallel flow stability theory. They found that the local growth rate of spatially growing waves increases as the total temperature of the jet is increased. This means that for heated jets there is a more unstable coherent structure, resulting in the widening of the mean jet velocity profile. Recently, Sohn (1986) found that cold jets are convectively unstable, whereas hot jets with an exit temperature 1.5 times the ambient temperature are absolutely unstable. By using a "quasi-linear" model, Ahuja et. al. (1982) concluded that the small-scale turbulence, which is induced by the passage of excited large-scale structures, is responsible for the jet spreading and mixing for both heated and unheated jets. Their theoretical and experimental studies have shown that both jet noise amplification and jet mixing decrease as the Mach number increases. The effect of heating is predicted to increase the turbulence intensity and to widen the jet width. They pointed out that their theoretical results for the heating effect on jets are inconsistent with limited experimental data and, therefore, are inconclusive. The "quasi-linear model," which requires empirical constants and certain turbulence closure assumptions, provides little physics governing the role of coherent structures in turbulent jet flows. Hence, the mystery and intricacies of coherent structures in heated jets have yet to be systematically unravelled.

Over the past few years, it has been established that linear inviscid stability theory can predict with surprising accuracy the phase velocity and the passage frequency of coherent structures, as well as the lateral distribution of the perturbations in excited jets (e.g.,

Crighton & Gaster 1976, Plaschko 1979, Strange & Crighton 1983). The convincing agreement obtained by Gaster, Kit & Wygnanski (1985) between experimental data and the linear inviscid stability theory for slowly diverging shear layers reconfirmed the preceding remark. Consequently, coherent structures can be viewed as (inviscid) instability waves of the mean flow, and fine-grain turbulence plays a passive role in the development of the coherent structures. They stressed that from the theoretical point of view, the large-scale structures offered a hope that certain characteristics — such as mixing enhancement and suppression — may be predicted and understood without resorting to the empirical requirement for the description of the fine-grain turbulence.

Although the linear parallel flow instability theory can describe accurately the local stability characteristics of the initial stages of the development of a large-scale instability wave, it is unable to predict the overall streamwise amplification of the disturbance. By retaining weakly nonparallel terms and using the method of multiple scales, Crighton & Gaster (1976) gained substantial improvement in the total streamwise growth, although there still exists discrepancies between their numerical results and experimental data. Petersen & Wygnanski (1987) attributed these differences to the neglect of the nonlinear terms in a linear analysis.

Another deficiency of linear (parallel flow) theory is that it is unable to predict the growth rate of a subharmonic disturbance in a periodic base flow. In the case of a planar mixing layer, this growth rate was first calculated by Kelly (1967) through the so-called linear secondary stability analysis. His temporal analysis predicted that a periodic fundamental component superimposed on a parallel mean flow destabilizes a subharmonic disturbance whose phase velocity matches that of the fundamental. Purely numerical work on the instability of a periodic flow has been carried out by Pierrehumbert and Widnall

(1982) who studied the linear (temporal) secondary instability of a row of Stuart vortices. Their results are in reasonable agreement with Kelly's analysis. Cohen (1986) extended Kelly's analysis to spatially growing waves in a planar mixing layer. While Kelly decoupled the predominant fundamental wave from the growth of the subharmonic, Cohen considered the exchange of energy between a fundamental disturbance and its subharmonic as both waves propagate downstream. Additionally, Cohen established subharmonic and azimuthal resonance conditions in low speed and unheated jets. In particular, he has shown that the nonlinear interaction between two azimuthal modes can produce a third mode which is initially absent in the flow. His theoretical results are in close agreement with his experimental studies. More recently, Monkewitz (1988) generalized Kelly's analysis and examined vortex pairing in more detail in incompressible mixing layers. By incorporating explicitly the weakly nonlinear interaction terms between two instability modes in his method of multiple scales analysis, he found that the development of the subharmonic depends crucially on its phase relation with the fundamental. He has also shown that a critical threshold fundamental amplitude is required for the subharmonic to become phase locked with the fundamental; this presence of the fundamental leads to an enhancement of a subharmonic growth rate.

It is perhaps appropriate at this point to mention briefly that the linear secondary stability mechanism is also important in the studies of the laminar-turbulent transition in walled-bounded boundary layer flows. By investigating the temporal instability of 3-D disturbances in a spatially periodic base flow consisting of a Blasius velocity profile and a finite amplitude 2-D Tollmien-Schlichting wave, Herbert (1984) found that the subharmonic resonance mechanism is the principal route to transition in low disturbance environments; hence the designation H-type breakdown. His numerical results agree closely with the experimental data of Saric (1983).

1.3 Scope of Present Research

The purpose of this research is to examine in detail the stabilities and resonances of coherent structures — assuming that they are synonymous with instability modes — in heated subsonic round jets. We choose temporal stability theory in favor of the spatial theory because the validity of a spatial theory was unclear at the initiation of this work (see remarks on convective instabilities of heated jets in Chapter 2). We believe that a temporal analysis of heated jets will contain all the essential physics and qualitative trends, although it is certainly true that the corresponding spatial analysis may provide a better agreement with experimental data. Of course, spatial instability arises naturally in convectively unstable flows when periodic excitation is present. The point is that the dispersion relation (i.e., the eigenvalue relation) is an analytic function of the complex wavenumber, and spatial instability is merely the analytic continuation of temporal instability. In addition, there are a number of conceptual difficulties associated with spatial instability — such as the calculation of the mean flow distortion — which we wish to circumvent through the use of temporal analysis. The present investigation is divided into the following two tasks:

1. Although the linear parallel flow instability theory of incompressible flows is presently understood and documented, the stability analysis of compressible and heated round jets is still rather sketchy. In the first part of this work, we focus on the systematic determination of the individual role of Mach number and temperature ratio in affecting jet instabilities. A good understanding of the primary instability characteristics is also a prelude to secondary instability calculations. In this work, an analytic mean flow (tanh shape) which provides a good local approximation to that obtained from measured experimental data is used in our stability calculations.

2. The principal task of this work is to study the linear subharmonic instability of a periodic flow consisting of the steady mean flow and a small but finite amplitude primary

wave. In order to make the physics governing this instability more transparent, we first establish the conditions — the so-called resonance conditions — which provide an effective mechanism for the destabilization of an instability wave. The resonant interactions between two waves allow us to determine the relevant parameters to be used as input for the secondary instability calculations.

We carry out the "secondary" instability analysis using the methods of multiple scales and a generalization of the normal mode analysis on a streamwise periodic flow. It may be noted that the secondary instability of round jets is, to date, still new, in the presence of heating and compressibility. The growth rate of the subharmonic disturbance as a function of the amplitude of the primary wave for different jet parameters — such as Mach number, temperature ratio, shear layer thickness and modal numbers — are determined.

In summary, this research will provide a deeper understanding of the relevant parameters (e.g., wavenumber of excitation, modal number, Mach number and jet temperature) that affect the secondary instability and the physical mechanisms governing vortex mergings in subsonic heated round jets.

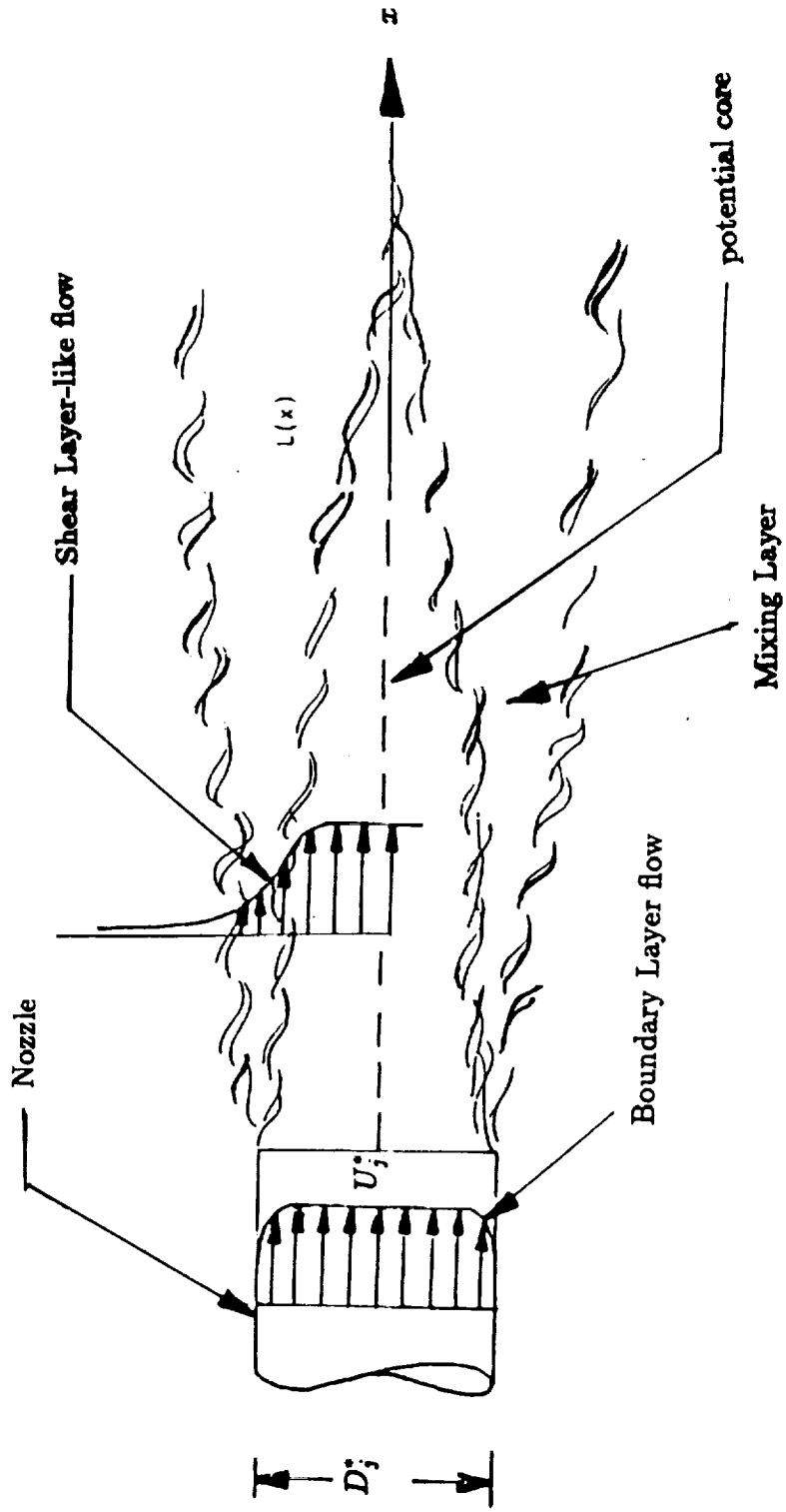

Fig. 1.1 The flow field of a jet.

Chapter 2

GOVERNING EQUATIONS AND PRIMARY STABILITY PROBLEM

2.1 Governing Equations

The governing equations for a viscous, heat conducting and compressible ideal gas in dimensional form (characterized by a superscript asterisk) are the conservation of mass, momentum, energy, and the thermodynamic equation of state. They are

$$\frac{\partial \rho^*}{\partial t^*} + \nabla^* \cdot (\rho^* \mathbf{v}^*) = 0 \tag{2.1}$$

$$\rho^* \frac{D^* \mathbf{v}^*}{D^* t^*} = -\nabla^* p^* + \rho^* \mathbf{g}^* + \nabla^* \cdot \boldsymbol{\tau}^* \tag{2.2}$$

$$\rho^* C_v^* \frac{D^* T^*}{D^* t^*} = -p^* \nabla^* \cdot \mathbf{v}^* + \nabla^* \cdot (k^* \nabla^* T^*) + \Phi^* \tag{2.3}$$

$$p^* = \rho^* \Re^* T^* \tag{2.4}$$

where ρ^*, $\mathbf{v}^*$, p^* and T^* represent the density, velocity, static pressure and the temperature, respectively. A point in space is denoted by the Cartesian coordinate $\mathbf{x}^*$, $\nabla^* = \partial/\partial \mathbf{x}^*$ and t^* stands for time. The convective derivative is defined by

$$\frac{D^*}{D^* t^*} = \frac{\partial}{\partial t^*} + \mathbf{v}^* \cdot \nabla^*, \tag{2.5}$$

$\mathbf{g}^*$ is the constant gravitational acceleration, C_v^* is the specific heat capacity at constant volume and $\Re^*$ is the gas constant. In (2.3), Fourier's Law of heat conduction is assumed; the heat flux is given by $(-k^* \nabla^* T^*)$. These equations may be found in Bird, Stewart and Lightfoot (1960).

Dissipative processes in the fluid are due to the viscosity, μ^*, and the thermal conductivity k^*. For a Newtonian fluid, the shear stress tensor, τ^*, and the "dissipation function", Φ^*, are defined by

$$\tau^* = 2\mu^*\mathbf{S}^* - \frac{2}{3}\mu^*(\nabla^* \cdot \mathbf{v}^*)\mathbf{I} \tag{2.6}$$

$$\Phi^* = \tau^* : \mathbf{S}^* = 2\mu^*\mathbf{S}^* : \mathbf{S}^* - \frac{2}{3}\mu^*(\nabla^* \cdot \mathbf{v}^*)^2 \tag{2.7}$$

where

$$\mathbf{S}^* = \frac{1}{2}[\nabla^*\mathbf{v}^* + (\nabla^*\mathbf{v}^*)^T] \tag{2.8}$$

$\mathbf{S}^*$ is the rate of strain tensor, $\mathbf{I}$ is the idemtensor and $(\cdot)^T$ denotes the transpose of a tensor or matrix.

2.2 Nondimensionalizing the Governing Equations and Simplifying Assumptions

Our principal interest is in the study of certain types of instabilities associated with compressible and heated round jets. For this purpose, the governing equations (2.1) - (2.4) can be made dimensionless by using the centerline values at the jet exit of the base flow (also called the mean flow or the unperturbed flow). We nondimensionalize all length, velocity and time scales by R^*, U_j^* and R^*/U_j^*, respectively — where R^* is the radius of the jet. The dimensionless physical variables become:

$$\mathbf{v} = \frac{\mathbf{v}^*}{U_j^*}, \quad p = \frac{p^*}{\rho_j^* U_j^{*2}}$$

$$T = \frac{T^*}{T_j^*}, \quad \rho = \frac{\rho^*}{\rho_j^*}$$

$$\mu = \frac{\mu^*}{\mu_j^*}, \quad k = \frac{k^*}{k_j^*},$$

and with the above normalizations, the governing equations (2.1) - (2.4) become

$$\frac{\partial \rho}{\partial t} + \nabla \cdot \rho \mathbf{v} = 0 \tag{2.9}$$

$$\rho \frac{D\mathbf{v}}{Dt} = -\nabla p + \frac{1}{Re}\nabla \cdot \boldsymbol{\tau} + \frac{\rho}{Fr}\hat{\mathbf{k}} \tag{2.10}$$

$$\rho \frac{DT}{Dt} = -(\gamma - 1)\gamma M_j^2 p \nabla \cdot \mathbf{v} + \frac{\gamma}{PrRe}\nabla \cdot k\nabla T + \frac{\gamma(\gamma - 1)M_j^2}{Re}\Phi \tag{2.11}$$

$$\gamma M_j^2 p = \rho T \tag{2.12}$$

where

$$\mathbf{S} = \frac{1}{2}[\nabla \mathbf{v} + (\nabla \mathbf{v})^T] \tag{2.13}$$

$$\boldsymbol{\tau} = 2\mu \mathbf{S} - \frac{2}{3}\mu(\nabla \cdot \mathbf{v})\mathbf{I} \tag{2.14}$$

$$\Phi = \boldsymbol{\tau} : \mathbf{S} \tag{2.15}$$

and $\hat{\mathbf{k}}$ is the unit vector in the direction anti-parallel to the gravity. The Reynolds number, Re, Mach number, M_j, Froude number, Fr, and Prandtl number, Pr, are given by

$$Re = \frac{\rho_j^* U_j^* R^*}{\mu_j^*}, \quad M_j = \frac{U_j^*}{a_j^*},$$

$$Fr = \frac{U_j^{*2}}{g^* R^*}, \quad Pr = \frac{\mu_j^* C_p^*}{k_j^*},$$

where a_j^* is the unperturbed sound speed at the jet exit, C_p^* is a constant representing the specific heat at constant pressure, γ = constant $= C_p^*/C_v^*$, and g^* is a constant representing the magnitude of the gravitational acceleration. The nondimensional convective derivative is given by

$$\frac{D}{Dt} = \frac{\partial}{\partial t} + \mathbf{v} \cdot \nabla \tag{2.16}$$

In order to make any progress with the relevant equations, a large number of assumptions must be made which are discussed in books on stability theory (Lin 1955, Betchov and Criminale 1967, Drazin and Reid 1981). To begin with, the last term in (2.10) is ignored because gravitational effects are unimportant at large Froude numbers; this is a

standard assumption in aerodynamics, for example, when $R^* = 5$ cm, $U_j^* = 5000$ cm/sec, $\rho_j^* = 1.3 \times 10^{-3}$ gm/ cm^3, $\mu_j^* = 1.8 \times 10^{-4}$ dynes sec/cm^2 (air at normal conditions), $Fr = 5 \times 10^3$, $Re = 1.4 \times 10^5$, $Pr = O(1)$. In instability theory, it is convenient to decompose the dependent variables into two parts: the base flow and the perturbations. At high Reynolds numbers, the base flow (i.e., unperturbed flow) will satisfy the boundary layer equations so that the unperturbed pressure will be a constant (approximately) throughout the flow field, and the jet will "diverge" with downstream distance on a long length scale of $(R^* Re^{\frac{1}{2}})$. Since the characteristic wavelength of the instability wave is on the order of R^*, the divergence of the base flow may be ignored for the purpose of calculating the instability wave. In other words, the base flow is assumed to be locally parallel. The precise form of this flow will be specified in the next section.

At high Reynolds number (say, above 10^3), the effects of viscosity and heat conductivity are negligible for the instability wave, except possibly for neutral modes and their derivatives in the cross-space. For this reason, we shall retain a highly simplified version of the viscous and conduction terms: these terms are only important in a thin layer of thickness $h = \mathrm{O}\ (Re^{-1/3})$, centered around the generalized inflection point. In this layer, the so-called the critical layer, μ and k are constants to a high degree of approximation so that $\nabla \cdot \boldsymbol{\tau}$ may be replaced by $\mu_c \nabla^2 \mathbf{v}$ and $\nabla.(k \nabla T)$ by $k_c \nabla^2 T$, where the subscript c denotes the value of a quantity in the critical layer. As a result of this approximation, the effects of heat conductivity and viscosity are correctly represented only in the critical layer where they may be important. Outside the critical layer, these effects are incorrectly represented in our analysis, but this is immaterial because they are unimportant.

Further, when the disturbances are small, the largest terms in Φ, in (2.11), are proportional to the product of the velocity gradient [which is O(1)] and the perturbation velocity gradient [which is at most O (δ/h), where $\delta \ll 1$ is the characteristic magnitude of the disturbance]. On the other hand, the perturbation temperature gradients in the conduc-

tion term of the energy equation scale as δ/h^2 because of the presence of the Laplacian and are, therefore, much more important in the critical layer than Φ. Consequently, the viscous dissipation, Φ, will be ignored here.

In summary, viscosity and heat conduction are included, but only to the extent needed to eliminate any possible singularity in the instability modes arising from the reduced inviscid and nonconducting equations. Although the viscosity and conductivity of a fluid vary with temperature, these variations will be negligible across the thin critical layer where they play an appreciable diffusive role. Consequently, the viscosity and conductivity are assumed to be uniform throughout the fluid. It may be remarked that outside the critical layer, the viscous and the conduction terms are negligible relative to the convection terms. With the preceding assumptions, the governing equations are approximated by

$$\frac{\partial \rho}{\partial t} + \nabla \cdot \rho \mathbf{v} = 0 \tag{2.17}$$

$$\rho \frac{D\mathbf{v}}{Dt} = -\nabla p + \frac{1}{Re_c}\nabla^2 \mathbf{v} \tag{2.18}$$

$$\frac{Dp}{Dt} = -\gamma p \nabla \cdot \mathbf{v} + \frac{\gamma}{Pr_c Re_c}\nabla^2 (\frac{p}{\rho}) \tag{2.19}$$

where Re_c and Pr_c are the Reynolds and Prandtl numbers based on the viscosity and thermal conductivity in the critical layer. The temperature has been eliminated in the energy equation in favor of the pressure via the equations of state and continuity. The Prandtl number and γ (ratio of specific heats) are taken to be 0.7 and 1.4, respectively. In the rest of this thesis, the subscript c on Re and Pr are dropped, with the understanding that these quantities are based on μ_c and k_c. The assumptions that lead to (2.17) - (2.19) are discussed more fully in Moore (1964; see the article by S. F. Shen).

2.3 The Base flow and Perturbation Equations

We shall now formally separate the disturbance from the base flow by writing

$$\rho \rightarrow \rho_0 + \rho$$

$$\mathbf{v} \rightarrow \mathbf{v}_0 + \mathbf{v} \tag{2.20}$$

$$p \rightarrow p_0 + p$$

where the subscript 0 hereafter refers to the base flow, and ρ, $\mathbf{v}$, p are perturbation quantities. After substituting (2.20) into (2.17) - (2.19) and collecting terms, we obtain a set of equations for the base flow and for the perturbations. The latter set is given vectorially as

$$\frac{D_0\rho}{Dt} + \rho_0 \nabla \cdot \mathbf{v} + \mathbf{v} \cdot \nabla \rho_0 = -\nabla \cdot (\rho \mathbf{v}) \tag{2.21}$$

$$\rho_0 \frac{D_0 \mathbf{v}}{Dt} + \rho_0 \mathbf{v} \cdot \nabla \mathbf{v}_0 + \nabla p - \frac{1}{Re} \nabla^2 \mathbf{v} = -\rho \frac{D\mathbf{v}}{Dt} \tag{2.22}$$

$$\frac{D_0 p}{Dt} + \gamma p_0 \nabla \cdot \mathbf{v} - \frac{\gamma}{PrRe} \nabla^2 \left(\frac{p}{\rho_0} - \frac{p_0 \rho}{\rho_0^2}\right) = -\mathbf{v} \cdot \nabla p - \gamma p \nabla \cdot \mathbf{v}$$

$$+ \frac{\gamma}{PrRe} \nabla^2 \left(\frac{p_0 \rho^2}{\rho_0^3} - \frac{p\rho}{\rho_0^2} + \cdots\right) \tag{2.23}$$

where,

$$\frac{D_0}{Dt} = \frac{\partial}{\partial t} + u_0 \frac{\partial}{\partial x}, \tag{2.24}$$

and the dots stand for terms for the product of perturbations that are cubic and higher. In deriving (2.21) - (2.23), we have made the assumption that the base flow is parallel; this implies that

$$\mathbf{v}_0 = [u_0(y,z), 0, 0] \tag{2.25}$$

$$\rho_0 = [\rho_0(y,z), 0, 0)] \tag{2.26}$$

$$p_0 = \text{constant} \tag{2.27}$$

where $\mathbf{x} = (x, y, z)$ is a cartesian coordinate system with x pointing along the axis of the jet. Although the numerical calculations and the theoretical developments are carried out in a cylindrical coordinate system (x, r, ϕ) with $y = r\cos\phi$, $z = r\sin\phi$, it is more compact to write down the perturbation equations in a Cartesian system. Note that $\nabla\rho_0 = (0, \partial\rho_0/\partial y, \partial\rho_0/\partial z)$ so that $\mathbf{v}\cdot\nabla\rho_0$ does not involve the x-component of the perturbation velocity. Similar remarks hold true for other terms of this type. In order to generate specific results, the mean flow is taken as

$$u_0 = u_0(r) = \frac{1}{2}\{1 - \tanh[(r - \frac{1}{r})/4\theta]\} \tag{2.28}$$

$$\rho_0 = \rho_0(r) = \frac{T_*}{1 + (T_* - 1)u_0 + \frac{(\gamma-1)}{2}M_j^2 T_* u_0(1 - u_0)} \tag{2.29}$$

$$p_0 = \text{constant} = \frac{1}{\gamma M_j^2} \tag{2.30}$$

where

$$\theta \text{ is the dimensionless momentum thickness} = \int_0^\infty u_0(1 - u_0)dr$$

$$T_* \text{ is the temperature ratio} = \frac{T_0(0)}{T_0(\infty)}$$

and,

$$T_0 \text{ is the base temperature} = T_0(y, z) = T_0(r)$$

Note that the steady unidirectional velocity profile (2.28) is not an exact solution of the Navier-Stokes equation. It is, however, a good local approximation to that obtained from the measured experimental data. This mean velocity profile, which has also been used by other investigators (e.g., Michalke & Hermann 1982), is capable of representing the top-hat profile at the jet nozzle exit and the fully developed Gaussian profile at around the end of the potential core as well as the profiles between these two extremes. This can be done by varying the parameter θ (momentum thickness) from (near) zero to a value which is a substantial fraction of unity (i.e., the nondimensional jet radius). The parameter θ can thus be used to characterize different velocity profiles at different axial locations.

For compressible ideal gas flows, the mean density profile, (2.29), is obtained from the mean velocity profile via the Busemann-Crocco law, which is valid for high Reynolds number flows and when the Prandtl number is unity (Schlichting 1979, p. 330). For a given velocity profile, u_0, the mean density distribution is governed by three dimensionless parameters: Mach number M_j, temperature ratio T_*, and the isentropic exponent γ. In this work, the isentropic exponent $\gamma = 1.4$, and T_* is taken to be greater than one, which means that the jet is hotter than the quiescent environment. For example, when $T_* = 2$, the jet is twice as hot as the environment.

Figure (2.1a) shows the dependence of velocity profiles on θ while the effect of θ, M_j, and T_* on the mean density distributions are shown in Figure (2.1b). It is interesting to note that in Figure (2.1b), T_* has a much greater influence than the (subsonic) Mach number M_j upon the base density profile, and therefore, is expected to produce a greater effect on the instability.

2.4 Primary Linear Stability Analysis

Although our principal goal is the study of the secondary instabilities and subharmonic resonances in a compressible and heated jet, we begin our discussion with the classical linear instabilities of a jet. A knowledge of these linear instabilities is needed in order to study the secondary instabilities and resonances. Perhaps it is worthwhile, first, to say a few words about the parallel flow assumption for the mean flow in view of some relatively recent developments.

Petersen & Samet (1988) have found that the local stability characteristics (e.g, eigenfunctions, phase velocity , Reynold stress, etc.) of an instability mode developing on a jet column can be predicted accurately from linear viscous stability theory based on the measured mean velocity profiles, which are again assumed to be locally parallel. They

found that the preceding observation is valid even when the local streamwise velocity disturbance reaches a level as high as 24% of the jet speed, when the flow is unquestionably nonlinear. The last remark lends considerable credibility to the generally accepted claim that even in "nonlinear" flows, the mode shape of the fundamental is given quite accurately by the linear mode. A large body of literature has been built on this assumption, beginning with the pioneering work of Ko, Kubota and Lees (1970).

In fact, this finding of Petersen & Samet is important in the instability analysis of a jet which has a finite-amplitude wave-like structure developed on its column. This structure is approximately both spatially and temporally periodic. In order to represent the fundamental component of this periodic flow, we shall use a linear instability mode. This makes the study of secondary instabilities much easier because we do not have to compute a finite amplitude primary disturbance. In our secondary instability analysis, this amplitude is a *given* quantity; the mode shape is given by linear theory.

Unfortunately, a shortcoming of linear instability based on parallel flow assumption is that it predicts poorly the total streamwise amplification of an instability mode. By retaining weakly nonparallel terms in an axisymmetric round jet, Crighton & Gaster (1976) [see also Gaster, Kit and Wygnanski 1985] gained a significant improvement on the total growth rate, although there still exists some unsatisfactory discrepancies between their results and experimental measurements. According to Wygnanski & Petersen (1987), these discrepancies are attributed to the neglect of the nonlinear interaction terms in the linear parallel flow analysis of a single wave train. Petersen et al. have, in fact, dispelled the skepticism surrounding the predictive capability of a parallel flow stability analysis for the mode shape. While there is no doubt that an accurate determination of the total growth rate still requires further studies on nonlinear analysis, it is not a concern in this work. The quantities of interest here are the local values of the phase velocity, growth rate and the shape of a specific mode, and that can be described well by linear parallel

flow analysis.

Because of the effects of compressibility and heating in a cylindrical geometry, the algebraic aspects of the analysis in this thesis are very lengthy. In order not to burden the reader, we use a compact operator notation; the specific elements of these operators may be found in the various appendices.

To recall, we use a cylindrical polar coordinate (x, r, ϕ), where x is along the axis of the jet and (r, ϕ) are the radial and azimuthal coordinates; the components of the perturbation velocity are $\mathbf{v} = (u, v, w)$ in this cylindrical system. To represent the entire perturbation field, we use the five-dimensional vector

$$\mathbf{F} = \delta\ \mathbf{f}_b = \delta\ (u, v, w, p, \rho)_b^T$$

After substituting the above equation into the (nonlinear) perturbation equations, (2.21) - (2.23), and neglecting all quadratic and higher order terms in δ, we arrive at the linearized disturbance equations

$$\mathbf{A}_b \mathbf{f}_b = 0 \tag{2.31}$$

Here $\mathbf{A}_b$ is a linear operator whose action on $\mathbf{f_b}$ is defined in detail in Appendix A. The various terms in $\mathbf{A}_b$ are functions of the base flow alone; $\mathbf{A}_b$ has variable coefficients which depend only on the radial coordinates. Here δ is a small parameter which measures the magnitude of a typical disturbance with respect to the base flow. Since $\mathbf{A}_b$ depends on r alone, we may extract the dependence of the disturbance on the other coordinates via Fourier (space) and Laplace (time) transforms. Because of the linearity, we consider a "single mode" (or wave component) and write

$$\begin{aligned} \mathbf{f}_b &= \mathbf{f}(r) e^{i(\alpha x + \beta\phi)} e^{\sigma t} + \text{ complex conjugate}; \qquad i = \sqrt{-1} \\ \mathbf{f}(r) &= [u(r), v(r), w(r), p(r), \rho(r)]^T \end{aligned} \tag{2.32}$$

where α and β are the wavenumbers in the axial and azimuthal directions, respectively, and σ is the complex growth rate. The disturbance is completely described by α, β, σ and the

complex amplitude function (also known as the mode shape) $\mathbf{f}(r)$. The modal form (2.32) is simply a single mode of a Fourier-Laplace component representing the wavenumber and frequency component of an arbitrary disturbance. This means that each individual mode evolves independently in the course of time, according to the the linearized equations. Because of the periodicity in ϕ, β must be an integer (0, 1,2 ... etc), and it is also called the mode number. In temporal theory, α is real, and σ is complex. The real part of σ determines the temporal growth rate of a disturbance. The imaginary value of σ is the radian frequency. In spatial stability, σ is usually written as $-i\omega$ where ω is the given real frequency, but α is complex. The spatial growth rate of a disturbance is given by the imaginary value of α. An approximate relation between the growth rates of these two forms of instability can be obtained by Gaster's transformation (Gaster 1962) under certain restrictive assumptions — such as for small growth rates.

Although there still exists some questions on the application of temporal or spatial theory (especially for nonlinear flows), it is now generally accepted that temporal analysis is meaningful for absolutely unstable flows while spatial analysis has physical meaning for convectively unstable flows. The basic concepts of absolute and convective instability are discussed in detail by Huerre & Monkewitz (1985). Suppose a jet is perturbed by a disturbance which is localized in space and is impulsive in time. Some time after the triggering of this disturbance, a wavetrain of finite extent evolves on the jet. If both the leading and trailing edges of this wavetrain propagate downstream, the flow is said to be convectively unstable. Otherwise, the flow is absolutely unstable. In an absolutely unstable flow, the trailing edge of the wavetrain propagates upstream and the group velocity is negative in some region of the wave. Because of this, disturbances which are generated downstream of the nozzle in an absolutely unstable flow can actually interact, through instability waves, with the nozzle to produce "feedback" or "resonance' loops.

Temporal stability is also applicable to flows which are required to be periodic in space.

Such flows may not actually exist in practice, but are at least fairly close approximations to those that do. Once a flow is forced to be periodic in space, its natural spatial evolution is inhibited and the (linear) instability will appear as an exponential growth in time. For this restricted class of flows, temporal instability is always valid. Since at the beginning of this study, the concepts of convective and absolute instabilities were not clarified, we opted for a study which is based on temporal instabilities and spatial periodicity. In retrospect, this was a good choice because it is now known that hot jets with $T_* > 1.5$ may be absolutely unstable (Sohn 1986); for such flows a study based on spatial instability would be meaningless.

The modal representation (2.32) of a disturbance transforms the system of linearized partial differential equations, (2.31), into a system of ordinary differential equations (hereafter ODE's) in r. These equations can be conveniently put into the matrix form

$$\mathbf{A}_1\mathbf{f} = \sigma\mathbf{B}_1\mathbf{f} \tag{2.33}$$

where the elements, which depend on the wavenumbers (α, β), of $\mathbf{A}_1$ and $\mathbf{B}_1$ are given in Appendix B. The principal task is to solve (2.33) for a given (α, β) and suitable boundary conditions in order to obtain the eigenvalue from the dispersion relation $\sigma = \sigma(\alpha, \beta)$. We now discuss the boundary conditions associated with (2.33).

2.5 Kinematic Boundary Conditions on the Linearized Disturbances

The appropriate boundary conditions for a disturbance superimposed on a subsonic jet require that $\mathbf{f}$ remains finite on the jet axis and vanishes at infinity. They are,

$$\mathbf{f} \to 0 \text{ as } r \to \infty \tag{2.34}$$

$$\mathbf{f} \text{ remains finite at } r = 0 \tag{2.35}$$

In fact, some of the boundary conditions to be satisfied at the origin are purely "kinematic" in nature, and therefore, are independent of the viscosity (Batchelor and Gill 1962). In order for a disturbance to remain single-value at the origin, these kinematic boundary conditions yield

$$u(0) = p(0) = \rho(0) = 0 \quad \text{for } \beta \neq 0 \tag{2.36}$$

and,

$$v(0) = w(0) = 0 \quad \text{for } \beta \neq 1 \tag{2.37}$$

Other boundary conditions at the origin, which cannot be determined from kinematic consideration alone, are derived from their asymptotic behavior developed in the next section; note that not all the boundary conditions are given by kinematic considerations.

2.6 Asymptotic Behavior of a Disturbance on a Uniform Base Flow

The numerical solutions of hydrodynamic stability problems in an unbounded domain, such as in round jets, are often solved over a finite domain. Consequently, the analytical structure of a disturbance for large r and small r is required. Because the base flow, u_0 and ρ_0, approaches a constant value, the asymptotic behavior can be obtained explicitly by solving a series of Bessel-like equations. In fact, for $r \to 0$, we can write

$$u = c_1 u_p + c_2 u_v \tag{2.38}$$

$$v = c_1 v_p + c_2 v_v \tag{2.39}$$

$$w = c_1 w_p + c_2 w_v \tag{2.40}$$

$$p = c_1 p_p \tag{2.41}$$

$$\rho = c_1 \rho_p \tag{2.42}$$

where

$$u_p = \frac{i\alpha}{\lambda_p} I_\beta(\lambda_p r)$$

$$v_p = I'_\beta(r\lambda_p)$$

$$w_p = \frac{i\beta}{r\lambda_p} I_\beta(r\lambda_p)$$

$$p_p = \left\{ \frac{\lambda_p^2 - \alpha^2}{Re} - \rho_0 i\alpha(u_0 - C) \right\} \frac{I_\beta(\lambda_p r)}{\lambda_p}$$

$$\rho_p = \rho_0 (\frac{\alpha^2}{\lambda_p} - \lambda_p) I_\beta(\lambda_p r)$$

$$\lambda_p = \frac{\alpha[1 - \rho_0(u_0 - C)^2 M_j^2 + i\alpha(u_0 - C)M_j^2/Re]^{\frac{1}{2}}}{[1 + i\alpha(u_0 - C)M_j^2/Re]^{\frac{1}{2}}}$$

$$u_v = \frac{i\lambda_v}{\alpha} I_\beta(\lambda_v r)$$

$$v_v = I'_\beta(\lambda_v r)$$

$$w_v = \frac{i\beta}{r\lambda_v} I_\beta(\lambda_v r)$$

$$\lambda_v = [\alpha^2 + i\alpha\rho_0(u_0 - C)Re]^{\frac{1}{2}}$$

where c_1 and c_2 are constants, the primes denote differentiation with respect to the argument in parenthesis, and the subscripts p and v refer to the so-called "pressure mode" and "viscous mode", respectively. Here I_β is the modified Bessel function whose order is the azimuthal wavenumber, β = integer, and $C = i\sigma/\alpha$ is the complex phase speed. Clearly, the kinematic boundary conditions are contained in the above asymptotic expressions. In order to maintain a highly accurate finite difference numerical procedure, the asymptotic boundary conditions are enforced. This not only fulfills the requirement of the value of a specific quantity at a specific point, but also the manner it behaves (e.g., in powers of r).

Similarly, as $r \to \infty$, the same asymptotic results hold provided that I_β is replaced by the modified Bessel function of the second kind, K_β (Abramowitz & Stegun 1972), and u_0 and ρ_0 are replaced by their values at $r = \infty$. Note that in all likelihood, the

viscous solution is unimportant for large r because the argument of K_β is large (i.e., $\lambda_v r \sim (\alpha Re)^{\frac{1}{2}} r \gg 1$).

2.7 The Behavior of Disturbances in the Critical Layer

Although we have retained the most important effects of viscosity and heat conductivity in the critical layer, it is instructive to examine the nature of the flow in this layer when (formally) $Re = \infty$ in equation (2.33). It is known that under certain conditions — to be made more precise momentarily — the instability modes will become singular at the critical point. It is desirable to know the "strength" of this singularity for numerical purposes, and to see under what conditions at least some of this singularity may be eliminated, even when $Re = \infty$. The latter condition gives us a generalization of the Rayleigh inflection point criterion to compressible and heated flows in round jets. We emphasize that, strictly speaking, there will be no singularity in the modes because the "diffusive" effects of viscosity and conductivity have been retained. However, at large Re, we will have a "near" singularity that does affect the accuracy of the numerical solutions.

By substituting $Re = \infty$ and $\sigma = -i\alpha C$ in equations (2.33), the linearized, inviscid and nonconducting disturbance equations can be obtained as

$$\rho_0 i\alpha(u_0 - C)u + \rho_0 u_0' v + i\alpha p = 0 \tag{2.43}$$

$$\rho_0 i\alpha(u_0 - C)v + p' = 0 \tag{2.44}$$

$$\rho_0 i\alpha(u_0 - C)w + \frac{i\beta p}{r} = 0 \tag{2.45}$$

$$i\alpha u + \frac{v}{r} + v' + \frac{i\beta w}{r} + i\alpha(u_0 - C)p = 0 \tag{2.46}$$

$$i\alpha(u_0 - C)\rho + \rho_0' v + \rho_0(\frac{v}{r} + v' + \frac{i\beta}{r}w + i\alpha u) = 0 \tag{2.47}$$

where primes denote differentiation with respect to r. After some algebraic manipulations in favor of the pressure, the above equations can be reduced to a second order ODE with

variable coefficients (essentially a Rayleigh equation) of the form

$$\frac{d^2p}{dr^2} + (\frac{1}{r} - \frac{2u_0'}{u_0 - C} - \frac{\rho_0'}{\rho_0})\frac{dp}{dr} + [\alpha^2(u_0 - C)^2\rho_0 M_j^2 - \frac{\beta^2}{r^2} - \alpha^2]p = 0 \tag{2.48}$$

When the instability wave is neutral, the differential equation (2.48) has a regular singular point at the point $r = r_c$ where $u_0(r_c) = C$ (C is real for a neutral wave); the subscript c hereafter refers to the value of a variable at the critical point. In the neighborhood of r_c, the coefficients of the differential equation can be expanded in terms of powers of $r - r_c$. For example,

$$\begin{aligned} u_0 &= C + u_c'(r - r_c) + u_c''(r - r_c)^2/2 + \cdots, \\ \rho_0 &= \rho_c + \rho_c'(r - r_c) + \rho_c''(r - r_c)^2/2 + \cdots \end{aligned} \tag{2.49}$$

where $u_c' = u_0'(r_c)$ etc. Substituting (2.49) into the differential equation (2.48), we obtain the approximate differential equation around the critical point for p, i.e.,

$$p'' - [\frac{2}{r - r_c} + D_1 + D_2(r - r_c) + \cdots]p' + [E_1 + E_2(r - r_c) + \cdots]p = 0 \tag{2.50}$$

where

$$D_1 = \frac{\rho_c u_c'' + \rho_c' u_c'}{\rho_c u_c'} - \frac{1}{r_c}$$

$$D_2 = -\frac{2u_c'''}{3u_c'} + \frac{u_c''^2}{2u_c'^2} - \frac{\rho_c''}{\rho_c} + \frac{\rho_c'^2}{\rho_c^2} - \frac{1}{r_c^2}$$

and

$$E_1 = -(\alpha^2 + \frac{\beta^2}{r_c^2})$$

$$E_2 = \frac{2\beta^2}{r_c^3}$$

According to the method of Frobenius (Bender & Orszag 1978), equation (2.50) has two linearly independent solutions of the form $r = r_c$,

$$p_a = (r - r_c)^3 g_1(r - r_c) \tag{2.51}$$

$$p_b = g_2(r - r_c) + K p_a \log(r - r_c) \tag{2.52}$$

where

$$g_1(r-r_c) = 1 + a_1(r-r_c) + a_2(r-r_c)^2 + \cdots$$

$$g_2(r-r_c) = 1 + b_1(r-r_c) + b_2(r-r_c)^2 + \cdots$$

The coefficients $a's$, $b's$ and K are found by substituting the Frobenius series (2.51) - (2.52) into the differential equation (2.50) and equating like powers of $(r-r_c)$:

$$a_1 = \frac{3D_1}{4}$$

$$a_2 = \frac{3D_2 + 4a_1D_1 - E_1}{10}$$

$$\vdots$$

$$b_1 = 0$$

$$b_2 = \frac{E_1}{2}$$

$$\vdots$$

$$K = \frac{D_1E_1 - E_2}{3}$$

The general solution of the differential equation (2.50) is of the form

$$p = \lambda_1 p_a + \lambda_2 p_b \tag{2.53}$$

where λ_1 and λ_2 are constants. The solution p_a is analytic, while p_b is a multi-valued function because of the logarithmic singularity unless $K = 0$. For the particular case of an unheated jet where ρ_0 is a constant, the condition $K = 0$ reduces to

$$\frac{d}{dr}\left(\frac{ru_0'}{\beta^2 + \alpha^2 r^2}\right) = 0 \quad \text{at} \quad r = r_c. \tag{2.54}$$

Condition (2.54), which was established by Batchelor & Gill (1962) to be a necessary condition for the existence of an amplified inflectional type of disturbance in an incompressible unheated round jet, is, in fact, valid even in the presence of compressibility. Furthermore,

the familiar generalized inflection point theorem for the existence of instability modes in planar mixing layers, derived by Lees & Lin (1946), i.e.,

$$\frac{d}{dy}(\rho_0 u_0') = 0, \tag{2.55}$$

at $y = y_c$ where y is the transverse coordinate, can be recovered by letting $1/r_c \to 0$ in the condition $K = 0$.

The behavior of the velocity and density perturbations in the vicinity of the critical point is obtained by substituting (2.51) and (2.52) into equations (2.43) - (2.47). The corresponding two independent solutions near the critical point, $r = r_c$, are

$$\begin{aligned}
v_a &= \frac{3i}{u_c'\rho_c\alpha}(r-r_c) + \left[\frac{3\rho_c u_c'' + (6\rho_c' - 8a_1\rho_c)u_c'}{2\alpha i\rho_c^2 u_c'^2}\right](r-r_c)^2 + \cdots \\
v_b &= \frac{2ib_2}{\alpha\rho_c u_c'} + \cdots + Kv_a\log(r-r_c) \\
u_a &= -\frac{3}{\alpha^2\rho_c u_c'} + \frac{(3\rho_c' - 4a_1\rho_c)}{\alpha^2\rho_c^2 u_c'}(r-r_c) + \cdots \\
u_b &= \frac{\beta^2}{r_c^2\alpha^2\rho_c u_c'(r-r_c)} + \cdots + Ku_a\log(r-r_c) \\
w_a &= -\frac{\beta}{\alpha r_c\rho_c u_c'}(r-r_c)^2 + \cdots \\
w_b &= -\frac{\beta}{u_c'\rho_c r_c\alpha(r-r_c)} + \cdots + Kw_a\log(r-r_c) \\
\rho_a &= \frac{3r_c u_c'' - (4a_1 r_c + 3)u_c'}{\alpha^2 r_c u_c'^3} + \cdots \\
\rho_b &= -\left\{\frac{(\alpha^2 r_c^3 + \beta^2 r_c)u_c'' + [3Kr_c^3 - (\alpha^2 r_c^2 + \beta^2)]u_c'}{\alpha^2 r_c^3 u_c'^3(r-r_c)}\right\} + \cdots + K\rho_a\log(r-r_c)
\end{aligned} \tag{2.56}$$

The above equations (2.56) show that the logarithmic term is present in all perturbations unless the generalized inflection point criterion is satisfied; that is $K = 0$. In addition, the leading order term in the pressure fluctuation and velocity perturbations of compressible

flows has the same analytical behavior as in incompressible flow. For example, the leading term for u and w has a simple pole unless the azimuthal mode number is zero, irrespective of compressibility. The density fluctuation, or the temperature fluctuation, which is a new quantity due to compressibility, has generally a simple pole at leading order. Consequently, for a neutral mode, the p and v perturbations are finite, the u and w modes becomes infinite for $\beta \neq 0$, and the ρ perturbation is generally infinite. It is precisely the singular nature of the perturbations at the critical point that creates difficulties in the numerical calculations for neutral modes. With the inclusion of dissipative effects, some of this difficulty disappears, although a very fine grid is needed in the vicinity of the critical layer to resolve the fluctuations.

2.8 Summary

In summary, the ODE's, which is symbolically expressed by (2.33), is solved by two independent numerical schemes (to be discussed later) with suitable boundary conditions on the jet axis and in the quiescent medium at infinity. Nontrivial solutions exist only for a certain set (α, β, σ), or equivalently in the more usual notation,

$$\sigma = \sigma(\alpha, \beta) \tag{2.57}$$

The above equation is called the dispersion relation whose real part (if positive) indicates instability and whose imaginary part is the frequency of the wave.

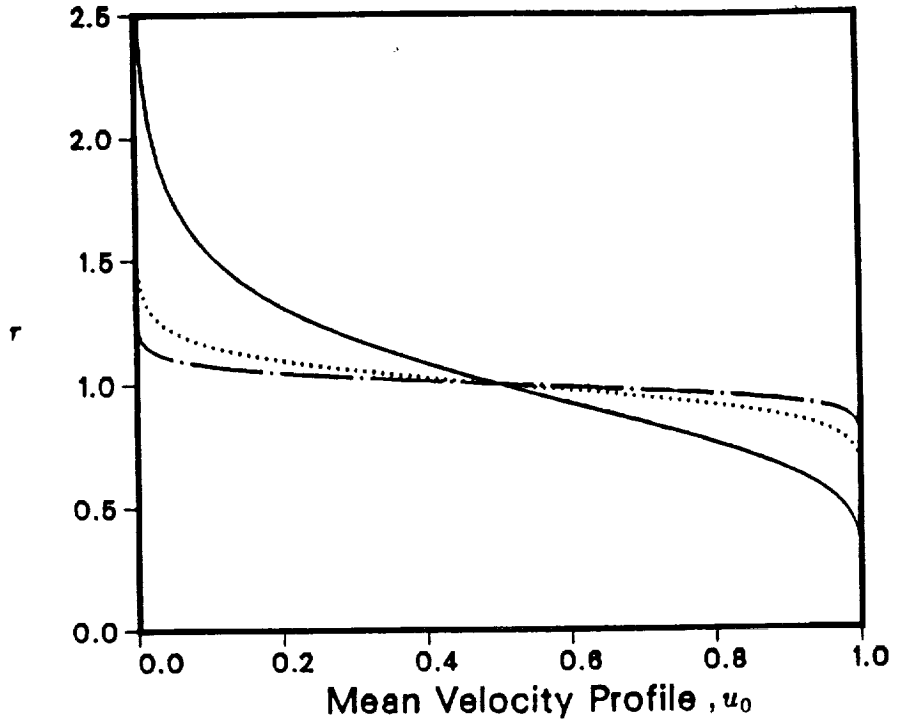

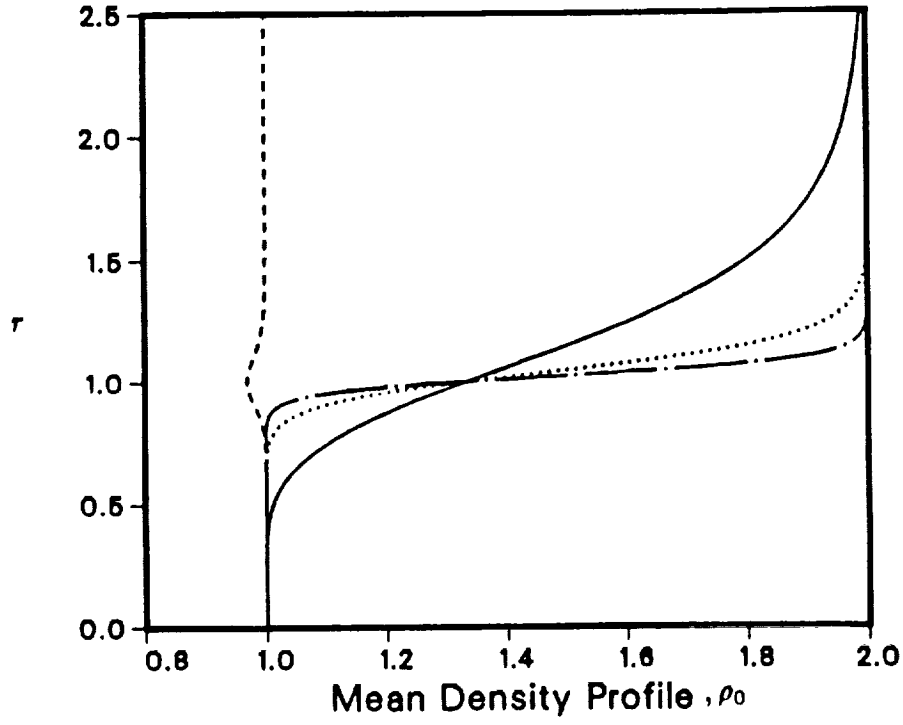

Fig. 2.1 Jet mean profiles: solid lines ($\theta = 1/5, M_j = 0.0, T_* = 2$), dot ($\theta = 1/15, M_j = 0.0, T_* = 2$), chaindot ($\theta = 1/30, M_j = 0.0, T_* = 2$), dash ($\theta = 1/15, M_j = 0.8, T_* = 1$).

Chapter 3

FORMULATION OF THE SECONDARY INSTABILITY PROBLEM

We begin our discussion in this section with a physical description of how an instability wave evolves on a jet and how the flow field may be approximated at a couple of diameters downstream of the jet nozzle.

When a jet is perturbed by an external excitation of a suitable wavenumber or frequency, an instability wave develops in the jet shear layer. For clarity, this instability wave will be called the fundamental wave or the primary wave. In this work, we will use the words "primary" and "fundamental" interchangeably. During the initial stages of development, where the amplitude of the disturbance is still small, the stability characteristics of this wave are described quite accurately by the primary stability analysis developed in Chapter 2. However, as this wave propagates downstream, its amplitude grows and the mean flow diverges. The mean flow divergence results in the reduction of the mean flow vorticity and hence, contributes to a decrease in the local growth rate of this wave. Farther downstream, at approximately one or two diameters from the jet nozzle, this wave reaches a finite-amplitude (i.e., saturation) as a result of nonlinear effects. The flow field arising from the presence of the fundamental wave may (roughly) be viewed as convecting discrete vortex rings. This flow is periodic (approximately) in time and in space.

A principal objective of this work is to determine the sensitivity of this periodic flow to various controllable jet parameters such as wavenumber of excitation, azimuthal mode

number, Mach number and jet temperature ratio.

The investigation is carried out via a secondary instability analysis. The instability analysis of small disturbances — which for clarity, will be called secondary disturbances — superimposed on a base flow consisting of the finite-amplitude fundamental wave and a long time averaged mean profile is termed secondary instability analysis. In order to make the secondary instability analysis as simple as possible, we invoke the following assumptions:

1. The locally parallel mean profile and the shape of the fundamental mode is minimally affected by the nonlinear self-interactions of the fundamental (i.e., shape assumption). In physical terms, this fundamental wave can be thought of as a coherent structure or a large scale instability wave.

2. The amplitude A of the fundamental wave, subject to an appropriate normalization, remains approximately constant during the evolution of the secondary instability disturbance.

3. The mean flow remains unchanged and the fundamental mode keeps its (initial) shape and phase velocity during the evolution of the secondary instability disturbance.

4. The magnitude of the secondary disturbance is kept sufficiently small to ensure that a linear secondary instability theory is valid.

The justification of the first assumption has been discussed in the primary stability analysis. Because of the nonlinear terms in the governing equations, a single linear instability mode can never exist, by itself, in the flow. It will interact with itself to produce higher harmonics and a mean flow distortion. The effects of the higher harmonics and of the mean flow distortion in subsonic round jets were recently investigated in detail by Jarrah (1989). His results indicate that the distortion of the mean flow due to wave Reynolds stresses is quite small locally and is probably unimportant for the secondary instability. The small

change in A during the course of its nonlinear evolution relative to an anticipated strong convective growth of a subharmonic disturbance justifies the use of assumption (2). This assumption is further supported by experimental studies on planar mixing layers; for example, Ho & Huang (1982) found that when discrete vortices develop on the flow, the subharmonic mode grows rapidly while the amplitude A remains approximately constant. The recent work of Petersen & Samet (1988) supports assumption (3), especially on the insensitivity of the mode shape to nonlinearities, although no detailed experimental results exist for heated and compressible round jets in this regard. Furthermore, in subsequent analysis, we find that the growth rate of the subharmonic wave is indeed very much larger than that of the primary wave; this finding will, in fact, justify the use of assumptions (2) and (3).

In order to have confidence in our results, two different approaches for secondary instability analysis are used here. The first is based on the method of multiple scales, while the second is done by generalizing the normal mode analysis from a parallel base flow to a periodic base flow.

3.1 Method of Multiple Scales

Kelly (1967) was the first to use the method of multiple scales to describe theoretically the strong growth of a subharmonic disturbance in an incompressible planar mixing layer. His results are consistent with the the experimental observations of the vortex-pairing phenomenon found by Sato (1956). By using full numerical simulations on the instability of an array of Stuart vortices in a mixing layer, Pierrehumbert & Widnall (1982) confirmed that the two-dimensional subharmonic modes responsible for the coalescence of vortices are indeed the most dominant instability modes. Recently, Monkewitz (1988) generalized Kelly's work and examined vortex pairing in more detail in incompress-

ible mixing layers.

The formulation of the secondary instability problem is based on Kelly's ideas, although a compact notation is used here. The finite-amplitude of the fundamental wave is regarded as a moderately small perturbation parameter δ [say, $\delta = O(A) \cong 0.1$]. The physical variable, which describes the perturbations, $\mathbf{F}$, is assumed to have a general asymptotic expansion of the form

$$\mathbf{F} = \delta\mathbf{F}_1 + \varepsilon\mathbf{F}_2 + \delta^2\mathbf{F}_{11} + \varepsilon\delta\mathbf{F}_{12} + 0(\varepsilon^2), \quad 0 < \varepsilon \ll \delta \ll 1 \tag{3.1}$$

where $\mathbf{F}_1$ is the fundamental (or primary) wave, $\mathbf{F}_2$ is the secondary disturbance (which will later be taken as a subharmonic disturbance), $\mathbf{F}_{11}$ denotes the quadratic nonlinear interactions of the fundamental wave with itself, and $\mathbf{F}_{12}$ represents all the quadratic interactions between $\mathbf{F}_1$ and $\mathbf{F}_2$. As the $\mathbf{F}_1$ mode propagates downstream, it travels into a shear flow whose transverse length scale continuously increases, the growth rate of this wave continuously decreases and the wave eventually becomes neutral. In shear layers, a strong interaction between the fundamental wave and its subharmonic (i.e., one half the fundamental frequency) occurs where the fundamental becomes neutral and its amplitude is a constant. This neutral state, which arises from the spreading of the shear layer and nonlinear effects, is really of no importance in this study. What really matters is that there is a region in the jet where the amplitude of the fundamental (or primary) wave is a constant and the growth rate of the subharmonic is enhanced from that given by parallel flow stability theory; of course, this amplitude is "unknown" to us, although experimental data suggests that it can be as large as 10% of the mean flow, and the cross-space structure of this wave may be represented by the local linear instability mode of the jet (Petersen & Samet 1988). In this region, the primary wave interacts with itself at $O(\delta^2)$ and higher. This interaction is assumed to have a negligible effect on the mean flow and the primary wave. Consequently, the $\mathbf{F}_{11}$ term in (3.1) can be ignored. Of course, the nonlinear interactions of primary wave will eventually lead to the appearance of higher harmonics,

but they play no significant role in the generation of the subharmonic at $O(\varepsilon\delta)$ because they occur at $O(\delta^2\varepsilon)$ and higher .

When the primary wave saturates, the characteristic magnitudes of the primary and secondary disturbances are δ and ε respectively. The focus of this work lies at order $\varepsilon\delta$ where the primary wave $\mathbf{F}_1$ interacts with the subharmonic disturbance $\mathbf{F}_2$ to form sum and difference modes. If the axial wavenumbers, frequencies, and azimuthal mode numbers satisfy the so-called resonance conditions, which will be discussed momentarily, then the growth rate of the disturbance $\mathbf{F}_2$ may be enhanced considerably from that given by linear parallel flow analysis.

3.2 Kinematic Resonance Conditions

We now illuminate the physics governing resonant interactions between two linear waves of the form

$$\mathbf{F}_1 = \mathbf{f}_1(r)E_1 + c.c. \tag{3.2}$$

$$\mathbf{F}_2 = \mathbf{f}_2(r)E_2 + c.c. \tag{3.3}$$

where

$$E_1 = \exp i(\alpha_1 x + \beta_1\phi)\exp\sigma_1 t$$

$$E_2 = \exp i(\alpha_2 x + \beta_2\phi)\exp\sigma_2 t$$

and *c.c.* denotes the complex conjugates of the preceding terms.

After substituting (3.1) - (3.3) into (2.17) - (2.19) and equating coefficients at various orders to zero, we obtain the corresponding disturbance equations. The zeroth order solutions come from the $0(\delta)$ and $0(\varepsilon)$ terms. They are the eigenmodes of linear parallel flow stability analysis (2.33), and consequently need no further exploration.

The equation which governs the quadratic nonlinear interaction between two linear waves, obtained at $0(\varepsilon\delta)$, is of the form

$$\mathbf{L}_{12}(\mathbf{F})_{12} = E_+\mathbf{R}_+ + E_-\mathbf{R}_- + c.c. \tag{3.4}$$

where

$$E_+ = \exp[i(\alpha_1+\alpha_2)x + (\beta_1+\beta_2)\phi]\exp(\sigma_1+\sigma_2)t \tag{3.5}$$

$$E_- = \exp[i(\alpha_1-\alpha_2)x + (\beta_1-\beta_2)\phi]\exp(\sigma_1+\tilde{\sigma}_2)t\,, \tag{3.6}$$

$\mathbf{R}_+$ and $\mathbf{R}_-$ are given in Appendix C, $\mathbf{L}_{12}$ is the linearized operator (given in Appendix A) which governs the evolution of small disturbances in a parallel base flow, the tilde denotes the complex conjugate of a quantity, and *c.c.* is the complex conjugate of the terms preceding *c.c.*.

Since $\mathbf{L}_{12}$ is a linear operator, the solution $\mathbf{F}_{12}$ consists of the superposition of the homogeneous solution and the particular solution due to the forcing function, namely the right hand side of (3.4). The homogeneous problem satisfies

$$\mathbf{L}_{12}(\mathbf{F}_{12})_{hom} = 0 \tag{3.7}$$

and the particular problem is determined from

$$\mathbf{L}_{12}(\mathbf{F}_{12})_{pat} = E_+\mathbf{R}_+ + E_-\mathbf{R}_- + c.c. \tag{3.8}$$

where the subscripts *pat* and *hom* respectively denote the particular and the homogeneous solutions of the inhomogeneous problem (3.4). Therefore, the physical variables can be written, up to order $\varepsilon\delta$, as

$$\mathbf{F} = \delta\mathbf{F}_1 + \varepsilon\mathbf{F}_2 + \varepsilon\delta[(\mathbf{F}_{12})_{hom} + (\mathbf{F}_{12})_{pat}] \tag{3.9}$$

Since the homogeneous solution $(\mathbf{F}_{12})_{hom}$ has an initial magnitude of $\varepsilon\delta$ and is described by linear eigenmode analysis, it will always continue to be smaller than $\mathbf{F}_2$ by an order δ,

and hence, can be neglected. The interactions between the two waves of the form given by (3.2) and (3.3) will produce the following four sets:

$$(\alpha_1+\alpha_2,\beta_1+\beta_2,\sigma_1+\sigma_2),\quad (-\alpha_1+\alpha_2,-\beta_1+\beta_2,\tilde{\sigma}_1+\sigma_2),$$

$$(\alpha_1-\alpha_2,\beta_1-\beta_2,\sigma_1+\tilde{\sigma}_2),\quad (-\alpha_1-\alpha_2,-\beta_1-\beta_2,\quad \tilde{\sigma}_1+\tilde{\sigma}_2) \tag{3.10}$$

As long as these four sets do not satisfy the dispersion relation (α,β,σ), a solution to (3.4) may be found, in principle, in a straightforward manner by the method of variation of parameters. In such cases, (3.4) represents an inhomogeneous equation for which a particular solution may be sought in the form

$$(\mathbf{F}_{12})_{pat} = E_+\mathbf{F}_{12}^+(r) + E_-\mathbf{F}_{12}^-(r) + c.c. \tag{3.11}$$

Equation (3.11) shows that the growth or decay of $(\mathbf{F}_{12})_{pat}$ is the same as that given by linear parallel flow analysis. Further, in order to satisfy the resonance conditions, which will be discussed momentarily, the disturbance $\mathbf{F}_2$ is required to be the most unstable wave given by parallel flow theory. This implies that, for the case where resonance conditions are not met, the $(\mathbf{F}_{12})_{pat}$ will remain smaller than $\mathbf{F}_2$ by $O(\delta)$, and it can therefore be similarly neglected.

On the other hand, when one of the four sets of α, β, and σ satisfies the dispersion relation, the operator $\mathbf{L}_{12}$, with the appropriate boundary conditions, admits nontrivial solutions which are, in fact, the linear instability modes of the base flow. This leads to the appearance of secular terms in (3.4) which results in the occurrence of resonance interactions. Accordingly, a solution is possible only if the right hand side of (3.4), which contains the resonance terms, satisfies the so-called solvability condition (or Fredholm alternative). In general, this constraint cannot be satisfied using a regular perturbation expansion. Before we proceed to consider how this constraint can be determined from a singular perturbation method, let us now explore the resonance interactions a step deeper. To do this, we consider the linearized inviscid primary disturbance equation (2.48) and its

conjugate; they are, respectively,

$$\frac{d^2p}{dr^2}+(\frac{1}{r}-\frac{2u_0'}{u_0-i\sigma/\alpha}-\frac{\rho_0'}{\rho_0})\frac{dp}{dr}+[\alpha^2(u_0-C)^2\rho_0 M_j^2-\frac{\beta^2}{r^2}-\alpha^2]p=0 \tag{3.12}$$

$$\frac{d^2\tilde{p}}{dr^2}+(\frac{1}{r}-\frac{2u_0'}{u_0+i\tilde{\sigma}/\alpha}-\frac{\rho_0'}{\rho_0})\frac{d\tilde{p}}{dr}+[\alpha^2(u_0-\tilde{C})^2\rho_0 M_j^2-\frac{\beta^2}{r^2}-\alpha^2]\tilde{p}=0 \tag{3.13}$$

where C is the complex phase velocity, $\sigma=-i\alpha C$, the primes denote differentiation with respect to r, and the tilde denotes the complex conjugate of a quantity. The complex phase velocity of an unstable mode which satisfies (3.12) and (3.13) can be expressed as

$$C(\alpha,\beta)=C_R(|\alpha|,|\beta|)+sgn(\alpha)iC_I(|\alpha|,|\beta|), \tag{3.14}$$

and the corresponding dispersion relation is

$$\sigma(\alpha,\beta)=|\alpha|C_I(|\alpha|,|\beta|)-i\alpha C_R(|\alpha|,|\beta|) \tag{3.15}$$

where $C=C_R+iC_I$, and $sgn(\alpha)$ means the sign of α. In view of (3.10), the complex equation (3.15) can be separated into two real equations — a growth rate equation and a frequency equation — which govern the resonance conditions between two unstable waves. These equations are, respectively,

$$|\alpha_1|C_I(|\alpha_1|,|\beta_1|)+|\alpha_2|C_I(|\alpha_2|,|\beta_2|)=|\alpha_2+\alpha_1|C_I(|\alpha_2+\alpha_1|,|\beta_1+\beta_2|) \tag{3.16}$$

$$\alpha_1 C_R(|\alpha_1|,|\beta_1|)+\alpha_2 C_R(|\alpha_2|,|\beta_2|)=(\alpha_2+\alpha_1)C_R(|\alpha_2+\alpha_1|,|\beta_1+\beta_2|) \tag{3.17}$$

where the α's and β's can be positive or negative, and are so far arbitrary. It may be noted that when $\beta_1=0$, the resonance conditions are valid independent of the direction to which a wave is propagating; this is because the inviscid equations (3.14) and (3.15) do not distinguish β from $-\beta$.

In order to satisfy the resonance conditions, the wavenumbers and mode numbers of two unstable waves are restricted to the following choices:

1. The fundamental mode is axisymmetric and has an axial wavenumber close to a neutral wavenumber. [i.e., $\beta_1=0$, $C_I(|\alpha_1|,0)\cong 0$].

2. The secondary disturbance, whether axisymmetric or helical, is an almost maximally amplified subharmonic wave. $[\alpha_2 \cong \alpha_1/2]$.

It may be remarked that although choices (1) and (2) are necessary, they do not guarantee resonance because when the waves are dispersive, condition (2) places a restriction on the phase velocity, C_R.

When the resonance conditions are (nearly) met, a subharmonic wave interacts effectively with the fundamental to produce an instability wave whose complex growth rate, σ, is (nearly) the same as that of the subharmonic. It is effective because resonant interactions produce secular terms which lead to a particular solution of (3.4) that grows more rapidly than the corresponding homogeneous solution by at least a factor t. Of course, the wavenumber and the mode number of the wave produced is always the sum of the wavenumbers and mode numbers of the two interacting waves. Consequently, an axisymmetric subharmonic which interacts with its fundamental will reproduce itself. On the other hand, a helical subharmonic mode which interacts with the fundamental will not reproduce itself but will produce a mode that propagates at an equal but opposite angle to the x-direction. For example, an axisymmetric mode with the wavenumber 2α and the mode number 0 — denoted by $(2\alpha, 0)$ — interacts with a helical mode $(-\alpha, \beta)$ to excite a mode (α, β). Similarly, the mode $(2\alpha, 0)$ interacts with mode $(-\alpha, -\beta)$ results in the mode $(\alpha, -\beta)$. Therefore, an interaction between mode $(2\alpha, 0)$ with modes $(-\alpha, \pm\beta)$ results in modes $(\alpha, \pm\beta)$. Because a helical mode which interacts with the fundamental mode does not reproduce itself, it is necessary to consider the secondary disturbance to be comprised of a pair of helical waves spinning at an equal but opposite direction to the x-axis. Consequently, if a non-axisymmetric subharmonic is involved, we need to assume that the secondary disturbance is of the form

$$\mathbf{F}_2 = \mathbf{F}_{2r} + \mathbf{F}_{2l} + c.c. \tag{3.18}$$

where

$$\mathbf{F}_{2r} = \mathbf{f}_{2r}(r) \exp i(\alpha_2 x + \beta_2 \phi) \exp \sigma_{2r} t + c.c. \tag{3.19}$$

$$\mathbf{F}_{2l} = \mathbf{f}_{2l}(r) \exp i(-\alpha_2 x + \beta_2 \phi) \exp \sigma_{2l} t + c.c., \tag{3.20}$$

where the subscripts r and l denote a helical wave propagating in the direction of positive and negative ϕ, respectively; for clarity, we call these waves right and left spinning (or propagating) waves, respectively. Since the terms involving the product of ϵ are truncated in the expansion (3.1), the left and right spinning waves of $\mathbf{F_2}$ do not interact with each other. Each will, however, independently interact with the primary wave $\mathbf{F_1}$. For example, $\mathbf{F}_{2l}$ interacts with $\mathbf{F_1}$, producing $\mathbf{F}_{2r}$, and $\mathbf{F}_{2r}$ interacts with $\mathbf{F_1}$, producing $\mathbf{F}_{2l}$. Consequently, $\mathbf{F_2}$ is again reproduced. Furthermore, since both the mean flow and the axisymmetric $\mathbf{F_1}$ are independent of the azimuthal angle, we can assume that the growth rate of the right and left spinning waves, as a result of resonant interactions between $\mathbf{F_2}$ (given by 3.18) and an axisymmetric primary wave, are modified exactly the same. In other words, there is no physical preference for the growth rates between the left and the right spinning waves. In fact, a second approach — which will be discussed in section 3.5 — shows that the growth rates of $\mathbf{F}_{2r}$ and $\mathbf{F}_{2l}$ in a frame of reference that moves with the phase velocity of $\mathbf{F_1}$ are indeed the same.

When the resonance conditions are met, the subharmonic disturbance interacts strongly with the fundamental to reproduce itself and therefore to increase its growth rate. The modified subharmonic growth rate, as a result of resonant wave interactions, will be accommodated by a set of slow scales.

We now proceed to obtain the governing equation for the modified growth rate using the method of multiple scales. The method of multiple scales is discussed in several books [e.g., Nayfeh 1973]. Accordingly, we can write

$$\mathbf{F} = \delta \mathbf{F_1} + \epsilon \mathbf{F_2} + \epsilon\delta \mathbf{F_{12}} + 0(\delta^2), \quad 0 < \epsilon \ll \delta \ll 1 \tag{3.21}$$

where

$$\mathbf{F}_1 = \mathbf{F}_1(x, t, \phi, r) \tag{3.22}$$

$$\mathbf{F}_2 = \mathbf{F}_2(x, x_1, t, t_1, \phi, \phi_1, r) \tag{3.23}$$

$$\mathbf{F}_{12} = \mathbf{F}_{12}(x, x_1, t, t_1, \phi, \phi_1, r) \tag{3.24}$$

and $t_1 = \delta t, \phi_1 = \delta\phi, x_1 = \delta x$ are the slow scales of time, azimuthal angle, and axial direction, respectively. It may be remarked that although this set of slow scales eliminates the nonuniformity caused by the secular terms in equation (3.4), it does not determine a uniform zeroth order expansion. This is because the amplitudes of the mean flow and the fundamental wave are assumed to remain unchanged with time, while the subharmonic wave, chosen from the resonance conditions, is strongly amplified. The series expansion (3.21) becomes disordered whenever the total magnitude of the growing subharmonic exceeds the preceding term; uniform validity only holds, at most, on a time scale δ^{-1}. This set of slow scales is compatible with (3.21) where the δ^2 term which arises from the third order interactions (i.e., $\delta^2\varepsilon$) is truncated. It is used to examine the influence of the fundamental wave on its subharmonic to linear order in terms of the amplitude δ. In the following equation (3.27), we shall assume that the shape of the primary subharmonic is unaltered by the appearance of the fundamental. This assumption is more fully justified by the second approach, to be discussed in the next section, which allows the shape of the subharmonic in the presence of its fundamental to be determined.

Since the physical variable $\mathbf{F}$ is a function of fast and slow scales, the partial derivatives in t, x, and ϕ become

$$\begin{aligned} \frac{\partial}{\partial t} &\to \frac{\partial}{\partial t} + \delta\frac{\partial}{\partial t_1} \\ \frac{\partial}{\partial x} &\to \frac{\partial}{\partial x} + \delta\frac{\partial}{\partial x_1} \\ \frac{\partial}{\partial \phi} &\to \frac{\partial}{\partial \phi} + \delta\frac{\partial}{\partial \phi_1}. \end{aligned} \tag{3.25}$$

As in the parallel flow analysis, we assume the normal mode concept and write

$$\mathbf{F}_1 = \mathbf{f}_1(r)E_1 + c.c. \tag{3.26}$$

$$\mathbf{F}_2 = B(x_1, t_1, \phi_1)\mathbf{f}_2(r)E_2 + c.c. \tag{3.27}$$

where

$$E_1 = \exp i(\alpha_1 x + \beta_1 \phi) \exp \sigma_1 t$$

$$E_2 = \exp i(\alpha_2 x + \beta_2 \phi) \exp \sigma_2 t$$

and c.c. denotes complex conjugate of the preceding terms. It should be noted that in (3.27), we have omitted the left propagating helical component — with the understanding that the left propagating helical wave which interacts with an axisymmetric primary wave produces and, therefore, enhances the growth of a right propagating helical wave; similarly, the left propagating helical wave can be reproduced through the interaction between a right propagating helical wave and an axisymmetric wave.

The amplitude function B is slowly varying in space and time, and will be determined at $0(\varepsilon\delta)$ by means of a solvability condition; the mode shape $\mathbf{f}_2$ is that given by the parallel flow theory.

It is now perfectly clear from equation (3.27) how the growth rate of the subharmonic is modified. Because of the departure of the growth rate of $\mathbf{F}_2$ from the parallel flow analysis, a set of slow scales is needed to reflect this change. For example, the slow scale δx implies a long length scale of $O(R^*/\delta)$, in addition to the usual length scale R^*. This means that as long as the evolution of the subharmonic is on a length scale that is much smaller than $O(R^*/\delta)$, its local growth is given by parallel flow theory. However, if the growth of the disturbance is on a distance that is comparable to $O(R^*/\delta)$, the change in the amplitude function B will then be of the same order as that provided by the parallel flow analysis. In temporal theory, it is clear that this change, which may be interpreted as an additional

(positive or negative) growth rate for the disturbance, is physically meaningful only over a time scale that is of $O(1)$.

3.3 Amplitude Equation

We now proceed to derive the amplitude equation of the subharmonic disturbance when the resonance conditions are met. The amplitude equation will be derived using two independent methods: the first is based on an "improved" inviscid analysis and the second is based on a viscous theory. These derived amplitude equations will be called an inviscid amplitude equation and a viscous amplitude equation, respectively. Here, the word "improved" signifies that the primary instability modes are actually obtained from viscous considerations. The inviscid amplitude equation is derived from a single ODE, while the viscous counterpart is based on a system of ODE's. Since the wavenumber of a subharmonic wave is near a maximally amplified wavenumber, the growth rate of the subharmonic obtained from an inviscid analysis will provide a good approximation to that obtained from a fully viscous analysis. We now proceed to derive the inviscid amplitude equation, while the viscous amplitude equation is given in Appendix D.

For the particular case where the product of $\mathbf{F}_1$ and $\mathbf{F}_2$ reinforces $\mathbf{F}_2$, the disturbance, $\mathbf{F}_{12}$, can assume the form:

$$\mathbf{F}_{12} = \mathbf{f}_{12}(x_1, t_1, \phi_1, r)E_2 + c.c. + \cdots \tag{3.28}$$

where

$$\mathbf{f}_{12} = (u_{12}, v_{12}, w_{12}, p_{12}, \rho_{12})^T,$$

$$E_2 = \exp i(\alpha_2 x + \beta_2 \phi) \exp \sigma_2 t$$

and the dots stand for the non-resonating terms that are unimportant.

We note that the linearized primary disturbance equations for an inviscid compressible jet at $O(\varepsilon\delta)$ can be manipulated to a single pressure perturbation $p_{12}(r)$ of the form

$$L(p_{12}) = \frac{d^2p_{12}}{dr^2} + \left[\frac{1}{r} - \frac{2u_0'}{u_0 - C_2} - \frac{\rho_0'}{\rho_0}\right]\frac{dp_{12}}{dr} + \left[\alpha_2^2(u_0 - C_2)^2\rho_0 M_j^2 - \frac{\beta_2^2}{r^2} - \alpha_2^2\right]p_{12} = rhs \tag{3.29}$$

where

$$rhs = h_1\frac{\partial B}{\partial t_1} + h_2\frac{\partial B}{\partial x_1} + h_3\frac{\partial B}{\partial \phi_1} + h_{12}\tilde{B} \tag{3.30}$$

$$h_1 = -i\alpha_2\rho_0 u_2 - [\frac{1}{r} - \frac{2u_0'}{u_0 - C_2} - \frac{\rho_0'}{\rho_0} + \frac{d}{dr}](\rho_0 v_2) - i\beta_2\rho_0 w_2/r + i\alpha_2(u_0 - C_2)\rho_0 M_j^2 p_2$$

$$h_2 = -i\alpha_2\rho_0 u_0 u_2 - [\frac{1}{r} - \frac{2u_0'}{u_0 - C} - \frac{\rho_0'}{\rho_0} + \frac{d}{dr}](u_0\rho_0 v_2) - i\beta_2\rho_0 u_0 w_2/r$$
$$+i\alpha_2(u_0 - C_2)\rho_0 M_j^2(u_0 p_2 + \gamma p_0 u_2)$$

$$h_3 = i\alpha(u_0 - C_2)\rho_0(w_2/r + M_j^2 r p_2)$$

$$h_{12} = i\alpha_2\hat{F}_{u-} + [\frac{1}{r} - \frac{2u_0'}{u_0 - C_2} - \frac{\rho_0'}{\rho_0} + \frac{d}{dr}]\hat{F}_{v-} + i\beta_2\hat{F}_{w-}/r - i\alpha_2(u_0 - C_2)\rho_0 M_j^2\hat{F}_{p-}$$

In the above equations, the tilde denotes the complex conjugate of a quantity, the prime denotes a differentiation with respect to r, C_2 is the complex phase velocity of the subharmonic mode, while $\hat{F}_{u-}$, $\hat{F}_{v-}$, $\hat{F}_{w-}$ and $\hat{F}_{p-}$ are given in Appendix E. Note that although (3.30) is derived based on an inviscid analysis, its coefficients, $h's$, are evaluated using viscous parallel flow instability theory. Further, h_{12} represents the particular set of the interaction terms between $\mathbf{F_1}$ and $\mathbf{F_2}$ that give rise to a subharmonic disturbance, while h_1, h_2, and h_3 come from the dependence of $\mathbf{F_2}$ on the slow scales.

We multiply (3.29) by $r/\{\rho_0(u_0 - C_2)^2\}$ to make it self-adjoint. The equation in the self-adjoint form becomes

$$\mathcal{L}(p_{12}) = \frac{r}{\rho_0}(u_0 - C_2)^2 L(p_{12}) = rhs\left\{\frac{r}{\rho_0}(u_0 - C_2)^2\right\} \tag{3.31}$$

In order for (3.31) to possess a nontrivial solution, its right hand side must be orthogonal to all $\grave{z}$'s such that $\grave{\mathcal{L}}\grave{z} = 0$ where $\grave{\mathcal{L}}$ is the adjoint operator and $\grave{z}$ is the adjoint solution. The orthogonality requirement, or solvability condition, is necessary and sufficient for the existence of solutions at order $\delta\epsilon$. We note that since the operator $\mathcal{L}$ is self-adjoint [i.e, $\grave{\mathcal{L}}$ = $\mathcal{L}$] and the boundary conditions on $\grave{z}$ are the same as those of the homogeneous solution [i.e., $\mathcal{L}(p_{12}) = 0$], the adjoint solutions are identical with the homogeneous solution.

The orthogonality requirement becomes

$$q_1\frac{\partial B}{\partial t_1} + q_2\frac{\partial B}{\partial x_1} + q_3\frac{\partial B}{\partial \phi_1} + q_4\tilde{B} = 0. \tag{3.32}$$

where

$$q_1 = \int_0^\infty p_2\frac{r}{\rho_0(u_0 - C_2)^2}\{i\alpha_2\rho_0 u_2 + (\frac{1}{r} - \frac{2u_0'}{u_0 - C} - \frac{\rho_0'}{\rho_0})\rho_0 v_2$$
$$+i\beta_2\rho_0 w_2/r - i\alpha_2(u_0 - C_2)\rho_0 M_j^2 p_2\} - (\frac{p_2 r}{\rho_0(u_0 - C_2)^2})'\rho_0 v_2 dr$$

$$q_4 = \int_0^\infty p_2\frac{r}{\rho_0(u_0 - C_2)^2}\{i\alpha_2\hat{F}_{u-} + (\frac{1}{r} - \frac{2u_0'}{u_0 - C_2} - \frac{\rho_0'}{\rho_0})\hat{F}_{v-}$$

$$+i\beta_2\hat{F}_{w-}/r - i\alpha_2(u_0 - C_2)\rho_0 M_j^2\hat{F}_{p-}\} - (\frac{p_2 r}{\rho_0(u_0 - C_2)^2})'\hat{F}_{v-}dr,$$

where the $(\cdot)'$ denotes a differentiation of its argument with respect to r, and q_4 contains the quadratic resonant wave interactions. Here q_2 and q_3 are included to allow the resonance to be manifested spatially. Their explicit expressions are not given here because this thesis focuses only on temporally growing waves. The integrands in the q's are evaluated from linear, viscous, parallel flow instability analysis. It may be noted that if we include the $\mathbf{F}_{11}$ term in the series expansion (3.21), an amplitude equation for the modified growth rate of the fundamental can similarly be obtained at order δ^2 (see Monkewitz 1988). This modified growth rate, which will be coupled into equation (3.32), provides a relationship for the mutual feedback between the subharmonic and the fundamental. In

accordance with our previous discussion, we shall not obtain the amplitude equation for the primary wave because this amplitude is assumed to be a constant. The constant amplitude A assumes a catalytic role in the enhancement of the growth rate of an infinitesimally small subharmonic secondary disturbance. Therefore, we called our instability analysis a linear "secondary" instability analysis instead of a "weakly" nonlinear analysis for two interacting waves.

The equation (3.32) together with its complex conjugate yields

$$|q_1|^2\frac{\partial^2}{\partial t_1^2}+|q_2|^2\frac{\partial^2}{\partial x_1^2}+|q_3|^2\frac{\partial^2}{\partial \phi_1^2}+$$

$$\text{Real}[2\tilde{q}_1 q_2\frac{\partial^2}{\partial t_1\partial x_1}+2\tilde{q}_1 q_3\frac{\partial^2}{\partial t_1\partial \phi_1}+2\tilde{q}_2 q_3\frac{\partial^2}{\partial x_1\partial \phi_1}]B=|q_4|^2 B \tag{3.33}$$

where the tilde stands for the complex conjugate of a quantity. The above equation is valid for temporal or spatial analysis because the amplitude B is a function of spatial and temporal variables. Since the coefficients in (3.33) are independent of the slow scales, we can write

$$B\sim\exp(\lambda_1 x_1+\lambda_2 t_1+\lambda_3\phi_1) \tag{3.34}$$

and substituting the above into (3.33) yields

$$|q_1|^2\lambda_1^2+|q_2|^2\lambda_2^2+|q_3|^2\lambda_3^2+(2\tilde{q}_1 q_2)_R\lambda_1\lambda_2+(2\tilde{q}_1 q_3)_R\lambda_2\lambda_3+(2\tilde{q}_2 q_3)_R\lambda_1\lambda_3=|q_4|^2 \tag{3.35}$$

The λ's are in general complex and $(\ \cdot\ )_R$ denotes the real part of a complex number. Each real part of $\lambda_1,\lambda_2,\lambda_3$ modifies the streamwise, temporal and azimuthal growth rate, respectively. Similarly, each imaginary part of λ's modifies its corresponding frequency (or wavenumber). Running parallel to Kelly's investigation of the mixing layer, our investigation is based on a disturbance of a fixed spatial wavenumber growing in time. Therefore, λ_1 and λ_3 are zero, while λ_2 is real. (3.35) can therefore be simplified to

$$\lambda_2=\pm\frac{|q_4|}{|q_1|}. \tag{3.36}$$

The secondary subharmonic disturbance can be expressed in terms of the original time variable as

$$\mathbf{F_2} = \mathbf{f_2} \exp i(\alpha_2 x + \beta_2 \phi) \exp(\sigma_2 + \lambda_2 \delta)t \tag{3.37}$$

The dependence of this growth rate as a function of various jet parameters is discussed in Chapter 6. Clearly, the growth rate of the subharmonic wave is changed by $\lambda_2 \delta$ due to parametric resonance.

3.4 Normal Mode Analysis

Our previous approach models the secondary instabilities of a round jet, which results in vortex pairing, by a perturbation analysis of two instability waves, $\mathbf{F_1}$ and $\mathbf{F_2}$, of different wave vectors undergoing interactions. When their product reproduces with $\mathbf{F_2}$, the growth rate of $\mathbf{F_2}$ is modified. While this model provides the physics of resonant interactions, it has at least three shortcomings.

1. The *finite amplitude* of the fundamental wave is regarded as a small perturbation parameter. Therefore the perturbation theory, can provide an accurate solution only for those values of δ for which the perturbation series is an accurate representation of the exact solution. As usual, the region of validity of an asymptotic analysis is not known a priori, and remains to be determined from a more complete analysis.

2. There is no mechanism for the determination of the threshold amplitude of the fundamental where the phase-locking with the subharmonic occurs. It is now known that this phase-locking is a mechanism for the onset of secondary instability.

3. As previously mentioned, this perturbation approach fails to determine the correction to the shape of a secondary subharmonic mode; it only provides information on its

growth rate.

These shortcomings can be circumvented by an alternative approach developed by Herbert (1983). He pioneered the development of the normal mode analysis of the secondary instability arising from the presence of TS waves in plane channel flows. His theory predicts with reasonable accuracy the growth rate of a 3-d secondary disturbance up to the stages prior to laminar breakdown and transition. In his subsequent analysis of the (linear) secondary instability of flat plate boundary layers, he has shown that this model is capable of explaining all the essential flow physics of staggered lambda vortex formation (1984) and peak-valley splitting (1985) in Blasius flows.

Motivated by Herbert's success, we will adapt his approach to subsonic heated round jets. In this approach, a sufficiently small disturbance $\mathbf{F}_2$ is superimposed on a periodic base flow consisting of the steady unidirectional mean flow $\mathbf{F}_0$ and a finite amplitude axisymmetric primary fundamental wave $\mathbf{F}_1$. We assume that the mean flow as well as the shape of $\mathbf{F}_1$ is minimally affected by the nonlinear self-interactions of $\mathbf{F}_1$. The choice of an axisymmetric wave is based on the resonance conditions established previously. Using a frame of reference moving downstream with the phase velocity of $\mathbf{F}_1$, it is appropriate to decompose the perturbation vector field $\mathbf{F}$ as

$$\mathbf{F}(x,r,\phi,t) = A\mathbf{F}_1(x,r) + \varepsilon\mathbf{F}_2(x,r,\phi,t) \tag{3.38}$$

where

$$\mathbf{F}_1 = \mathbf{f}_1(r)e^{i\alpha x} + c.c. \quad , \tag{3.39}$$

A, as discussed earlier, is assumed to be a constant, and x now refers to the streamwise coordinate of the moving frame of reference. In (3.38), A is usually small but finite (say, $A \cong 0.1$), not a perturbation parameter, while ϵ is assumed to be sufficiently small to allow linearization about a steady and spatially periodic base flow. Of course, the range of ϵ for which linear theory is valid remains to be determined by comparing it with future work,

say, direct numerical simulations. The finite value of A will remove the usual accuracy issue associated with an asymptotic analysis. Further, since the amplitude A has a physical meaning provided the eigenfunction $\mathbf{f}_1$ is suitably normalized, we choose, for convenience,

$$\max_{0\leq r\leq\infty} |u_1(r)| = 1/2 \tag{3.40}$$

so that A is the maximum magnitude of the streamwise velocity perturbation. This normalization, which is also used in our multiple scales approach, is not unique and is rather subjective because $\mathbf{f}_1$ is an eigenfunction. Herbert normalized A so that it is the maximum rms value of the streamwise velocity fluctuation. The magnitudes of eigenfunctions of Cohen (1986) are normalized such that the experimental and theoretical profiles have identical areas. At this point, it is important to note that this secondary instability analysis is still linear, as is the classical instability analysis. In the latter, the flow is linearized about a locally parallel flow. The coefficients in the resultant equations depend solely on r since the (x, ϕ) and t dependences of the (primary) disturbance are trivially extracted by Fourier-Laplace transforms. This leads to the mode shape $\mathbf{f}_1(r)$. In the present (secondary instability) analysis, linearization is made about a flow which is periodic in the streamwise coordinate x. This streamwise periodic flow becomes independent of time in a reference frame that moves with the phase velocity of the fundamental wave, and is independent of ϕ since $\mathbf{F}_1$ is axisymmetric. Therefore, the ϕ and t dependence of the secondary disturbance can again be extracted by Fourier - Laplace transforms, but the x dependence requires a more careful consideration and additional assumptions, to be discussed shortly. We can now apply the normal mode analysis in ϕ and t and write

$$\mathbf{F}_2 = \hat{\mathbf{f}}_2(x, r) e^{i\beta_2\phi} e^{\hat{\sigma}_2 t} + c.c.\,, \tag{3.41}$$

where $\hat{\sigma}_2$ is the complex growth rate, and β_2 is the azimuthal mode number. After substituting (3.38), (3.39) and (3.41) into the governing equations (2.17) - (2.19), and neglecting quadratic and higher order terms in ϵ, we obtain a system of linear partial differential equa-

tions which govern the instability of the linearized secondary disturbance, $\mathbf{F}_2$. Apart from a complicated r dependence and numerous other terms, these equations are essentially of the classical Mathieu type because the coefficients are (streamwise) periodic. It is known that, according to Floquet theory of linear periodic differential equations, a Mathieu equation whose coefficients are π-periodic has two important classes of Floquet solutions: a π-periodic and a 2π-periodic function. With guidance from Floquet theory (Ince, 1956), we can therefore express the secondary disturbance in the Floquet form as

$$\hat{\mathbf{f}}_2(x,r) \rightarrow e^{\partial_x x}\breve{\mathbf{f}}_2(x,r) \tag{3.42}$$

where σ_x is the characteristic exponent and $\breve{\mathbf{f}}_2$ is periodic in x. The solutions with period λ_1 — where λ_1 is the wavelength of the primary wave — are called the primary (fundamental) resonance, while the solutions with period $2\lambda_1$ are known as the principal parametric (subharmonic) resonance. The instability modes which arise from these resonances can, in general, be expressed in terms of Fourier series as

$$\breve{\mathbf{f}}_2 = \sum_{j=-\infty}^{\infty} \mathbf{f}_{2,j}(r)e^{ij\alpha_1 x/2} \tag{3.43}$$

The fundamental modes are the harmonic series whose period is the same as the streamwise wavelength of the primary wave and are given by j = even. The subharmonic modes have odd j, and therefore, constitute a subharmonic series whose basic wavelength is twice that of the primary wave. The fundamental and subharmonic modes are completely uncoupled since the wavelength of the basic flow is different from the basic wavelength of the subharmonic series. In this work, we shall investigate only the parametric resonance case.

We now digress briefly to present some known results in incompressible boundary layer flows. The fundamental modes produce the peak-valley splitting of the lambda-shaped vortical structures, while the subharmonic modes cause the staggered formation of lambda vortices. By approximating the Fourier series (3.43) to consist of merely two oblique waves

propagating at equal and opposite angles to the x direction, Herbert (1984) has shown that these two oblique subharmonic modes, which provide a reasonably accurate approximation to the streamwise structure of the subharmonic disturbance, are sufficient to give rise to the formation of staggered lambda vortices.

We return to equation (3.43). Its substitution into the linearized disturbance equations yields an infinite set of ODE's for the complex growth rate $\hat{\sigma}_2$ and the mode shape $\mathbf{f}_{2,j}$. Numerically, the streamwise structure of the secondary disturbance is expanded in terms of a finite Fourier modes whose stability is governed by a system of N_a ODE's — where N_a is 5 times the number of Fourier modes used. Numerically, these (stability) equations are approximated by a complex algebraic eigenvalue problem whose computation requires $O(N_b^2)$ storage and $O(N_b^3)$ operations (see Chapter 4) — where N_b equals N_a times the number of grid points in the computation domain. In order to be practical in the numerical evaluation of the secondary stability problem and in order to make a direct comparison with the previous perturbation approach, simplification of equation (3.43) is deemed desirable. The justification of this simplification will now be discussed.

In controlled jet experiments, a primary instability wave, which is often generated by an acoustic source or through vibrating ribbons, produces a vortex structure that is responsible, at least partially, for the mixing and spreading of jet shear layers. In order to control the global spreading rate via the manipulation of this vortex structure, a discrete subharmonic disturbance can be excited simultaneously with the primary (or fundamental) frequency. In accordance with our discussion in section 3.3, when the subharmonic disturbance is axisymmetric, it is assumed to be a subharmonic wave; when the subharmonic is helical, it is comprised of a pair of helical waves whose propagation angles are equal but opposite with respect to the mean flow direction. As dictated by the resonance conditions, these excited discrete modes are sufficient to promote a strong growth of a subharmonic disturbance. In order to compare the two approaches, we assume that the (secondary) subharmonic growth rate is minimally affected by the unexcited higher

terms in the subharmonic series. In other words, we assume that the (two) Fourier modes ($\alpha_1/2$ and $-\alpha_1/2$) are reasonably sufficient to represent the the streamwise structure of the subharmonic disturbance.

With the preceding assumptions, we can approximate the subharmonic disturbance by

$$\mathbf{F}_2 = e^{\delta_x x} e^{\delta_2 t} e^{i\beta_2 \phi} (\mathbf{f}_{2,1} e^{i\alpha_1/2} + \mathbf{f}_{2,-1} e^{-i\alpha_1/2}) + c.c., \tag{3.44}$$

where

$$\mathbf{f}_{2,1} = (u_{2,1}, v_{2,1}, w_{2,1}, p_{2,1}, \rho_{2,1}),$$

and,

$$\mathbf{f}_{2,-1} = (u_{2,-1}, v_{2,-1}, w_{2,-1}, p_{2,-1}, \rho_{2,-1})$$

As in primary stability analysis, we employ temporal theory, which implies that $\hat{\sigma}_x = 0$ and $\hat{\sigma}_2 \neq 0$ is the complex eigenvalue to be solved. Thus, in a temporal theory, we can write

$$\mathbf{F}_2 = e^{\delta_2 t} e^{i\beta_2 \phi} (\mathbf{f}_{2,1} e^{i\alpha_1/2} + \mathbf{f}_{2,-1} e^{-i\alpha_1/2}) + c.c. \tag{3.45}$$

Note that in the moving frame of reference, (3.45) shows that the complex growth rates $\hat{\sigma}_2$ of a pair of helical modes, whose propagation angles (with respect to the x-axis) are equal and opposite, are exactly the same.

To recall, a main result of the multiple scales analysis is that the secondary disturbance can interact with its fundamental to produce a wave whose wavenumber and frequency are the same as the disturbance itself and can therefore reinforce it. Since such a destabilization of the subharmonic requires the matching of its phase velocity with the fundamental, our calculations focus on the particular case where the subharmonic becomes phase-locked with the fundamental and $\hat{\sigma}_2$ becomes purely real. The modal representation of $\mathbf{F}_2$, given by (3.45), will transform the linearized secondary disturbance equations from a system of partial differential equations into a system of ODE's. These ODE's are obtained after substituting (3.38), (3.39) and (3.45) into (2.17) - (2.19), and by neglecting quadratic and

higher order terms in ϵ. The resulting equations become

$$(\boldsymbol{\Delta}_0 + A\boldsymbol{\Delta}_1 + A^2\boldsymbol{\Delta}_2 + A^3\boldsymbol{\Delta}_3)\mathbf{g} = \hat{\sigma}_2\hat{\mathbf{B}}\mathbf{g} \tag{3.46}$$

where

$$\mathbf{g} = (u_{2,1}, u_{2,-1}, v_{2,1}, v_{2,-1}, w_{2,1}, w_{2,-1}, p_{2,1}, p_{2,-1}, \rho_{2,1}, \rho_{2,-1})^T \tag{3.47}$$

Recall that when the secondary disturbance is axisymmetric, we need only to consider one subharmonic wave. In this case, $\mathbf{f}_{2,-1} = \tilde{\mathbf{f}}_{2,1}$ where tilde is the complex conjugate of a quantity. In (3.46) the precise elements of $\boldsymbol{\Delta}_0$, $\boldsymbol{\Delta}_1$ and $\hat{\mathbf{B}}$ can be extracted from Appendix F, the A^2 term arises from the cubic interaction, $A^2\epsilon$, while the A^3 term originates from the quartic interaction, $A^3\epsilon$. The quartic term stems from the $\nabla^2(p/\rho)$ term of the energy equation; of course, this term would have disappeared if the temperature had been used as a dependent variable. Note that for incompressible and unheated flows, $\boldsymbol{\Delta}_2$ and $\boldsymbol{\Delta}_3$ do not exist because the nonlinearity in the governing equations is quadratic. Further, since our representation of the flow arising from the finite-amplitude saturation of the primary wave is approximated only to order A (see Chapter 6), we ignored, for consistency, the A^2 and A^3 terms. Hence, the secondary disturbance equations become

$$(\boldsymbol{\Delta}_0 + A\boldsymbol{\Delta}_1)\mathbf{g} = \hat{\sigma}_2\hat{\mathbf{B}}\mathbf{g} \tag{3.48}$$

We should recognize that when $A \neq 0$ in (3.48), the parallel jet mean flow is slightly distorted by the presence of the fundamental mode. This leads to a modified growth rate of the subharmonic from that obtained through a parallel flow analysis.

At this point, it is crucial to realize that the difference between our two different approaches lies in the treatment of the terms representing the interactions between two waves. When using the normal mode approach, the interaction terms appear explicitly as the coefficients in the disturbance equations (3.48). In contrast, these terms, when using the method of multiple scales, appear as inhomogeneous terms in the equation (3.4).

The boundary conditions at $r = 0$ and $r = \infty$ for the secondary disturbances are identical with those of the primary stability analysis. The system of ODE's (3.48) together with the appropriate boundary conditions constitute an eigenvalue problem that yields, for a given mean flow and primary eigenmodes, a dispersion relation of the form

$$\hat{\sigma}_2 = \hat{\sigma}_2(\alpha_2, \beta_2) \tag{3.49}$$

The evaluation of the eigenvalues and their corresponding eigenfunctions is described in Chapter 4, and the secondary instability results are discussed in Chapter 6.

Chapter 4

NUMERICAL METHODS

This section deals with the numerical formulation of the eigenvalue problem which arises from the analysis of the stability of subsonic round jets. The primary stability problem can be cast in a system of 5 coupled ODE (2.33), while the normal mode analysis of the secondary (subharmonic) instability problem is approximated by a system of 10 coupled ODE (3.48). The numerical solution of these systems of equations is obtained by a spectral collocation method with Chebyshev polynomials, and the primary instability problem is checked by a finite difference method. For both methods, a function, say $f(z)$, is approximated by a discrete set of values of $f(z)$ on a set of nodal points z_i. The discrete pointwise approximation of the function $f(z)$ will eventually convert a linear differential equation into a system of algebraic equations which can be solved by several techniques. We begin by outlining an application of spectral method to the instabilities of shear layer generated from a jet emanating from an axisymmetric nozzle.

4.1 Spectral Method

The spectral method has now been successfully implemented in many types of hydrodynamic stability problems such as boundary layers, wakes and mixing layers. A detailed and extensive discussion of the theory and application of spectral methods, particularly with regard to fluid dynamic problems, can be found in the monograph of Canuto,

Hussaini, Quarteroni, and Zang (1987). The starting point of a spectral method is to expand a function $u = u(z)$ in an infinite complete set of orthogonal functions of the form

$$u(z) = \sum_{k=0}^{\infty} a_k T_k(z) \tag{4.1}$$

where the $T_k(z)$ are the known basis functions and the coefficients a_k $(k = 0, 1, \cdots)$ are called the spectrum of $u(z)$. Numerically, the function $u(z)$ is expanded in terms of a truncated set of the basis functions T_k. For example,

$$u \approx u_N(z) = \sum_{k=0}^{N} a_k T_k(z) \tag{4.2}$$

where $u_N(z)$ is an approximation to $u(z)$ for each $N \geq 0$. For a smooth function with periodic boundary conditions, the natural choice of the basis functions is sines and cosines. This leads to the usual Fourier series and its finite version. On the other hand, for non periodic boundary conditions, the most widely used basis functions are the Chebyshev polynomials. In any expansion, the task is either to find the set of values of u at the nodal grids through an appropriate interpolation or the spectral coefficients a_k $(k = 0, 1, \cdots N)$. Intuitively, when the number of grid points is sufficiently large, they are equivalent to each other.

The Chebyshev polynomial of degree k, $T_k(z)$, is defined by

$$T_k(z) = \cos(k \cos^{-1} z) \quad -1 \leq z \leq 1. \tag{4.3}$$

Therefore, $T_0 = 1$, $T_1 = z$, and the higher polynomials can be generated by the recursion relation,

$$2zT_k = T_{k+1}(z) + T_{k-1}(z), \quad k \geq 1 \tag{4.4}$$

Details of various identities, orthogonal properties, and numerical quadratures can be found in the book by Gottlieb and Orszag (1977). The Chebyshev polynomials are even for even k and odd for odd k, as illustrated in Figures (4.1a) and (4.1b). They are the

solutions of the Sturm-Liouville differential equation

$$\sqrt{1-z^2}\frac{d}{dz}\left(\sqrt{1-z^2}\right)\frac{dT_k}{dz}+k^2T_k=0 \tag{4.5}$$

which are bounded at $z=-1$ and $z=1$.

It is known that if a smooth function is expressed in terms of the eigenfunctions of a suitable Sturm-Liouville problem, "spectral accuracy" is obtained. This means that the spectrum a_k, according to this basis function, decays more rapidly than any power of k. To be more specific, the Fourier cosine series for an even function $f(x)$ is used for illustration. The appropriate expansion is

$$f(x)=\sum_{k=0}^{\infty}a_k\cos(kx) \qquad 0\le x\le\pi \tag{4.6}$$

where

$$a_k=\frac{2}{\pi}\int_0^{\pi}f(x)\cos(kx)dx, \qquad k=0,1,2,\cdots \tag{4.7}$$

If a periodic function $f(x)$ has $\mathcal{M}-1$ continuous derivatives, and the $\mathcal{M}^{th}$ derivative is integrable, then, after integrating (4.7) by parts $(\mathcal{M}-1)$ times, we find that

$$a_k=\frac{2}{\pi k^{(\mathcal{M})}}\int_0^{\pi}f^{(\mathcal{M})}(x)\cos(\chi\pi/2-kx)dx \tag{4.8}$$

where $\chi=1$ when $\mathcal{M}$ is even and 0 otherwise, and the $f^{(\mathcal{M})}$ is the $\mathcal{M}$-th derivative of f. It is worth noting that the integral in equation (4.8) is bounded by some constant which is independent of k but may depend on $\mathcal{M}$. Therefore, the truncation error, say e, using the $\mathcal{N}+1$ modes to represent an infinitely smooth function by (4.2) can be estimated to be

$$|e|<\frac{constant(\mathcal{M})}{\mathcal{N}^{\mathcal{M}}}, \quad for\ any\ \mathcal{M} \tag{4.9}$$

This is because each of the coefficients a_k [for $k\ge\mathcal{N}$] satisfies (4.8) and the neglected series expansion for f,

$$\sum_{k=\mathcal{N}}^{\infty}a_k\cos(kx),$$

will be of the order given by the right hand side of (4.9). [More precise error estimates for the eigenfunction expansion in terms of Chebyshev polynomials is discussed in Canuto et al]. It may be remarked that a finite difference method with N grid points usually has an error estimate of N^{-p} where p is the order of the accuracy of a particular scheme used; for example, a second order method has $p = 2$. Thus, if a function is infinitely smooth, then, according to (4.8), the spectrum a_k decays faster than any finite power of k, or, simply, it decays "spectrally". An important consequence of this spectral accuracy is that accurate numerical results can be obtained by using relatively "few" grid points, and it is precisely this accuracy that makes spectral methods an emerging powerful computational tool.

Further, after making the substitution $z = \cos(x)$ into (4.5), we find that

$$\frac{d^2T_k}{dx^2} + k^2T_k = 0 \tag{4.10}$$

so that the Chebyshev polynomials are the usual trigonometric functions of the argument $kx = k\cos^{-1} z$. From (4.3) and (4.6), we obtain

$$f(x) = \sum_{k=0}^{\infty} a_k T_k(z), \tag{4.11}$$

where $x = \cos^{-1}(z)$. Therefore, according to equations (4.11) and (4.1), the Chebyshev series has the same convergence properties as the Fourier cosine series, since the former is really the latter in disguise.

If we expand an arbitrary function u in $(N + 1)$ Chebyshev polynomials, (4.2) will contain $(N + 1)$ unknown coefficients, $a_0, a_1, ..., a_N$. In order to evaluate these using collocation methods, the approximate expansion of $u(z)$ is satisfied exactly at a set of $(N + 1)$ points, say $z_0, z_1, .., z_N$. These points are called collocation points; they are arbitrarily subjected to a rather qualitative constraint. In order to see how to choose these collocation points, we go back to (4.8) and note that the required coefficients $a_k (k = 0, 1, .., N)$ are given by a trigonometric integral. This integral can be evaluated extremely

accurately by a trapezoidal formula because, in fact, this scheme is equivalent to an $\mathcal{N}$-point Gaussian quadrature rule. Therefore, an optimum way is to divide the interval $0 \leq x \leq \pi$ into equal increments:

$$x_j = \frac{j\pi}{\mathcal{N}} \quad j = 0, 1, ..., \mathcal{N} \tag{4.12}$$

or in terms of the original variable, z,

$$z_j = \cos\frac{j\pi}{\mathcal{N}} \quad j = 0, 1, ..., \mathcal{N} \tag{4.13}$$

The set $\{z_j\}$ is called the Gause-Lobatto points where $dT_{\mathcal{N}}/dz = T'_{\mathcal{N}} = 0$. Since $T_k(z)$ is a polynomial in z of degree k, $u_{\mathcal{N}}$ is an $\mathcal{N}$-polynomial approximation to $u(z)$.

In order to represent the derivative of the function at the collocation points, Lagrange interpolating polynomials of degree $\mathcal{N}$ are used, i.e.,

$$u(z) = \sum_{k=0}^{\mathcal{N}} \lambda_k(z) u(z_k) \tag{4.14}$$

where the interpolant $\lambda_k(z)$ can be expressed in an explicit form:

$$\lambda_k(z) = \frac{(1-z^2)}{(z-z_k)} \frac{T'_{\mathcal{N}}(z)}{c_k \mathcal{N}^2} (-1)^{k+1} \tag{4.15}$$

where $c_0 = c_{\mathcal{N}} = 2$ and $c_k = 1$ for $0 < k < \mathcal{N}$. Of course, this Lagrangian polynomial representation provides perfect accuracy for all functions with polynomials of degree $\leq \mathcal{N}$. The p^{th} derivative of $u(z)$ at the j^{th} collocation point, in terms of the values of u at all the collocation points, is given as

$$\frac{d^p u}{dz^p}|_j = \sum_{k=0}^{\mathcal{N}} D^p_{jk} u_k \tag{4.16}$$

where $u_k = u(z_k)$, the D_{jk} are the elements of the derivative matrix given in Canuto, et al. (1987) as

$$\begin{aligned} D_{00} &= \frac{2\mathcal{N}^2+1}{6} = -D_{\mathcal{N}\mathcal{N}} \\ D_{jk} &= \frac{c_j}{c_k} \frac{(-1)^{k+j}}{(z_j - z_k)} \quad \text{for } j \neq k \\ D_{jk} &= \frac{-z_j}{2(1-z_j^2)} \quad \text{for } j = k \end{aligned} \tag{4.17}$$

and,

$$D^p_{jk} = (D_{jk})^p$$

With approximate representations (4.14) and (4.16) for a function $u(z)$ and its derivatives, it is possible to convert any ODE into a system of algebraic equations for the $(N+1)$ unknowns $u(z_0)$, $u(z_1)$,.. $u(z_N)$, where z_0, z_1... z_N are the collocation points. These (linear) algebraic equations may be solved by several powerful methods [see Wilkinson 1965], although a principal difficulty is that the matrix associated with these equations is not very sparse.

Clearly, in order to apply a spectral method with the Chebyshev polynomials, the physical semi-infinite domain $0 \leq r \leq \infty$ must first be transformed onto the finite Chebyshev domain, $|z| \leq 1$. For boundary layer flows, the two mappings which have been successfully employed in transforming the infinite domain $(0, \infty)$ onto the half interval of the Chebyshev domain $(0, 1)$ are the exponential mapping (Laurien & Kleiser 1985) and the algebraic mapping (Herbert 1984). These mappings, which cluster the collocation points near the "wall" at $r = 0$ and become more widely spaced away from the wall, are inefficient in subsonic round jets where steep gradients occur in a very thin critical layer of thickness $0(Re^{-\frac{1}{3}})$ located in the neighborhood of the jet radius, not on the jet centerline. The thin critical layer in jets requires sufficiently dense collocation points in this layer. In fact, a difficult numerical task that arises from the coupled system of ODE is that any numerical scheme must be capable of capturing accurately the eigenfunctions and their derivatives up to second order, simultaneously. The viscous and conduction terms, which contribute to the second derivatives, are included to eliminate any singular behavior of inviscid neutral eigenmodes. We utilize two different mapping methods for the stability calculation of compressible subsonic jets. The first method maps the infinite physical domain onto a finite Chebyshev domain. The second approximates the unbounded physical domain by a finite domain which is mapped onto the Chebyshev domain. We now outline these two

mappings.

Mapping A

The first mapping maps from $r = 0, \infty$ into $z = 0, 1$ via

$$z = \frac{l_1}{2(r + l_1)} + \frac{1}{2}\exp[-\frac{r^n}{l_2}] \tag{4.18}$$

The parameters l_1 l_2 and n are adjustable constants which control the amount of stretching in the r direction. Note that when $n = 1$ and $l_1 = 0$, the mapping reduces to the classical exponential mapping. For a given l_1 and l_2, n controls the number of grid points in the neighborhood of the critical point (near $r = 1$) When the value of n increases, more nodal points are clustered around the critical layer. The parameters l_2 and n redistribute some of nodal points near $r = 0$ to the region where strong gradients exist (near $r = 1$). For a given number of collocation points, the concentration of nodes in the physical domain is governed by the metric coefficient:

$$z' = \frac{dz}{dr} = -\frac{l_1}{2(r + l_1)^2} - \frac{n}{l_2}r^{n-1}\exp[-\frac{r^n}{l_2}] \tag{4.20}$$

The higher the value $|z'|$ in the neighborhood of the critical layer, the greater the concentration of nodal points. As a caveat, in order not to decrease the exponential convergence rates associated with a spectral method, a mapping, $r = r(z)$, which maps the physical domain onto the Chebyshev domain must not be too complicated [Canuto et al.]. In other words, if we expand

$$r_N(z) = \sum_{k=0}^{N} a_k T_k(z),$$

the truncation error, e, which arises from using the $N + 1$ modes to represent r, is

$$e = \sum_{k=N}^{\infty} a_k T_k(z)$$

This error e must be so exponentially small that it will not affect the accuracy of a spectral method. In (4.18), the point $r = 0$ is mapped onto $z = 1$, while the point $r = \infty$

is mapped onto $z = 0$. The point $z = 0$ is not used as a collocation point, and we used odd polynomials expansion so that the boundary conditions at this point are automatically satisfied.

In general, a function and its higher order derivatives which are regular at infinity in the physical domain r might not necessarily be regular in the computational domain z (Spalart 1984). In order not to destroy a spectral accuracy, the function and all its higher order derivatives at $z = 0$ must be sufficiently well behaved so that the formula (4.8) for the spectral decay of the spectrum a_k is valid. We now examine the behavior of $u(z)$ as $z \to 0$. As $r \to \infty$, z vanishes algebraically according to the first term on the right hand side of (4.18). Since a disturbance decays exponentially (2.38) - (2.42), we can conclude that all the derivatives of the disturbance $\to 0$ as $z \to 0$, i.e.,

$$\lim_{z \to 0} \frac{d^j u}{dz^j} \to 0 \quad for\ all\ j \tag{4.19}$$

Although no studies have been done here, we suspect that when a function is properly resolved, *mapping A* will preserve the rapid convergence rates associated with a spectral method. Further, the algebraic term of this mapping provides an adequate resolution of nodal points far away from the origin.

The cylindrical geometry of a round jet inherits a coordinate singular point at $r = 0$ which requires a little care. To remove this singularity, we imposed explicitly the boundary conditions at $r = 0$. These boundary conditions, which are independent of the viscosity, can be obtained from (2.38) - (2.42). For $\beta = 0$ or $\beta =$ an even integer, they are

$$v = w = \frac{du}{dr} = \frac{dp}{dr} = \frac{d\rho}{dr} = 0 \tag{4.21}$$

and, for $\beta =$ odd integer

$$u = p = \rho = \frac{dv}{dr} = \frac{dw}{dr} = 0. \tag{4.22}$$

Mapping B

For a disturbance which is confined to the critical layer at $r \cong 1$ and which vanishes rapidly away from the origin, an alternate approach is to transform a truncated finite physical domain $0 < r \leq R_{\max}$ onto the computational interval $0 < z \leq 1$ according to

$$\begin{aligned} z &= \cos\theta \\ \overline{y} &= 1 - 2\theta\pi \\ r &= r_c\left\{1 + \frac{\sinh[\tau(\overline{y} - B)]}{\sinh(\tau B)}\right\} \end{aligned} \tag{4.23}$$

where

$$B = \frac{1}{2\tau} ln\left[\frac{1 + (e^{\tau} - 1)(r_c/R_{\max})}{1 + (e^{\tau} - 1)(r_c/R_{\max})}\right], \quad 0 < \tau < \infty,$$

τ is the concentration parameter which varies from zero for no stretching to high values which concentrate more grid points near r_c, and r_c is the approximate location of the critical layer. Figure (4.3) shows the distribution of collocation points for various values of τ. [See Anderson et al. 1984 for a part of this mapping]. Since the slope, dz/dr, is large in the region of the critical layer, the mappings (4.23) provide high resolution for a suitable value of τ. Unfortunately, because dz/dr vanishes at $R_{\max}$, any disturbance under this mapping has zero slope at $R_{\max}$, unless the asymptotic behavior of this disturbance is implemented appropriately (see remarks in section 4.1) into the discretization. As a consequence, this mapping will work only for the case where a disturbance is confined mainly in a narrrow region and decays rapidly. Extensive sensitivity studies were performed to determine the effect on the eigenmodes due to the zero slope approximation of a disturbance at $R_{\max}$. We found that when $\alpha R_{\max}$ is sufficiently large, typically 4 to 7, the stability characteristics are rather insensitive to the value of $R_{\max}$ as long as there is an adequate clustering of points in the critical layer. This insensitivity of the numerical results can be attributed to the sufficiently rapid decay of a disturbance. According to the asymptotic solutions (2.38) - (2.42), a disturbance is of order $R_{max}^{-1/2}\exp(-\alpha R_{\max})$ at $r = R_{max}$, which is small enough to be approximated by zero derivative whenever αR_{max} is sufficiently large. In this work, τ is between 5 to 10, while r_c ranges from 0.95 to 1.2.

In either mapping, as a result of using either odd or even polynomials over the half interval, the spectral derivative operators (4.16) need to be modified accordingly. The matrix elements of odd and even derivative operators become

$$D^p_{jk}(\text{odd}) = D^p_{jk}(\text{full}) - D^p_{j,N-k}(\text{full}) \tag{4.24}$$

$$D^p_{jk}(\text{even}) = D^p_{jk}(\text{full}) + D^p_{j,N-k}(\text{full}) \tag{4.25}$$

where

$$N = \frac{\mathcal{N}+1}{2}$$

$$j = 0, 1, \cdots, N$$

$$k = 0, 1, \cdots, N$$

The superscript p denotes the p^{th} derivative, $\mathcal{N}$ is an odd integer, and N is the actual number of collocation points in the half Chebyshev domain. The derivatives in the physical domain can be expressed in the computational domain by using the chain rule of differentiation. For example,

$$\begin{aligned} u(r) &= u(z(r)) \\ \frac{du}{dr} &= \frac{du}{dz}\frac{dz}{dr} \end{aligned} \tag{4.26}$$

$$\frac{d^2u}{dr^2} = \frac{d^2u}{dz^2}(\frac{dz}{dr})^2 + \frac{du}{dz}\frac{d^2z}{dr^2} \tag{4.27}$$

where

$$\frac{dz}{dr} = \frac{dz}{d\theta}\frac{d\theta}{d\overline{y}}\frac{d\overline{y}}{dr} \tag{4.28}$$

$$\frac{d^2z}{dr^2} = \frac{dz}{d\theta}(\frac{d\overline{y}}{dr})^2\frac{d^2\theta}{d\overline{y}^2} + \frac{d^2z}{d\theta^2}(\frac{d\overline{y}}{dr})^2(\frac{d\theta}{d\overline{y}})^2 + \frac{dz}{d\theta}\frac{d\theta}{d\overline{y}}\frac{d^2\overline{y}}{dr^2} \tag{4.29}$$

In an implementation of a spectral collocation method, the spectral derivative operators are replaced by full matrices, non-constant coefficient terms are represented by diagonal matrices, and the boundary conditions (when exists) are imposed by replacing the appropriate rows of matrix. The spectral matrix representation of the stability equations

converts them into the generalized algebraic problem

$$\mathbf{AX} = \sigma\mathbf{BX} \tag{4.30}$$

where $\mathbf{A}$ and $\mathbf{B}$ are complex general square matrices of size N^*; N^* is $5\times N$ for the primary stability problem, $10\times N$ for the secondary subharmonic analysis, and N is the number of collocation points in the computational domain.

There are generally two different classes of numerical approaches for computing the eigenvalues σ of (4.30), global and local methods. Global methods, which require no initial guess on the eigenvalues and compute all the eigenvalues of the discretized system, are based on the QZ algorithm (Wilkinson 1965). For a matrix of dimension N^*, it requires $0(N^{*2})$ storage and $0(N^{*3})$ operations. Local methods, however, require a starting guess for the eigenvalue and an iteration scheme based on an accelerated inverse Rayleigh iteration method (Wilkinson). The global algorithm requires much more computer time and storage than the local method since they compute the whole spectrum of eigenvalues of the discretized system. Therefore, in order to maximize the numerical efficiency, it is desirable to minimize the number of Chebyshev polynomials used in a global method. On the other hand, the main shortcoming of a local method is that it converges to the true eigenvalue only if an initial guess is sufficiently close to it. As a rule of thumb, in the absence of any prior guidance on the eigenvalue, we select the physically desirable eigenvalue from a global method and use it as input to a more refined local method (using more collocation points) to obtain a more accurate eigenvalue and its corresponding eigenfunction.

For the tanh mean profiles of (2.28) - (2.30), we found that the eigenvalues obtained from the global method and the local method agreed to at least six decimal places when the same number of grid points were used. The typical rapid convergence of complex phase velocity C corresponding to the most unstable eigenvalue of a near maximally amplifying disturbance is reflected in the values below:

N	C_R	C_I
15	0.57644	0.18860
21	0.57656	0.18866
31	0.57656	0.18866
41	0.57656	0.18866

The above results, obtained using *Mapping B*, are for $\alpha = 3.5, \beta = 1, M_j = 0.1, Re = 10^6, T^* = 1$ and $\theta = 1/15$. The corresponding value of C obtained by an independent inviscid finite difference code (see Section 4.2) using 200 grid points is $C = 0.57656 + 0.18867i$.

For a near neutral wave the convergence of the unstable eigenvalue with N is observed to be much slower than that of a maximally amplified wave. For example, the least stable eigenvalue for a near-neutral wave of a heated and compressible jet [$\alpha = 5.8, \beta = 0, M_j = 0.8, Re = 5000, T^* = 2$ and $\theta = 1/15$] is found, using *Mapping A*, to be

N	C_R	C_I
35	0.4821	0.0096
45	0.4840	0.0109
65	0.4840	0.0100

This slow convergence is attributed to the near singular behavior of the eigenmodes in the vicinity of a critical point at high Reynolds number flows (see section 2.7). In fact, as heating and compressibility increase for high Reynolds numbers flows, we have found that the structures of the near-neutral eigenmodes become increasingly more difficult to resolve.

Figures (4.4) - (4.9) exhibit the typical transverse distributions of the shape and phase of the most amplified and near neutral eigenfunctions. These eigenfunctions are normalized such that the maximum magnitude of the eigenfunction of the streamwise velocity is 0.5. The pressure eigenfunction is seen to exhibit the "smoothest" structure. This behavior is sensible since the pressure perturbation has the weakest form of singularity at the critical point. Numerically, it is precisely this relatively smooth behavior of the pressure that

makes it the most useful variable to work with in connection with a Rayleigh equation (when one exists). It is interesting to note that for a near maximally amplified wave, the streamwise perturbation u has a typical distinct peak and the radial component v has a plateau-like structure at the critical layer. For a near neutral wave, the peak structure of u perturbation changes drastically to a shape with two local maxima and is accompanied by a significant change of the phase, while the plateau feature of the v component transforms to a smooth shape with a single maximum point. Note also that the amplitude of a highly amplified u perturbation is large at the jet lipline and becomes progressively small as the wave approaches the neutral point.

4.2 Some Remarks on Spectral Methods

1. The imposition of the asymptotic boundary conditions (see section 2.6) forbids the use of a global method because the eigenvalue σ then enters nonlinearly into the eigenvalue problem through the boundary conditions. In addition, since the analytic far field behavior of a disturbance in a periodic base flow is still unknown, it is suitable to use the set of mappings (4.18) and (4.23) with a sufficient number of grid points to resolve the disturbance structure in the critical layer.

2. The extension to spatial stability analysis can be done without much difficulty. Since the basic instability mechanism is essentially inviscid, the viscous terms which contribute to a quadratic nonlinearity in α, can be neglected in a global method for spatial stability problems. This is because $\alpha^2 \sim \partial^2/\partial x^2$ and in the critical layer (where the effects of viscosity and heat conductivity are small), this derivative is negligible compared to $\partial^2/\partial y^2$ (i.e., the boundary layer assumption). This inviscid spatial analysis can be reduced to a generalized eigenvalue problem for α. The physically meaningful α, usually the most unstable mode selected from a global scheme,

is used as a starting guess for the eigenvalue of a more refined viscous local code.

4.3 Fourth-Order Finite-Difference Method

In order to have confidence in the spectral method, the eigensolutions of the viscous problem as viscosity vanishes, or equivalently as the Reynolds number becomes infinite, were checked by an independent fourth order inviscid finite difference method. Eigensolutions of the linear stability problem of unidirectional round jets have been obtained using finite difference methods by Paragiri (1985) for inviscid analysis and by Jarrah (1989) for viscous modes. For completeness, a brief description of the method is discussed here. In the absence of viscosity (and conductivity), the governing disturbance equation for an inviscid compressible parallel flow can be reduced to a single Rayleigh-type second order ODE for the pressure disturbance (2.48)

$$\frac{d^2p}{dr^2} + \left[\frac{1}{r} - \frac{2u_0'}{u_0 - C} - \frac{\rho_0'}{\rho_0}\right]\frac{dp}{dr} + \left[\alpha^2(u_0 - r)^2\rho_0 M_j^2 - \frac{\beta^2}{r^2} - \alpha^2\right]p = 0. \qquad (2.48)$$

Since u_0' and ρ_0' vanish as $r \to 0$ and as $r \to \infty$, the asymptotic solutions are

$$p = C_1 I_\beta(\alpha r\sqrt{1 - M_j^2\rho_0(u_0 - C)^2}) \quad as\ r \to 0 \qquad (4.31)$$

$$p = C_2 K_\beta(\alpha r\sqrt{1 - M_j^2\rho_0(u_0 - C)^2}) \quad as\ r \to \infty \qquad (4.32)$$

where I_β and K_β are modified Bessel functions of the first and second kind, respectively, and C_1 and C_2 are constants. Numerically, the asymptotic far field boundary condition is satisfied at approximately $r = R_{max} = 4.0$ and the boundary condition on the jet axis is satisfied at the first two grid points where constant mean flow prevails to a good degree of approximation. Details and some sample calculations may be found in Paragiri (1985). A fourth order central difference scheme is employed which translates the ODE (2.48) together with the boundary conditions (4.31) and (4.32) into a pentadiagonal system of

complex algebraic equations. The complex eigenvalue C is then found by a local method based on the Newton-Raphson scheme where iterations on the eigenvalue are performed until a prescribed convergence criterion is met. In this work, the eigenvalues are iterated to five decimal places for highly amplified modes, and to three decimal places for near neutral modes. Note that a physical eigenvalue can easily be distinguished from a spurious (unphysical) one because the latter does not converge as the number of computational grid points is increased.

4.4 Some Remarks on the Linear Inviscid Calculation

The inviscid pressure equation (2.48) has a regular singular point whenever the mean flow velocity equals the phase velocity of a neutral wave. This singularity often creates numerical difficulties. For sufficiently amplified modes, the imaginary part of the complex phase velocity C removes the singularity from the differential equation along the real axis and hence poses no numerical problem. However, for eigenmodes that are merely slightly unstable, the almost singular nature of the differential equation requires some care. To make matters worse, the secondary instability calculations require an accurate determination for all the primary disturbances (not just the pressure) and their higher order derivatives. As shown from section (2.7), compressible flows introduce density fluctuations whose leading order behavior in the neighborhood of the critical point is

$$\rho_b = -\left\{ \frac{(\alpha^2 r_c^3 + \beta^2 r_c)u_c'' + [3Kr_c^3 - (\alpha^2 r_c^2 + \beta^2)]u_c'}{\alpha^2 r_c^3 u_c'^3 (r - r_c)} \right\} + \cdots + K\rho_a \log(r - r_c) \qquad (2.56)$$

This singularity, which is a pole of order one, may create a change in density fluctuation across the critical layer that is too rapid for an accurate determination of an inviscid near-neutral eigenmode. Therefore, we conclude that although the instability is predominantly inviscid, the inclusion of viscosity is mandatory in secondary instability calculations because the primary wave is very nearly neutral.

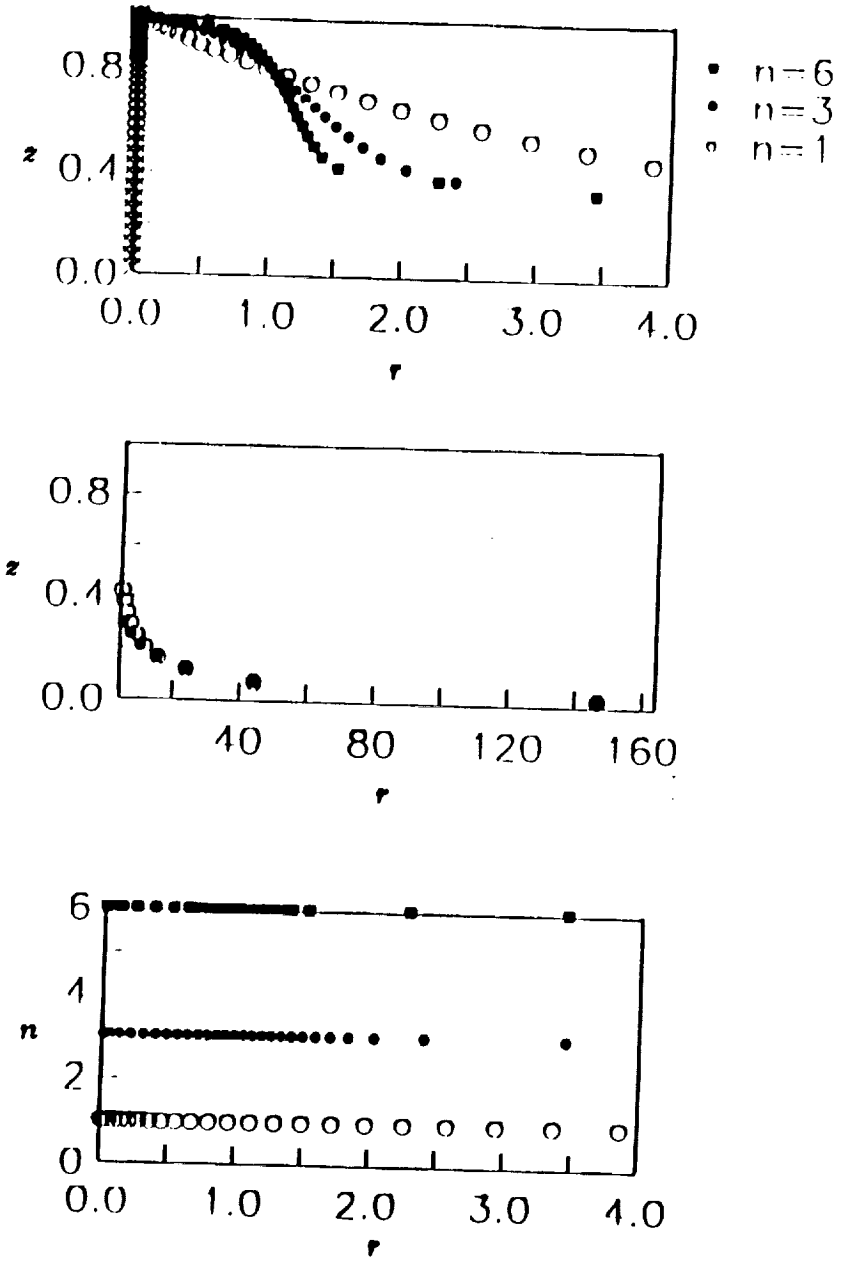

Fig. 4.2 (a) and (b) z as a function of the radial variable r for various n. Crosses are the collocation points. (c) collocation points on r. The number of collocation points is 35 using *Mapping-A* with $l_1 = 7$ and $l_2 = 3$.

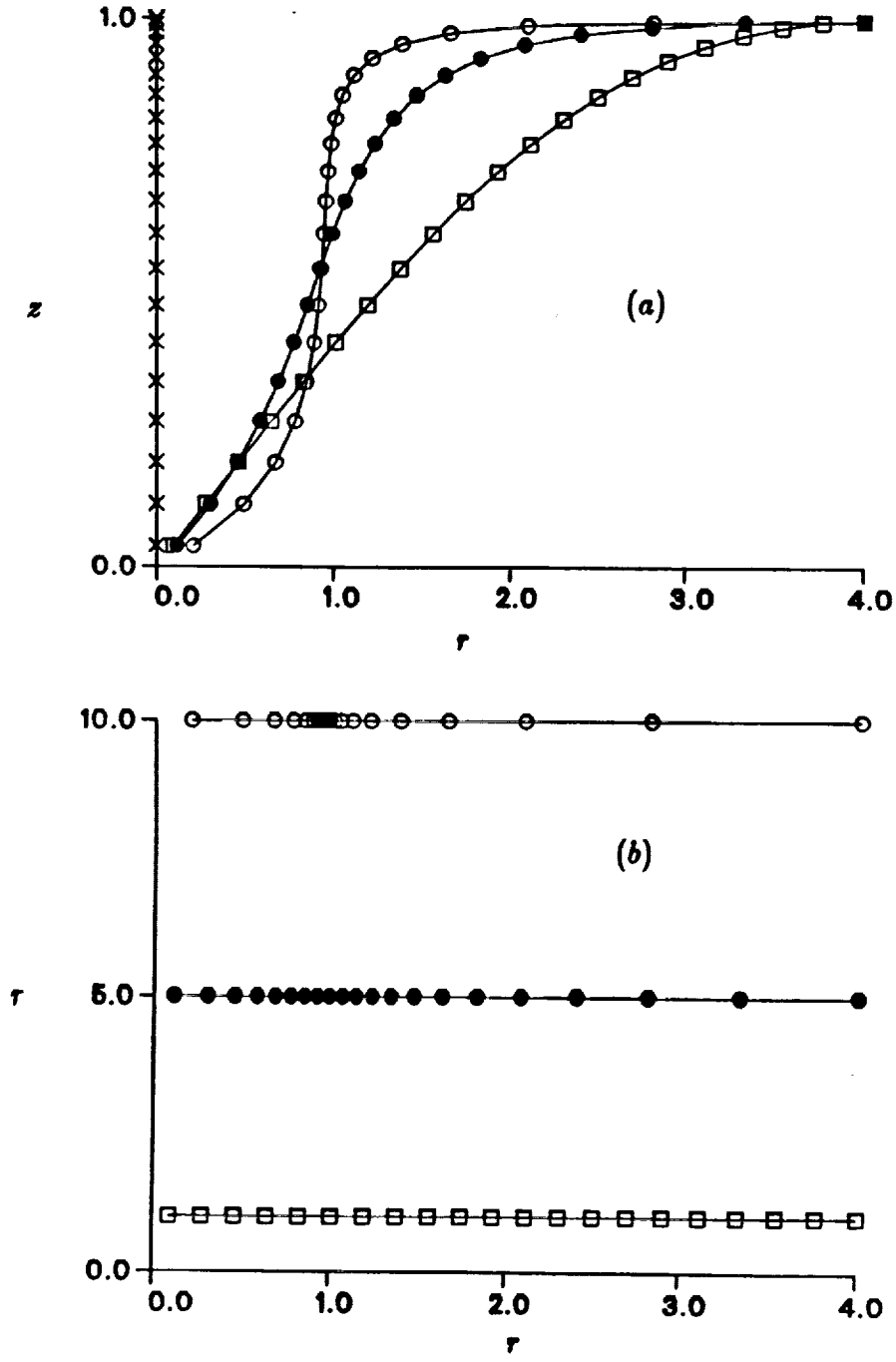

Fig. 4.3 (a) z as a function of the radial variable r for various stretching parameter τ (b) collocation points on r. The number of collocation points is 21 using *Mapping-B*. Crosses are the collocation points. Bullets ($\tau = 5$), circles ($\tau = 10$), and squares ($\tau = 1$).

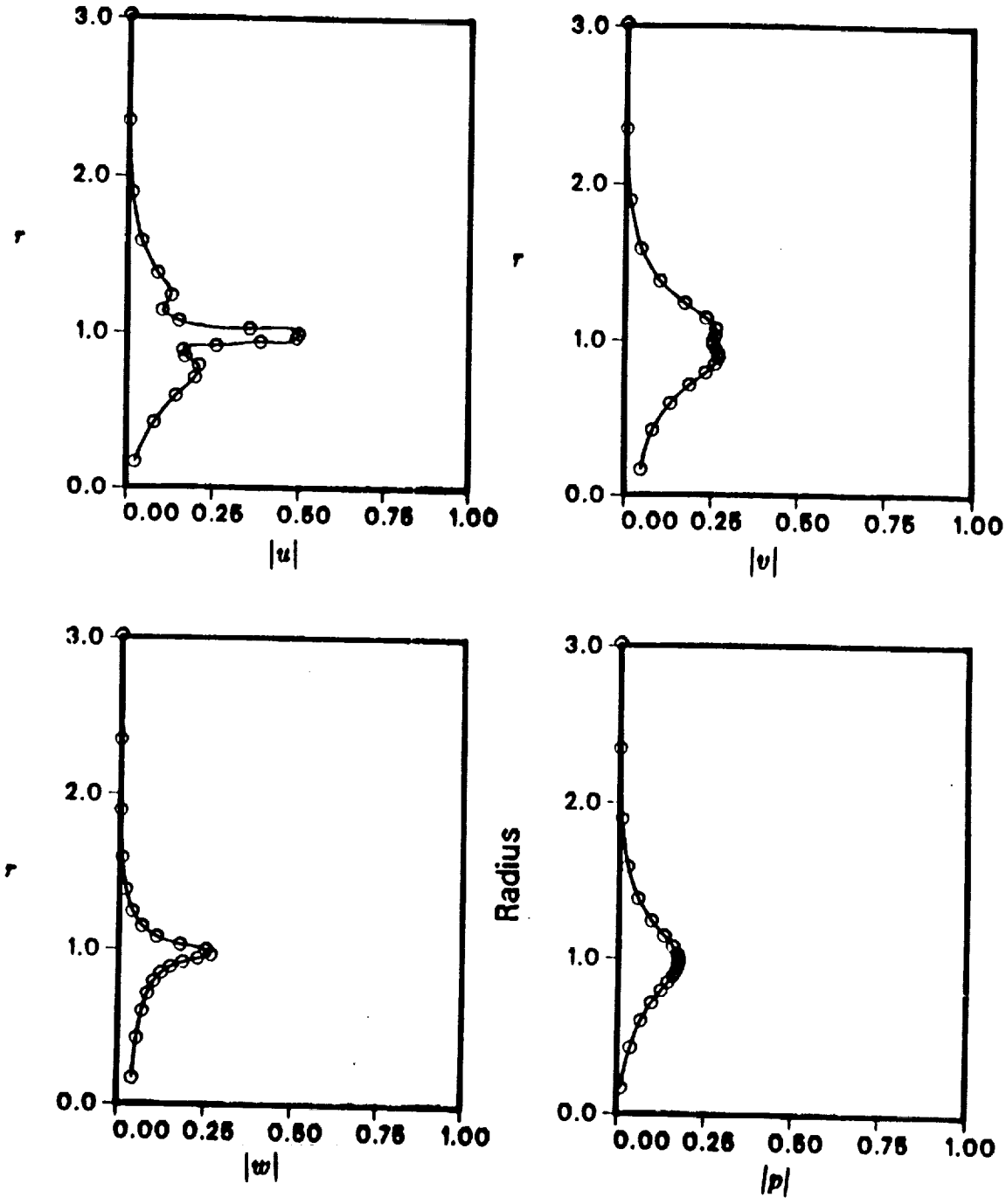

Fig. 4.4 Distributions of the |eigenfunction| of a near maximally amplified disturbance for $Re = 1.0E+6, T_s = 1.0, M_j = 0.1, \theta = 1/15, \alpha = 3.5, \beta = 1$, and the complex phase velocity C = (0.577,0.189).

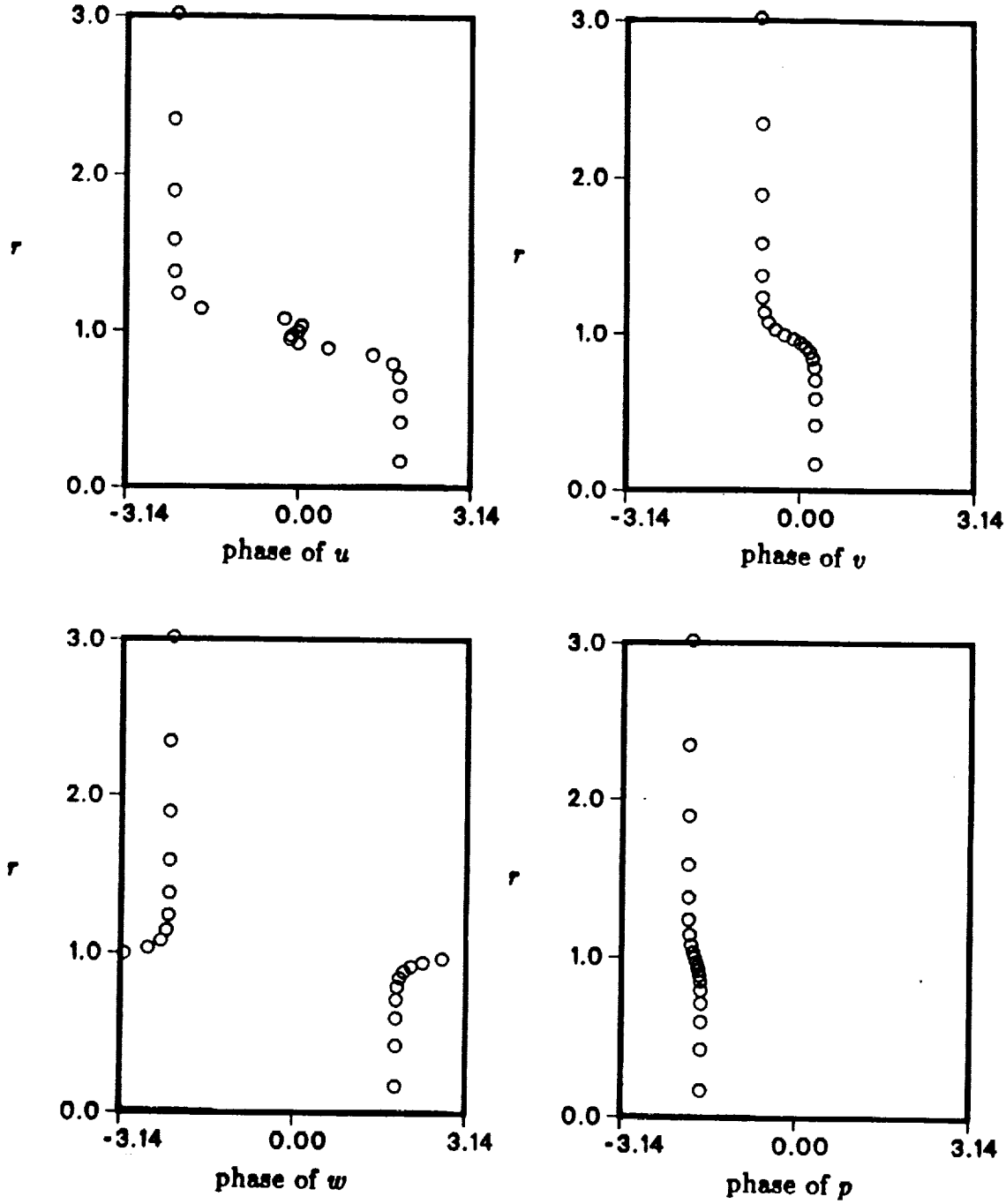

Fig. 4.5 Distributions of the phase of the eigenfunction of a near maximally amplified disturbance for $Re = 1.0E+6, T_s = 1.0, M_j = 0.1, \theta = 1/15, \alpha = 3.5, \beta = 1$, and the complex phase velocity C = (0.577,0.189).

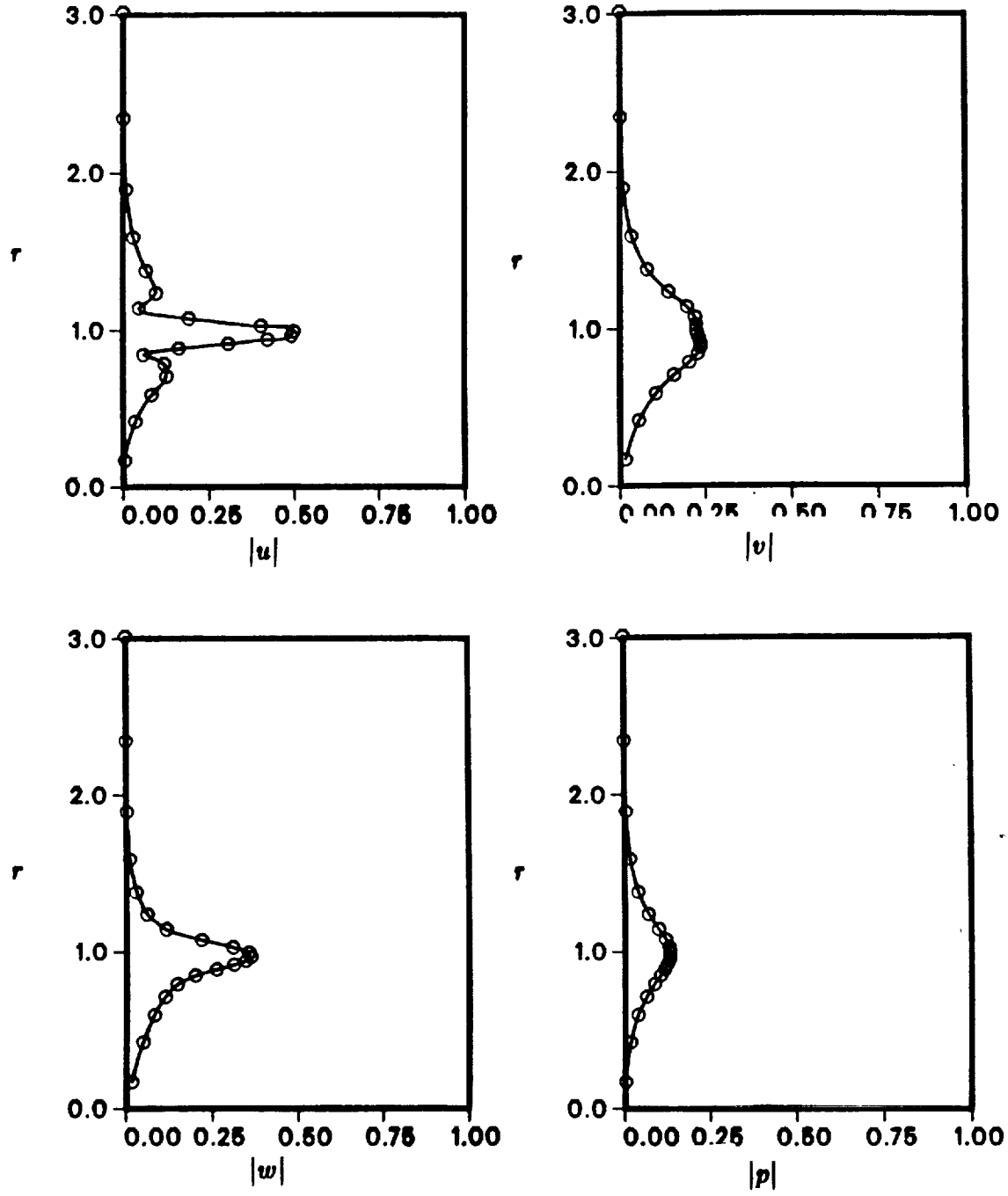

Fig. 4.6 Distributions of the |eigenfunction| of a near maximally amplified disturbance for $Re = 1.0E+3, T_s = 1.0, M_j = 0.1, \theta = 1/15, \alpha = 3.5, \beta = 2$, and the complex phase velocity C = (0.557,0.142).

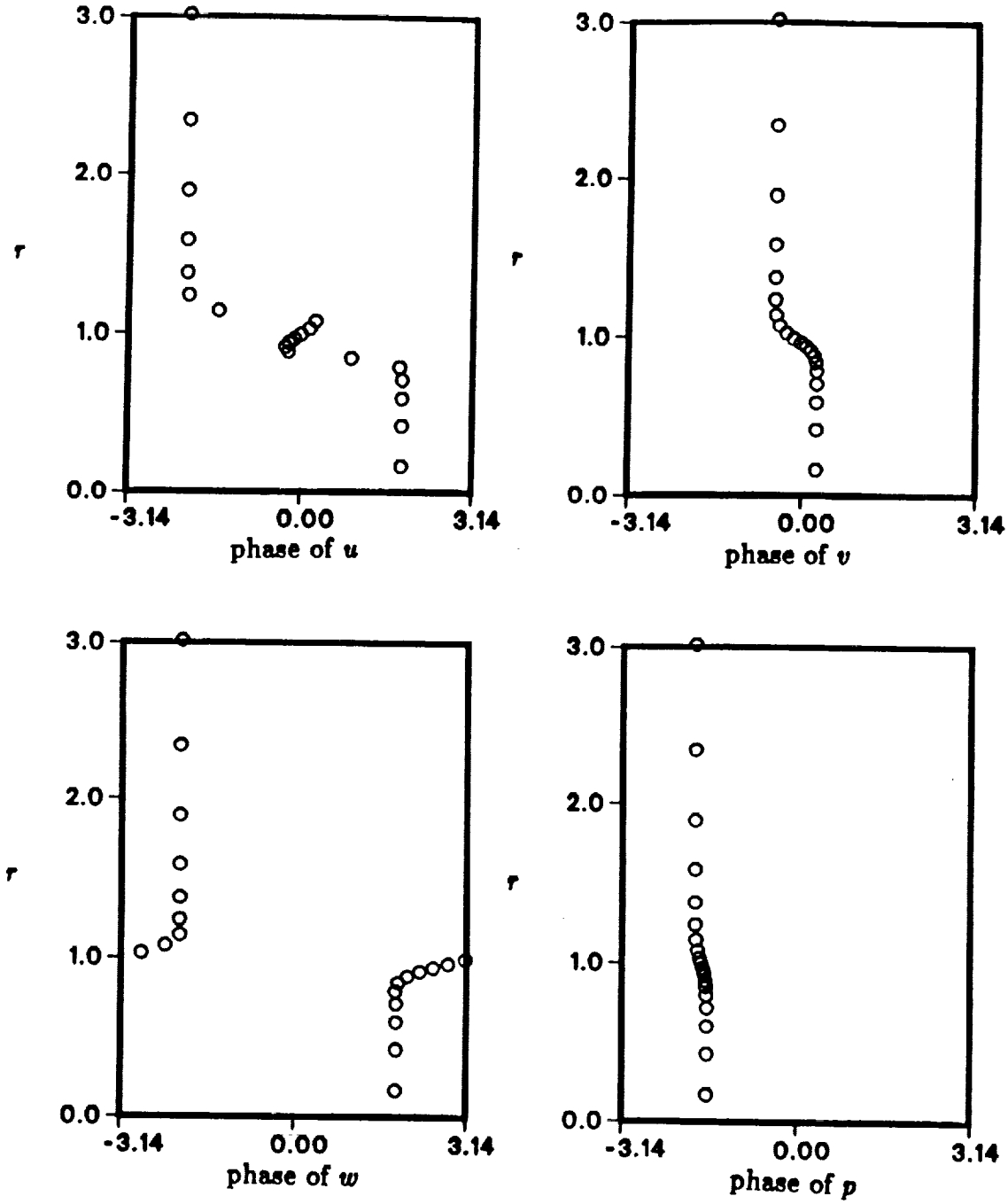

Fig. 4.7 Distributions of the phase of the eigenfunction of a near maximally amplified disturbance for $Re = 1.0E+3, T_s = 1.0, M_j = 0.1, \theta = 1/15, \alpha = 3.5, \beta = 2$, and the complex phase velocity C = (0.557,0.142).

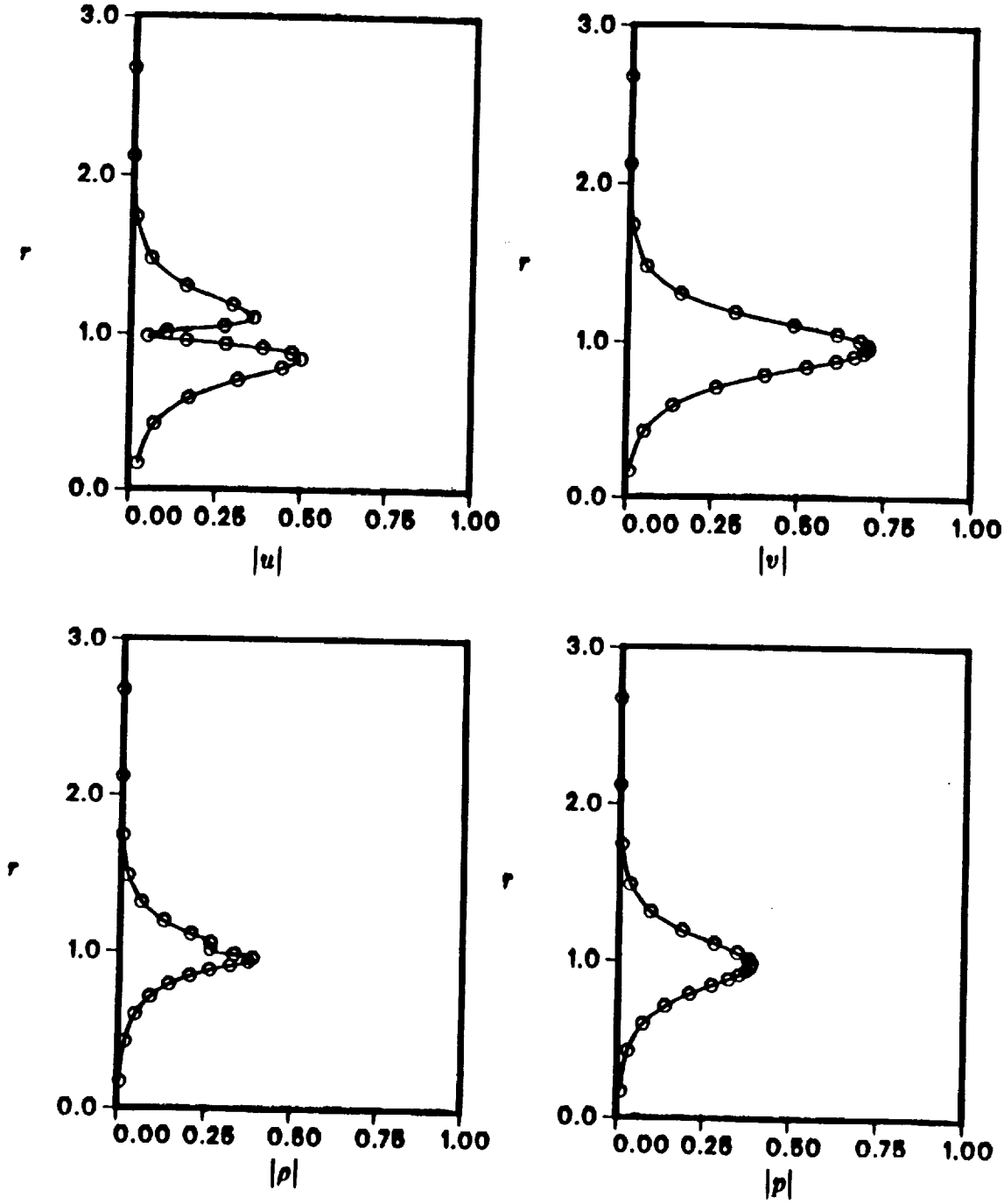

Fig. 4.8 Distributions of the |eigenfunction| of a near neutral disturbance for $Re = 5.0E+3, T_s = 1.0, M_j = 0.8, \theta = 1/15, \alpha = 6.55, \beta = 0$, and the complex phase velocity C = (0.569,0.001).

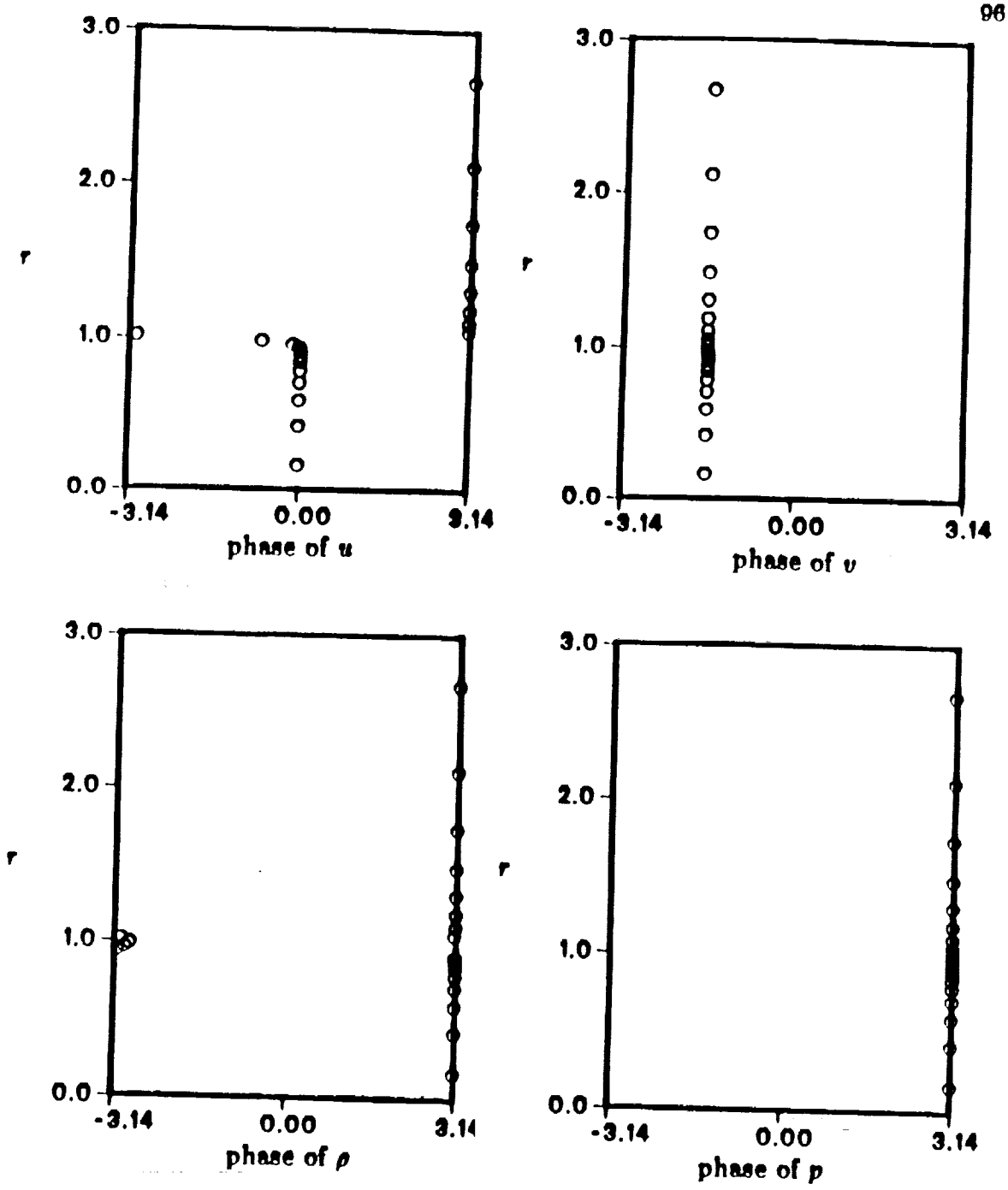

Fig. 4.9 Distributions of the phase of the eigenfunction of a near neutral disturbance for $Re = 5.0E+3, T_s = 1.0, M_j = 0.8, \theta = 1/15, \alpha = 6.55, \beta = 0$, and the complex phase velocity C = (0.569,0.001).

Chapter 5

LINEAR STABILITY OF PARALLEL JETS

The linear stability of a parallel jet is important in its own right. In order to be able to manipulate the downstream evolution of jet shear layers, the early stages of jet instability must be understood. We reiterate that linear analyses can reveal accurately not only the stability characteristics of the initial stages of development of the large-scale instability wave, but also, rather surprisingly, it can predict the cross-space structure of the perturbation, even when the local disturbance level is as high as 24% of the jet exit velocity (Petersen & Samet 1988). This linear analysis, being the first cascade of instability, is used as input to fully nonlinear numerical simulations, weakly nonlinear analysis, and secondary instability theory. This section considers some features of the linear stability of subsonic heated round jets. The different parameters affecting jet instability mechanism are discussed separately in order to elucidate their individual influences. The important parameters are the jet Mach number M_j, the temperature ratio T_*, the jet momentum thickness θ, wavenumbers (α, β), and the Reynolds number Re.

5.1 Viscosity Effect

There are now a number of investigations on the inviscid stability characteristics of round jets, although studies on the viscous instability analysis remain scarce. Batchelor & Gill (1962) pioneered a theoretical framework on the inviscid stability of a top hat

velocity profile which characterizes the mean flow close to the jet exit. This top hat velocity, which ignores the presence of the jet nozzle, as is customary in all parallel flow analysis, provides a closed form solution of the stability characteristics of a cylindrical vortex sheet. By using more realistic profiles, which depend continuously on r, Michalke (1971) and Mattingly & Chang (1974) obtained a good agreement with the experimental results of Crow & Champagne (1971). Morris (1976) went further to investigate the effect of viscosity on the instability of various jet mean velocity profiles for different values of the jet parameters. He found that for jet velocity profiles with thin shear layers, i.e., close to the jet nozzle, viscosity has a slight stabilizing effect on the growth rate for flows above a Reynolds number of 1000, based on jet centerline velocity and jet nozzle radius. In other words, viscosity for instability modes in jets is predominantly passive in character, and can be ignored for flows at high Reynolds number (except for neutral waves).

Typical results exhibiting the influence of Reynolds number on the linear (temporal) instability of subsonic heated round jets with the tanh base profiles of (2.28) - (2.30) are summarized in Figures (5.1) - (5.6). In particular, the effect of Reynolds number on the full spectrum of eigenvalues using 31 Chebyshev polynomials for $\alpha = 3.66$ and $\theta = 1/15$ are plotted for various jet parameters in Figures (5.1) - (5.3). We caution the reader that the discretized eigenvalues in these figures, except for the unstable ones, are only "roughly" determined since their associated eigenfunctions did not adequately satisfied the far field boundary conditions. Nevertheless, these eigenvalues may provide a rough guide on the the full spectrum of the primary instability problem. The salient features that can be extracted from these figures are

1. As the viscosity tends to zero ($Re \to \infty$), the spectrum consists of a string of neutral modes and a complex conjugate pair of eigenvalues.

2. The string of eigenvalues, which probably constitutes part of the continuous spectrum, generally becomes increasingly stable with decreasing Reynolds number. The

inclusion of viscosity (at high Reynolds number) only slightly stabilizes the unstable (discrete) eigenvalue, and breaks down the symmetry of an inviscid complex conjugate pair. In other words, viscosity has a considerable effect on damped waves but exerts only a slightly stabilizing effect on unstable (inflectional) waves.

3. The "continuous modes", whether viscous or inviscid, have phase velocities lying between the minimum (free stream value) and the maximum (jet center line value) of the jet mean flow.

Observation (1) is perfectly consistent with the well-known properties of the reduced inviscid equation (2.48). Since this equation admits a complex conjugate pair of eigenvalues, it has either neutral modes or growing modes which have corresponding "damped" modes moving with the same phase velocity. Furthermore, since the mean velocity profile used in this work has only one generalized inflection point, the spectrum is thus restricted to an assembly of a single unstable mode, its conjugate damped mode, and the remaining neutral modes. The fact that an inviscid equation describes the same instability mechanism as the viscous problem in the limit of vanishing viscosity is reinforced by (2). Although the continuous spectrum of free shear flows is still not completely understood, observation (3) suggests that the complex eigenvalues of the highly damped continuous modes move toward the real axis. This observation is again consistent with the theoretical results of the continuous spectrum of boundary layers (Grosch & Salwen, 1978); they found that the phase velocity of the highly damped continuous mode matches the mean flow velocity. In view of the physical insignificance of the damped waves compared to the rapidly amplified unstable waves of round jets, the continuous spectrum will not be pursued further in this work. Nevertheless, the continuous spectrum obtained from a numerical discretization scheme can influence the results of an unstable mode. The inclusion of viscosity will generally increase the rate of numerical convergence of the unstable mode by moving the continuous spectrum away from it. This implies that viscosity will play an important role

in the convergence of a near neutral unstable eigenvalue (see Santos, 1987).

In Figures (5.4) - (5.6), the growth rate and phase velocity as functions of wavenumber are plotted for $\theta = 1/15$. These figures show the typical influence of Reynolds number on the unstable mode of subsonic heated round jets. Note that the eigenvalues asymptotically approach the inviscid limit at a Reynolds number of about 5000. In contrast, the inviscid limit of a planar mixing layer occurs at a Reynolds number of about 200 (Jarrah 1989). This means that viscosity plays a more important role in the instability of round jets than in mixing layers. This is because in a mixing layer, where there are two external streams, the viscous solution (see section 2.6) is completely negligible; but this solution is not negligible on the jet axis unless the jet momentum thickness is extremely small. Thus the viscous solution will affect the eigenvalue through the boundary condition near the jet axis, even when the Reynolds numbers is on the order of several thousand. For jet flows at $Re \leq 5000$, viscosity not only slightly reduces the range of unstable wavenumbers but also the growth rate. Viscosity is also seen to have virtually no effect on the phase velocity of unstable disturbances, even though the Reynolds number can be as low as 500. These results agreed perfectly with the viscous calculations of Jarrah (1989), and are consistent with the numerical results for the spatial and viscous instability calculations of Morris (1976).

5.2 Mach Number Effect

The new quantity in compressible flows is the density fluctuation, which occurs simultaneously with the velocity and pressure fluctuations. The new parameters which will generally influence compressible flows are the Mach number M_j, the temperature ratio T_*, the Prandtl number Pr, and the ratio of the heat capacity coefficients, $\gamma = C_p/C_v$. In this section, the influence of Mach number on the stability of jet shear layers is given, the

effect of temperature ratio will be discussed in next session, while the last two parameters are assumed to be constants [$\gamma = 1.4$, $Pr = 0.72$], and hence, will not be addressed in this work. The Mach number can influence the instability via the base density profiles as well as through the disturbance equations. For example, in the unheated jet, the jet Mach number appears explicitly in the disturbance equations as well as in the base density distribution.

Although the stability of incompressible shear layers has been studied extensively, a systematic determination of the role of Mach number on the instability of jet shear layers is still unavailable. In the case of mixing layers, on the other hand, there are now several fairly complete studies [see Gropengiesser 1967, Jackson & Grosch 1988]. In his spatial stability calculations, Michalke (1971) found that increasing Mach number reduces the range of unstable waves as well as stabilizes the flow. Furthermore, he found that the phase velocity is sensitive to Mach number only for lower frequencies (or, wavenumbers) while in contrast, the growth rates become almost independent of Mach numbers. His results also show that the stabilizing effect due to Mach number is slightly more significant for an axisymmetric mode than for the first helical mode.

Eckart (1963) extended the Rayleigh stability criterion and Howard's (Howard 1961) semi-circle theorem to a compressible, adiabatic plane jet. By using a different approach, Blumen (1970) found that the influence of αM_j on the complex wave velocity of an unstable mode is the same as that of the Richardson number in Howard's results. He concluded that compressibility reduces the range of unstable wavenumbers and stabilizes the mixing layer. We will show that Howard's semicircle analysis can similarly bound the complex wave speed and illuminate the role of compressibility in jet shear layers. We will do this by generalizing Blumen's approach to a round jet.

The linear disturbance equations for an inviscid compressible jet can be reduced to a

single equation for the pressure perturbation $p(r)$:

$$L(p) = \frac{d^2p}{dr^2} + \left[\frac{1}{r} - \frac{2u_0'}{u_0 - C} - \frac{\rho_0'}{\rho_0}\right]\frac{dp}{dr} + \left[\alpha^2(u_0 - C)^2\rho_0 M_j^2 - \frac{\beta^2}{r^2} - \alpha^2\right]p = 0. \quad (2.48)$$

We multiply the above by $r/\{\rho_0(u_0 - C)^2\}$ to make it self-adjoint. The equation in the self-adjoint form becomes

$$\frac{d}{dr}\left\{\frac{r}{\rho_0(u_0 - C)^2}\frac{dp}{dr}\right\} + q_1 p = 0 \quad (5.1)$$

where $q_1 = r\left[\alpha^2(u_0 - C)^2\rho_0 M_j^2 - \beta^2/r^2 - \alpha^2\right]/\{\rho_0(u_0 - C)^2\}$. After multiplying (5.1) by the complex conjugate of p and integrating over the range of r, we find that

$$\int_0^\infty \left[\frac{r}{\rho_0(u_0 - C)^2}|p'|^2 - q_1|p|^2\right]dr = 0. \quad (5.2)$$

Separating (5.2) into the real and imaginary parts, we obtain

$$\int_0^\infty [(u_0 - C_R)^2 - C_I^2]rq_2 dr = \int_0^\infty r\alpha^2 M_j^2|p|^2 dr \quad (5.3)$$

$$2C_I\int_0^\infty (u_0 - C_R)rq_2 dr = 0 \quad (5.4)$$

where

$$q_2 = \frac{1}{\rho_0|u_0 - C|^4}[|p'|^2 + (\alpha^2 + \frac{\beta^2}{r^2})|p|^2]$$

$$C = C_R + iC_I.$$

For unstable waves ($C_I > 0$) which vanish at infinity, (5.3) and (5.4) can be simplified to

$$\int_0^\infty u_0 q_2 dr = C_R\int_0^\infty q_2 dr \quad (5.5)$$

$$\int_0^\infty u_0^2 q_2 dr = (C_R^2 + C_I^2)\int_0^\infty q_2 dr + \int_0^\infty \alpha^2 M_j^2|p|^2 dr \quad (5.6)$$

If we let a and b be, respectively, the maximum and minimum of the base velocity [i.e., $a \le u_0(y) \le b$], then (5.5) and (5.6) can be reduced to

$$0 \ge \int_0^\infty (u_0 - a)(u_0 - b)q_2 dr \quad (5.7)$$

$$0 \geq \left\{[C_R - \frac{1}{2}(a+b)^2] + C_I^2 - [\frac{1}{2}(a-b)]^2\right\} \int_0^\infty q_2 dr + \int_0^\infty (\alpha M_j)^2 |p|^2 dr \qquad (5.8)$$

The above expression can be simplified to the equation governing the Howard's semicircle theorem:

$$\left\{[C_R - \frac{1}{2}(a+b)]^2 + C_I^2\right\} \leq [\frac{1}{2}(a-b)]^2 \qquad (5.9)$$

Hence, the stability of inviscid compressible round jets, here $a = 0$ and $b = 1$, can be reduced to exactly the same form as in Howard's investigation of the stability of variable density parallel shear flows.

Therefore, the complex wave velocity for an unstable mode of jet shear layers is also restricted to the semicircle which has the range of u_0 for diameter, just as in unbounded planar mixing layers. Furthermore, since equations (5.5) and (5.6), which govern the instability of round jets, are exactly the same as equations (3.4) and (3.5) in Howard's results, we can conclude that compressibility stabilizes jet instability modes.

For the tanh profile, with $\theta = 1/15$, the typical role of subsonic Mach number in jet instability for the axisymmetric and the first helical modes is illustrated in Figures (5.7) and (5.8), respectively. Compressibility is found to be stabilizing and reduces the range of unstable wavenumbers. For example, when the jet Mach number, M_j, is increased from 0 to 0.8, the maximum growth rate of the axisymmetric and the first helical modes for an unheated jet is reduced from 0.68 to 0.55, and from 0.66 to 0.55, respectively. Compressibility also reduces, but only slightly, the phase velocity of waves whose wavenumbers are smaller than the maximally amplified wavenumber, and has no apparent effect on higher wavenumbers. In other words, the phase velocities of disturbances, whether axisymmetric or helical, are only weakly dependent on the subsonic Mach number.

In the limiting case as $\alpha \to 0$, these figures also show that long waves are unaffected by compressibility, i.e., waves with axial symmetry travel with the base flow velocity on the center line, whereas helical modes travel with half that velocity. Our calculations are consistent with the results of Jarrah (1989) and are in reasonable agreement with

the *spatial* stability calculations of Michalke & Hermann (1982). Physically, according to Blumen (1970), the mean flow energy, which provides the energy for an unstable mode, is diminished by working against the elastic force associated with a compressible medium, and consequently the growth rate of an unstable disturbance is reduced.

5.3 Heating Effect

In the previous section, we have discussed the effects of jet Mach numbers on the instability. An extension of the Howard semicircle theorem provided some analytical understanding for the reduction of the growth rates with increasing compressibility. We would now like to gain some understanding of the effects of heating. To do this, we shall begin by generalizing the vortex sheet problem of Batchelor & Gill (1962) to a hot jet. In order to obtain simple results, we set $M_j = 0$ in the final expressions.

As mentioned in section (5.2), the presence of density fluctuations in a zero Mach number flow is caused by a variable base density profile which is a function of θ and T_*. Although stability calculations have now been successfully carried out for unheated jets, studies on the influence of heating on jet instability characteristics remain scarce. Michalke (1971) and Michalke & Hermann (1982) are among the few who investigated the stability characteristics of subsonic heated round jets by using linear spatial (parallel flow) stability theory. They found that the local growth rate of the spatially growing instability wave in a zero Mach number flow (i.e., $M_j = 0$) increases as the total temperature is increased.

In order to shed light on the effect of heating and to increase the understanding of the stability characteristics of a viscous heated round jets with continuous velocity and density profiles, the solution for a cylindrical inviscid and heated vortex sheet is investigated here. The stability analysis of a vortex sheet has a closed form analytical solution, and has been given by Batchelor & Gill (1962) for the incompressible case. We now consider the corresponding compressible case.

The base profiles of a compressible vortex sheet are

$$\begin{aligned} u_0 = U_a = \text{constant}, \quad \rho_0 = \rho_a = \text{constant} \quad \text{for } r < 1 \\ u_0 = 0, \quad \rho_0 = \rho_o = \text{constant} \quad \text{for } r > 1 \end{aligned} \tag{5.10}$$

On both sides of the vortex sheet, given by $r = 1$, where irrotational flows persist, the

pressure perturbations are

$$p_a = E_h I_\beta(\alpha \Upsilon_a r) \; for \; r \; < \; 1 \tag{5.11}$$

$$p_b = D_h K_\beta(\alpha r) \; for \; r > \; 1 \tag{5.12}$$

where

$$\Upsilon_a = \sqrt{1 - (U_a - C)^2 M_j^2 \rho_a}$$

where I_β and K_β are Bessel functions, and E_h and D_h are arbitrary constants. The corresponding radial velocity can be obtained from the linearized radial momentum disturbance equation. They are

$$v_a = -\frac{E_h I'_\beta(\alpha \Upsilon_a r)}{i\alpha\rho_a(U_a - C)} \tag{5.13}$$

$$v_b = \frac{D_h K'_\beta(\alpha r)}{i\alpha\rho_b C} \tag{5.14}$$

where primes denote differentiation with respect to the argument in parenthesis. Let η be the radial displacement of the vortex sheet which assumes a normal mode representation of the form

$$\eta = A_h \exp i[\alpha(x - Ct) + \beta\phi] + c.c. \tag{5.15}$$

where A_h is a free constant which denotes the arbitrary amplitude.

The kinematic boundary condition that the interface I is a material surface (i.e., the interface is formed by the same fluid particles at all times) can be expressed as

$$\frac{DI}{Dt} = 0 \quad \text{for } r = 1^+ \tag{5.16}$$

$$\frac{DI}{Dt} = 0 \quad \text{for } r = 1^- \tag{5.17}$$

where

$$\frac{D}{Dt} = \frac{\partial}{\partial t} + (\mathbf{v} + \mathbf{v}_0) \cdot \nabla$$

and,

$$I = I(x, r, \phi, t)$$

Substituting equations (5.10) - (5.15) into (5.16) - (5.17) and after linearizing the disturbance equations, we obtain

$$i\alpha(U_a - C)A_h = \frac{E_h I'_\beta(\alpha\Upsilon_a)}{\rho_a(U_a - C)i\alpha} \tag{5.18}$$

$$i\alpha C A_h = \frac{D_h K'_\beta(\alpha)}{\rho_b C i\alpha} \tag{5.19}$$

Furthermore, the dynamic condition that the pressure is continuous at the interface yields

$$E_h I_\beta(\alpha\Upsilon_a) = D_h K_\beta(\alpha) \tag{5.20}$$

(5.18) - (5.20) provide the the equation for the determination of A_h, E_h and D_h. In order to have a nontrivial solution, these equations yield

$$\left(\frac{U_a - C}{C}\right)^2 = -L_\beta(\Upsilon_a\alpha)\frac{\rho_b}{\rho_a} \tag{5.21}$$

where

$$L_\beta(\Upsilon_a\alpha) = \frac{K_\beta(\alpha)I'_\beta(\Upsilon_a\alpha)}{K'_\beta(\alpha)I_\beta(\Upsilon_a\alpha)}$$

The complex wave velocity in equations (5.21) cannot be solved analytically for a nonzero Mach number. In order to investigate the individual influence of heating, the solution for an incompressible heated jet is examined. In this case, an explicit analytical expression for the real and imaginary parts of the complex wave velocity can be obtained as below:

$$C_R = \frac{U_a}{1 + T_* L_\beta(\alpha)} \tag{5.22}$$

$$C_I = \frac{U_a\sqrt{T_* L_\beta(\alpha)}}{1 + T_* L_\beta(\alpha)} \tag{5.23}$$

where $T_* = \rho_b/\rho_a$. Since the jet centerline velocity is used in the normalization in this work, $U_a = 1$. Thus, the incompressible vortex layer is unstable to all disturbance wavenumbers, as in the classical Kelvin-Helmholtz problem. Since very short waves for real flows with a finite shear layer thickness are stable, this vortex sheet model is applicable to disturbances

whose wavelength is much longer than the shear layer thickness. This will be further elucidated in subsequent discussion. Since the wavelength of a disturbance is inversely proportional to its wavenumber, long wave approximations are, therefore, characterized by small wavenumbers and thus low frequencies.

Using (5.22) and (5.23), the typical influence of heating on the value of C_I and C_R as functions of the axial wavenumbers for $\beta = 0$ and $\beta = 1$ are plotted in Figures (5.9a) and (5.9b), respectively. It is found that, except for long axisymmetric waves, heating reduces the phase velocity substantially; for example, the phase velocity of an axisymmetric wave with axial wavenumber 7.5 is reduced from 0.53 to 0.36. For waves with α approximately less than 1.5, this reduction is more pronounced for the first helical mode than for the axisymmetric mode.

In the limiting case, the values of C for long wave approximation ($\alpha \rightarrow 0$) can be obtained from (5.22) - (5.23). They are

$$C_R = 1,\ C_I = 0, \quad \text{for } \beta = 0 \tag{5.24}$$

$$C_R = \frac{1}{1+T_*},\ C_I = \frac{\sqrt{T_*}}{1+T_*} \quad \text{for } \beta \neq 0 \tag{5.25}$$

Therefore, a heated vortex sheet is always stable to long axisymmetric modes, but is unstable to all non-axisymmetric modes whose growth rates are reduced by heating. For a cold jet ($T_* = 1$), long waves with axial symmetry travel with the speed of the center of the jet, whereas all helical modes travel with half that speed (Batchelor & Gill 1962). The phase velocity of long axisymmetric waves is independent of heating, whereas that of non axisymmetric waves is substantially reduced by heating.

The stability characteristics of a continuous base velocity profile are in general not expressible in closed form, and, therefore, must be determined numerically. The phase velocity and growth rate as functions of wavenumbers for the tanh velocity profile with $\theta = 1/15$ are displayed in Figure (5.7) for $\beta = 0$ and in Figure (5.8) for $\beta = 1$. Note that axisymmetric disturbances are more unstable in heated jets than in cold jets only at small

axial wavenumbers, and that heating reduces the range of unstable waves. Except for very small axial wavenumbers, heating generally decreases significantly the phase velocity; for example, the phase velocity of a near neutral axisymmetric disturbance is decreased from 0.562 to 0.476. While the phase velocity is rather insensitive to Mach number, it is, except for long axisymmetric waves, substantially reduced by heating.

By using a slightly different velocity profile (profile 1 of Michalke 1984), we found that these stability characteristics are virtually indistinguishable from those of profile (2.28) - (2.30). This insensitivity of the stability characteristics to the details of the (two slightly different mean velocity profiles) convinces us that our results are representative of what might be obtained for a wide class of mean flows with reasonable shapes.

By comparing Figures (5.9 a-b) and Figures (5.10 a-b), the phase velocities obtained from a tanh velocity profile with $\theta = 1/15$ and the vortex sheet model are seen to exhibit very similar behavior. In contrast, the quantitative values of the amplification factors from these two profiles are considerably different (except at small wavenumbers); this shows the true limitation of a vortex sheet theory.

Further, the long wave results for $\theta = 1/15$ are consistent with Jarrah's (1989) calculations on mean velocity profiles with a different momentum thickness, namely $\theta = 1/5$. For shear flows, as previously mentioned, the stability behavior of a disturbance which has a large wavelength in comparison to a characteristic profile length (e.g., shear layer thickness) is unaffected by the form of velocity profiles. The validity of the preceding statement needs some clarification, though. For round jets, we found that this statement is true for axisymmetric modes but not strictly valid for helical modes. To be precise, the phase velocities of long waves (i.e., $\alpha \to 0$) in a tanh velocity profile with a finite shear layer thickness, whether axisymmetric or helical, agreed with that obtained from simple vortex models. For the corresponding growth rates, this agreement is found in axisymmetric modes but not in helical modes. This disagreement is exacerbated as the helical

mode number and the shear layer thickness is increased.

5.4 Mode Number and Shear Layer Thickness Effects

Since the evolution of instability modes in an axisymmetric jet is affected by the shear layer thickness and the mode number, these effects are concurrently discussed in this section. The length scale characterizing the effect of shear layer thickness is the dimensionless momentum thickness θ which, in this work, is normalized with the jet radius. There have now been a number of theoretical studies on the stability characteristics of incompressible round jets. In their theoretical work, Batchelor & Gill (1962) found that a top-hat jet velocity profile (i.e, $\theta \rightarrow 0$), which represents the mean flow very close to jet exit, is unstable to a small disturbance for all axial and azimuthal wavenumbers. Their analysis is supported by Plaschko (1979) who found that the thin jet shear layer (i.e., small θ) for a slowly diverging jet is unstable to a large number of discrete azimuthal modes. The importance of the parameter θ in the initial evolution of an axisymmetric jet is further explored in detail by Cohen (1986). By using a scaling analysis, he found that all azimuthal modes will amplify at identical rates whenever $\theta \ll 1$ and $(\lambda_x/\lambda_\beta)^2 \ll 1$; where λ_x and λ_β are the streamwise and the azimuthal wavelengths. This implies that the results obtained from the thin jet shear layer are equivalent to the planar mixing layer where the stability characteristics depend only on a single parameter α.

Although the shear layer near the jet nozzle exit is unstable to a large number of azimuthal modes, only the first few are considered since these are the modes that dominate the coherent structures experimentally (Cohen 1986). In fact, the geometrical design of most laboratory jets, which consists of a small nozzle emanating from a large chamber where an acoustic excitation signal is introduced, cuts off higher azimuthal modes. It is for this reason that azimuthal excitation of a jet is usually accomplished by a series of circumferentially placed acoustic "drivers". To be more precise, a linearized monochromatic pressure wave traveling inside a plane duct, where for simplicity the mean flow in the duct is set to zero, before exiting downstream to the jet nozzle is used for illustration. This

wave is of the form

$$\exp(-i\omega_e t)\cos(\frac{n_d \pi y}{h})\exp i\left[\frac{\omega_e^2}{a_{\infty^2}} - \frac{n_d^2\pi^2}{h^2}\right]^{\frac{1}{2}} x \tag{5.26}$$

where ω_e is the excitation frequency, h is the duct height, a_∞ is the sound speed, y is the cross stream direction, x is the downstream direction, and n_d is the duct mode number. Equation (5.26) shows that the fundamental mode ($n_d = 0$) will always propagate sinusoidally downstream. However, if the excitation frequency ω_e is small such that $\omega_e < n_d \pi a_\infty / h$, then the behavior of the acoustic mode along the x axis is purely exponential, and the wave is said to be cut-off. Therefore, at a given frequency, only a finite number of modes can propagate out of the jet nozzle exit. In order to excite the instability wave whose frequency is on the order of the ratio of the dimensional jet exit speed (U_j) and the shear layer thickness (θ), the excitation frequency of acoustic waves corresponding to most laboratory experiments is often quite low. Consequently, only the fundamental plane acoustic wave survives through the nozzle exit. This implies that if the nozzle is round, then an axisymmetric low frequency acoustic wave, which accentuates an axisymmetric instability wave, will be observed at the nozzle exit. Farther downstream where the rolling-up of coherent structure occurs, the axisymmetric and the first azimuthal components have been experimently observed to predominate the flows. Therefore, the stability calculations are focused mainly on these modes.

The parameter θ appears explicitly in the velocity profile (2.28) - (2.30). If the flow is compressible, θ also appears as a parameter in the base density via the coupling with the velocity profile. In order to single out the effect of the shear layer thickness, the base density profile is taken to be constant (i.e., $M_j = 0$ and $T_* = 1$). In this work, the tanh velocity profiles for two different axial locations are investigated, although the analysis can be carried out to include profiles at an arbitrary location, provided that the mean profiles are known a priori. The values of momentum thickness which characterize the two locations are chosen to be $\theta = 1/15$ and $\theta = 1/5$. Crighton & Gaster (1976) reported

that these values of θ correspond to axial positions 0.5 and 2.7 diameters downstream of the nozzle exit in the experimental measurements of Crow & Champagne (1971). Of course, the functional relation between θ and the streamwise direction, which depends on M_j and T_*, will vary from experiment to experiment.

The growth rate and phase velocity of the first three azimuthal disturbances for a cold and incompressible jet for $\theta = 1/15$ and $\theta = 1/5$ are summarized in Figure (5.11) and Figure (5.12), respectively. In Figure (5.11), the jet shear layer is dispersive to waves longer than the most amplified wave and relatively nondispersive for shorter waves; $\beta = 1$ produces the largest range of (approximately) nondispersive waves. The phase velocity of axisymmetric modes decreases with α from unity to 0.56. In contrast, the phase velocities of helical modes ($\beta = 1, 2$) increases with α from 0.5 to 0.56. In particular, the phase velocity for a neutral wave is approximately 56 % of the jet centerline velocity, and it is independent of the mode numbers when the shear layer is very thin. An important consequence of the almost nondispersive character of azimuthal modes over a broad range of wavenumbers is that it allows waves to interact resonantly. We shall show in Chapter 6 that this resonance wave interaction phenomenon is, in fact, a mechanism for the strong growth of a subharmonic disturbance. Further, the axisymmetric ($\beta = 0$) mode has the highest maximum growth rate of 0.680, the $\beta = 1$ mode amplifies at a slightly lower rate of 0.663, while the most unstable rate of $\beta = 2$ is 0.595. This is reasonable, since as $\theta \rightarrow 0$, the results of the tanh profiles tend to that obtained from vortex sheet analysis where all azimuthal modes amplify at the same rate at large enough axial wavenumbers.

It is interesting to recall that the phase velocity for all azimuthal waves for a simple vortex sheet (i.e. for $\theta = 0$) is at approximately 50% of the jet centerline velocity. This shows that although the vortex layer under-estimates the phase velocity of the tanh velocity profiles at $\theta = 1/15$ by about 11 %, it correctly predicts that all azimuthal disturbances with high axial wavenumbers propagate at the same phase velocity.

Farther downstream at $\theta = 1/5$, Figure (5.12a) shows the $\beta = 1$, $\beta = 2$, and $\beta = 0$, are respectively the most, the second, and the third unstable modes. The maximum growth rates of the disturbances with $\beta = 1$, $\beta = 0$, and $\beta = 2$ are 0.173, 0.134 and 0.039, respectively. Therefore, if both the axisymmetric and helical modes have the same initial amplitudes, the helical mode will eventually dominate downstream of the end of the potential core. The emergence of $\beta = 1$ mode as the dominant instability mode towards the end of the potential core is also observed by Michalke & Hermann (1982), Cohen (1986) and Miles & Raman (1988). Batchelor & Gill (1962) theoretically demonstrated that the " fully developed" jet, after the end of a potential core, is unstable only to the $\beta = 1$ mode. For the tanh profiles, the phase velocities of axisymmetric modes are seen to decrease with wavenumbers from unity to 0.71. In contrast, the phase velocities of modes $\beta = 1$ and $\beta = 2$ increase with wavenumbers from 0.5 to 0.67 and from 0.5 to 0.56, respectively. Owing to a greater value of θ, the near-neutral azimuthal modes now travel with different phase velocities.

By comparing Figure (5.11) and Figure (5.12), we found that as the shear layer thickness grows, not only does the wavenumber of the maximum local growth rate and the range of unstable waves becomes smaller, but the range of nondispersive waves is significantly reduced. It should be noted that, as pointed out by Petersen (1978), each coalescence of coherent structures will result in a bigger value of θ, making the layer more dispersive to unstable waves . These results are consistent with the numerical results of Petersen (1978), Michalke & Hermann (1982) and Cohen (1986) which are based on spatial stability calculations.

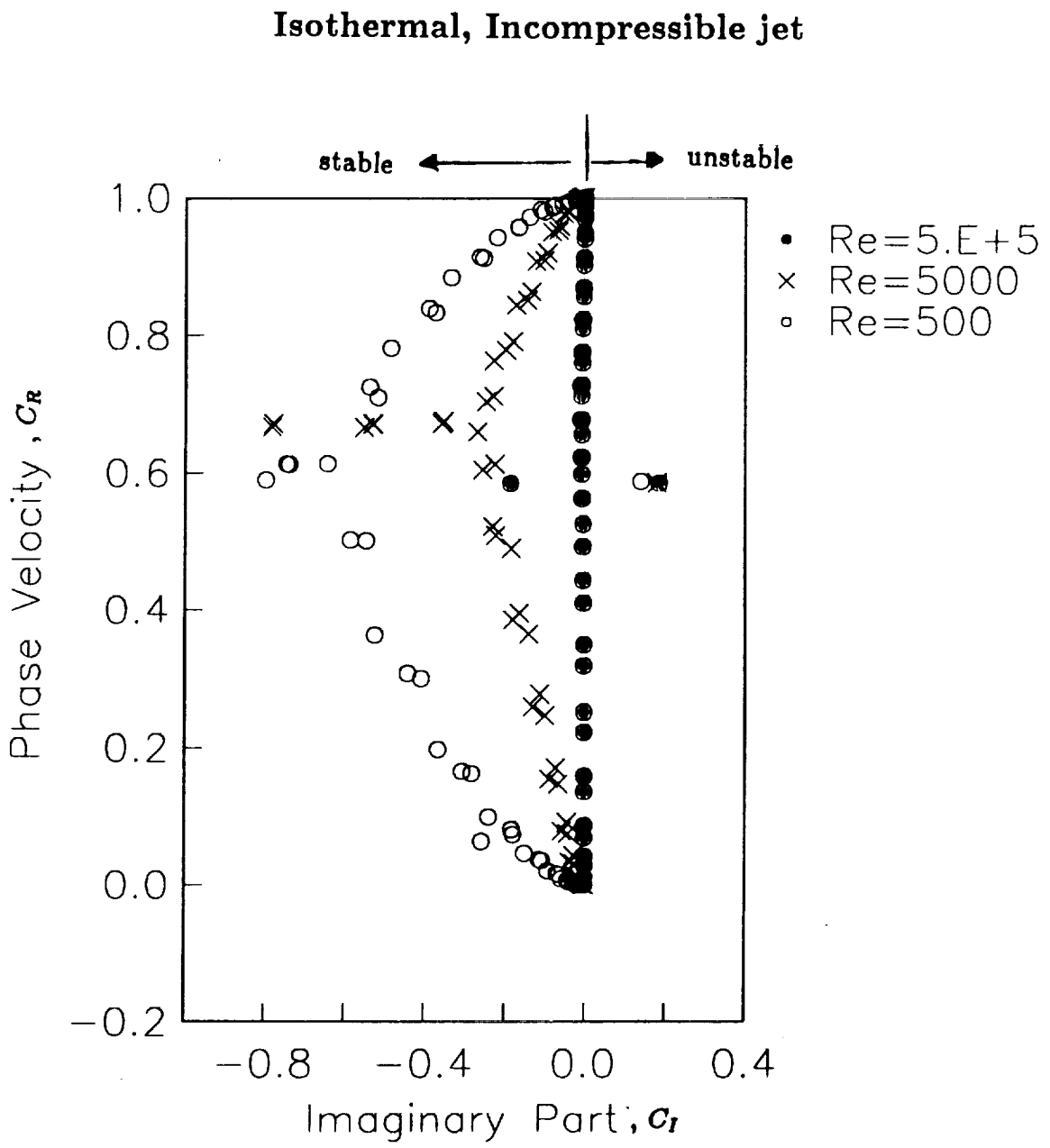

Fig. 5.1 The effect of Re on the spectrum of linear, parallel flow, temporal eigenvalues using 31 collocation points for $\theta = 1/15$, $M_j = 0$, $T_* = 1$, $\alpha = 3.66$, and $\beta = 0$.

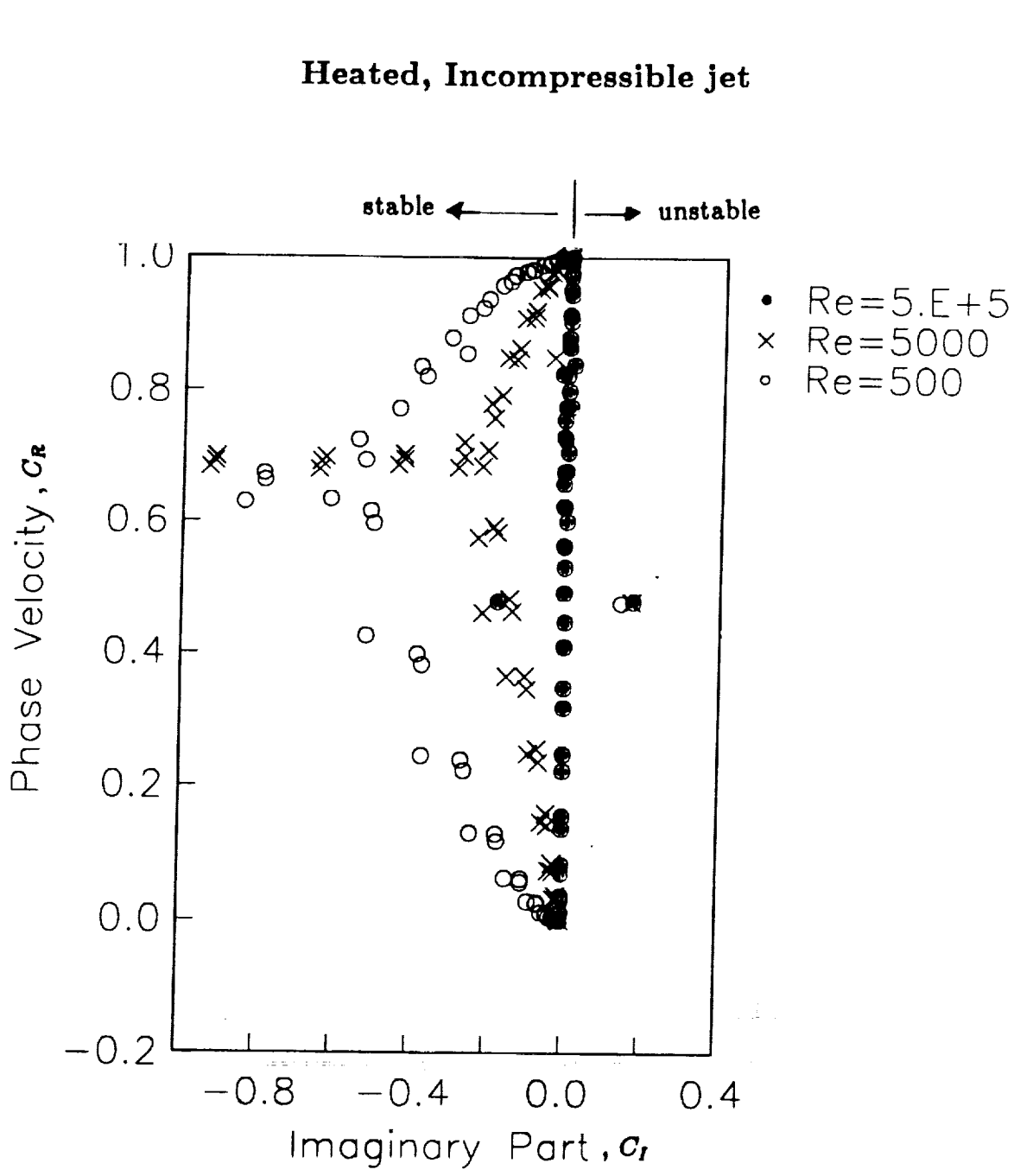

Fig. 5.2 The effect of Re on the spectrum of linear, parallel flow, temporal eigenvalues using 31 collocation points for $\theta = 1/15$, $M_j = 0$, $T_* = 2$, $\alpha = 3.66$, and $\beta = 1$.

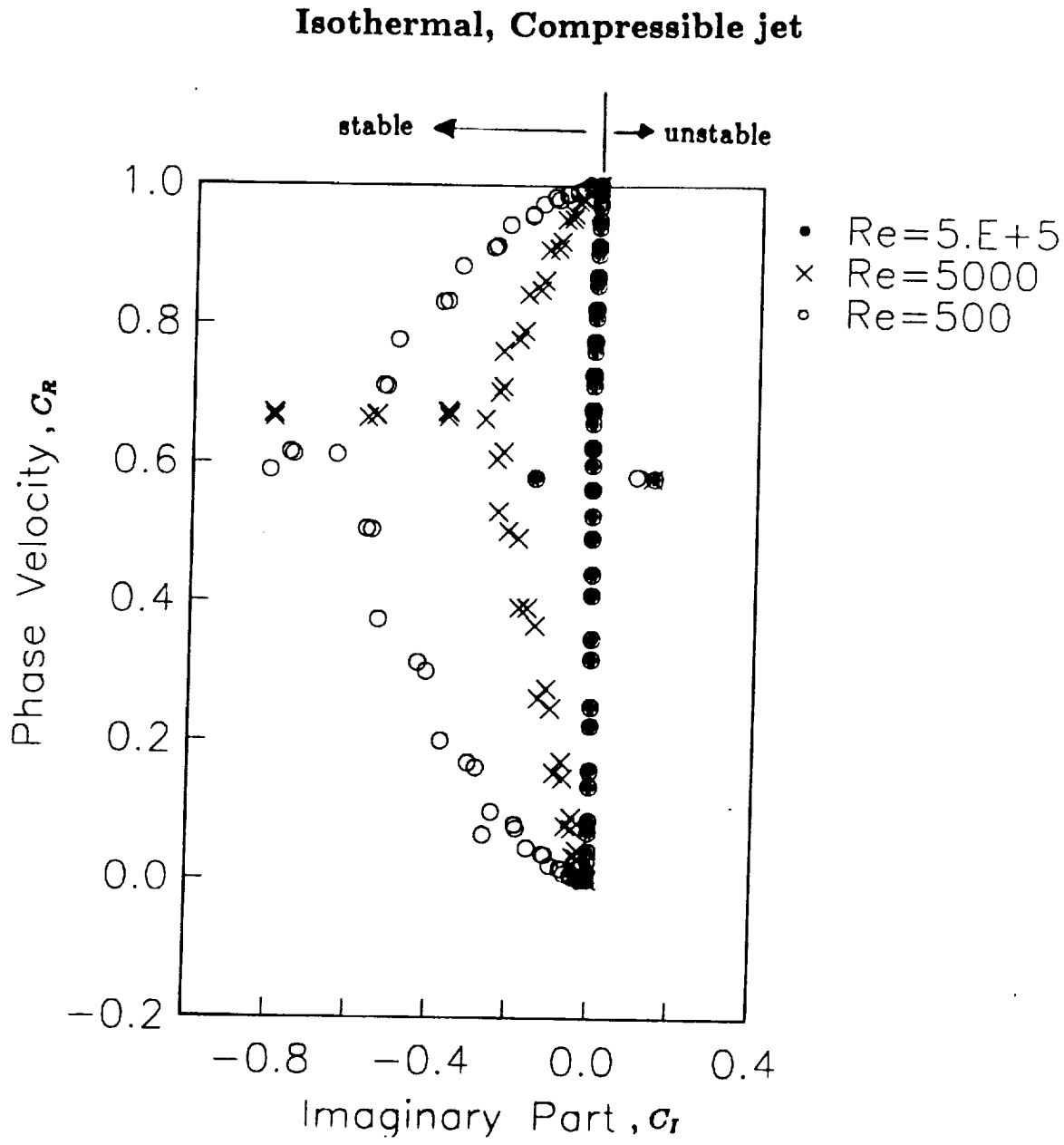

Fig. 5.3 The effect of Re on the spectrum of linear, parallel flow, temporal eigenvalues using 31 collocation points for $\theta = 1/15$, $M_j = 0.8$, $T_* = 1$, $\alpha = 3.66$, and $\beta = 0$.

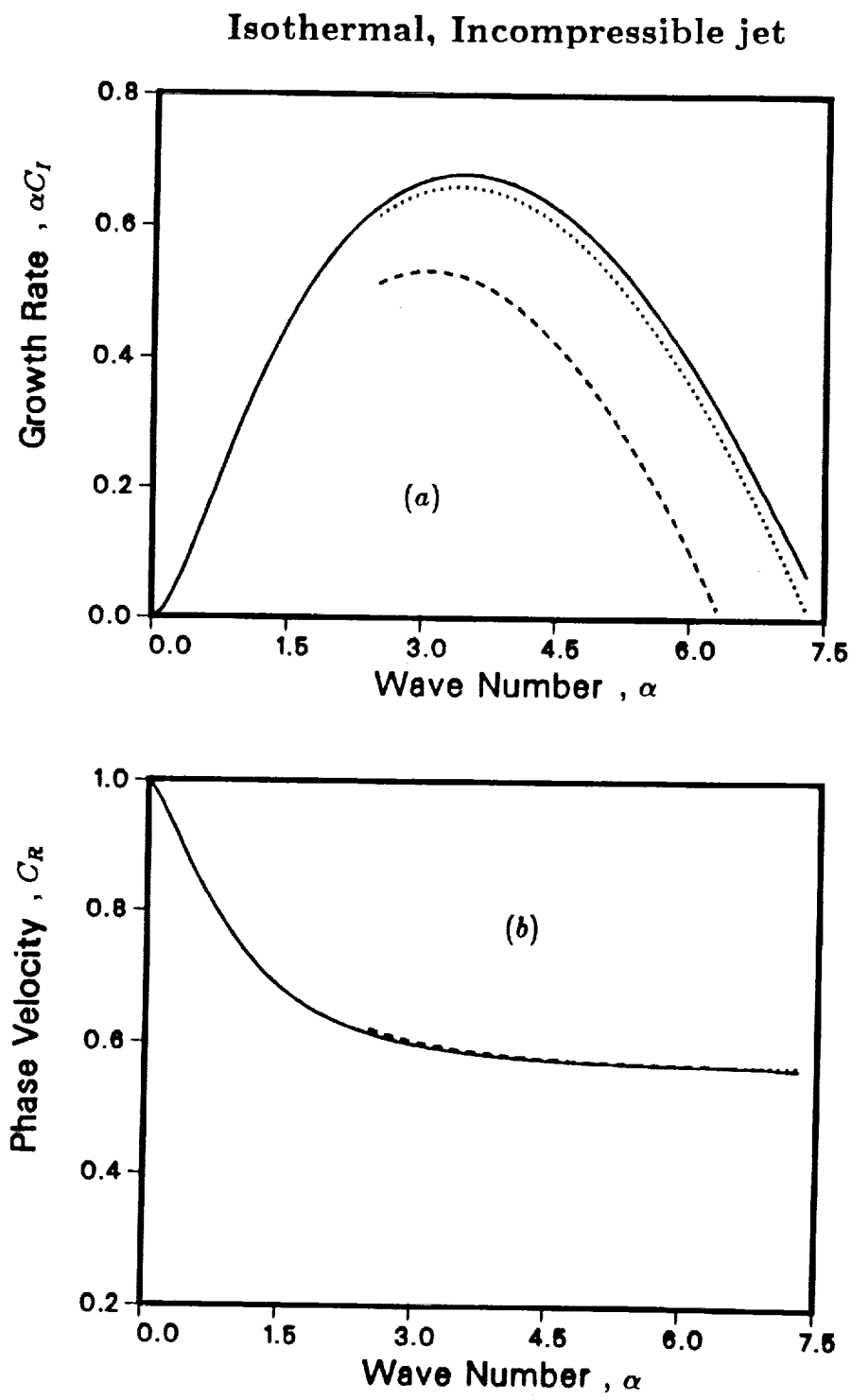

Fig. 5.4 (a) Growth rate and (b) phase velocity of unheated, axisymmetric modes for various Re: $Re = \infty$ (solid lines), $Re = 5000$ (dot), Re =500 (dash). Calculations are for $\theta = 1/15$, $M_j = 0$, $T_* = 1$.

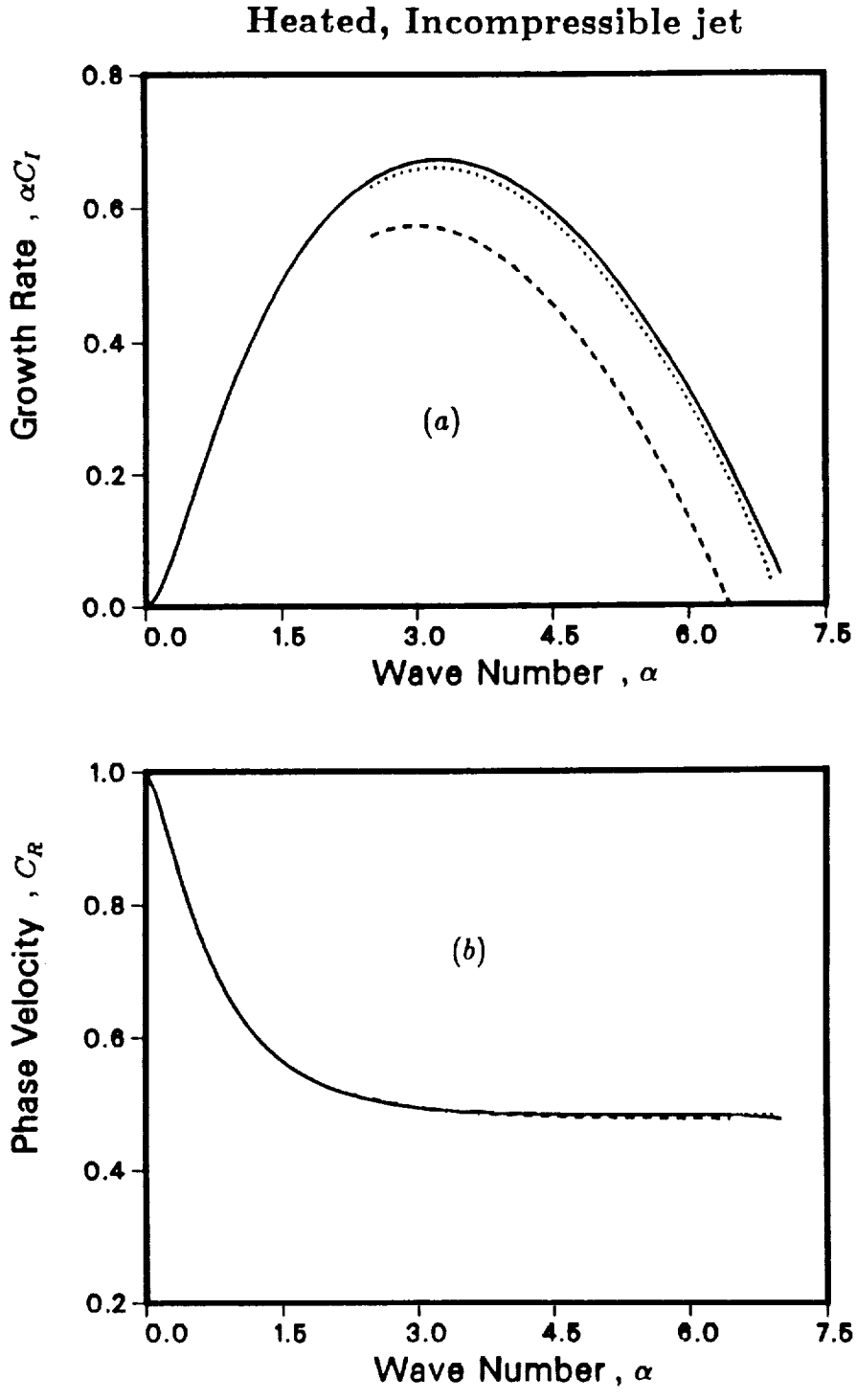

Fig. 5.5 (a) Growth rate and (b) phase velocity of heated, axisymmetric modes for various Re: $Re = \infty$ (solid lines), $Re = 5000$ (dot), Re =500 (dash). Calculations are for $\theta = 1/15$, $M_j = 0$, $T_* = 2$.

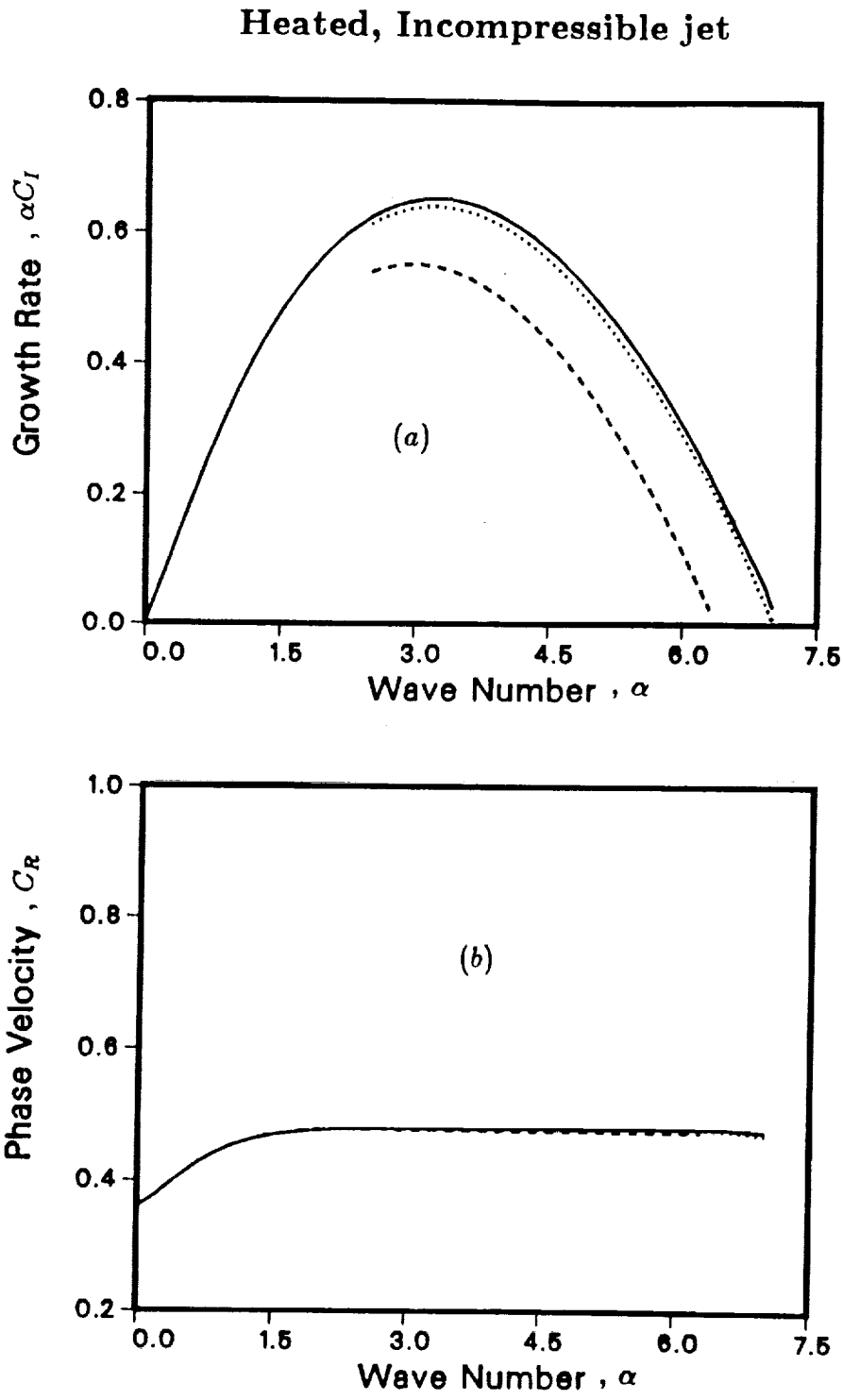

Fig. 5.6 (a) Growth rate and (b) phase velocity of heated, $\beta = 1$ modes for various Re: $Re = \infty$ (solid lines), $Re = 5000$ (dot), Re =500 (dash). Calculations are for $\theta = 1/15$, $M_j = 0$, $T_* = 2$.

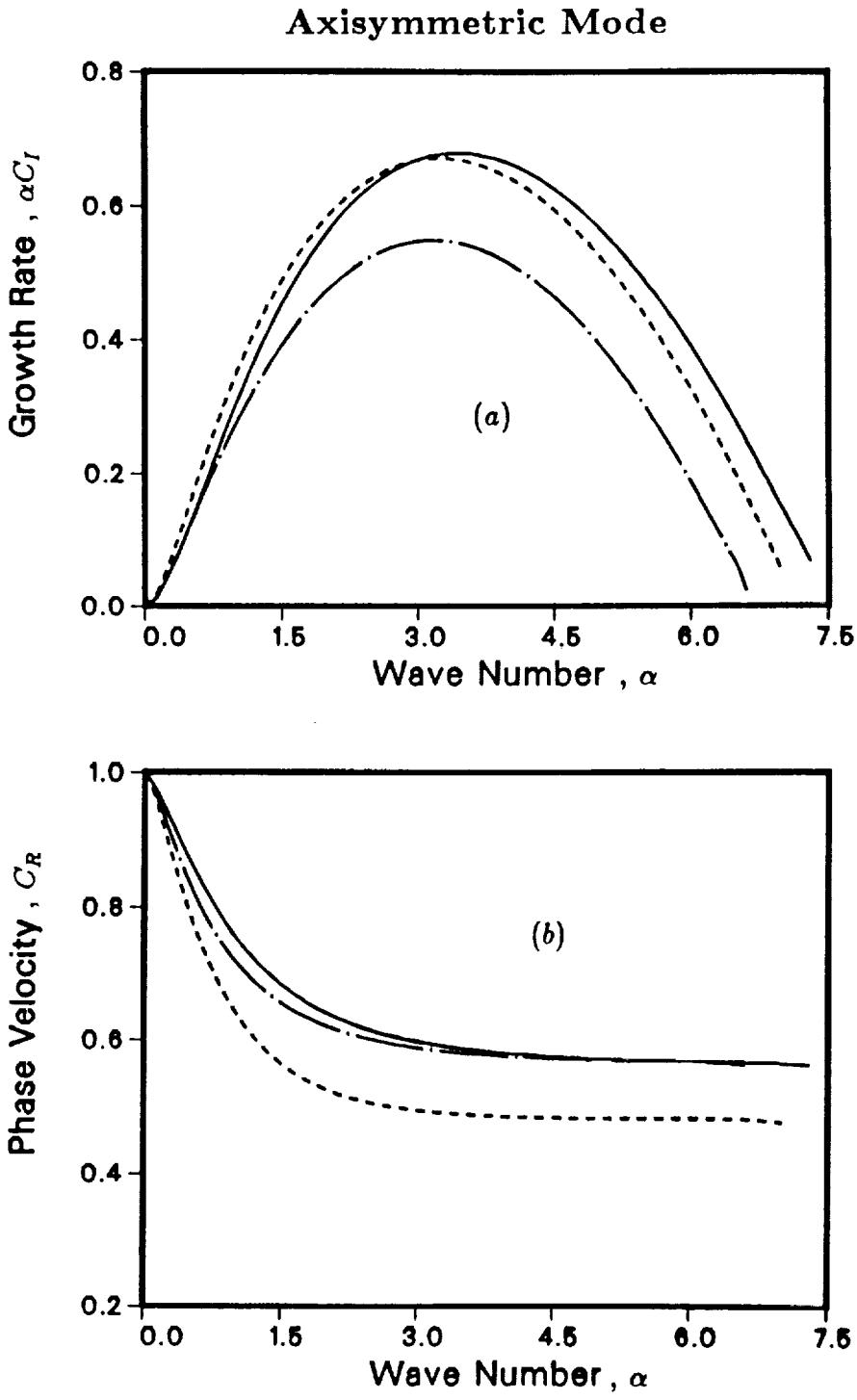

Fig. 5.7 Inviscid (a) growth rate and (b) phase velocity of the azimuthal modes $\beta = 0$ and $\theta = 1/15$ for various M_j and T_j. $M_j = 0$, $T_* = 1$ (solid lines). $M_j = 0.8$, $T_* = 1$ (chaindot). $M_j = 0$, $T_* = 2$ (dash).

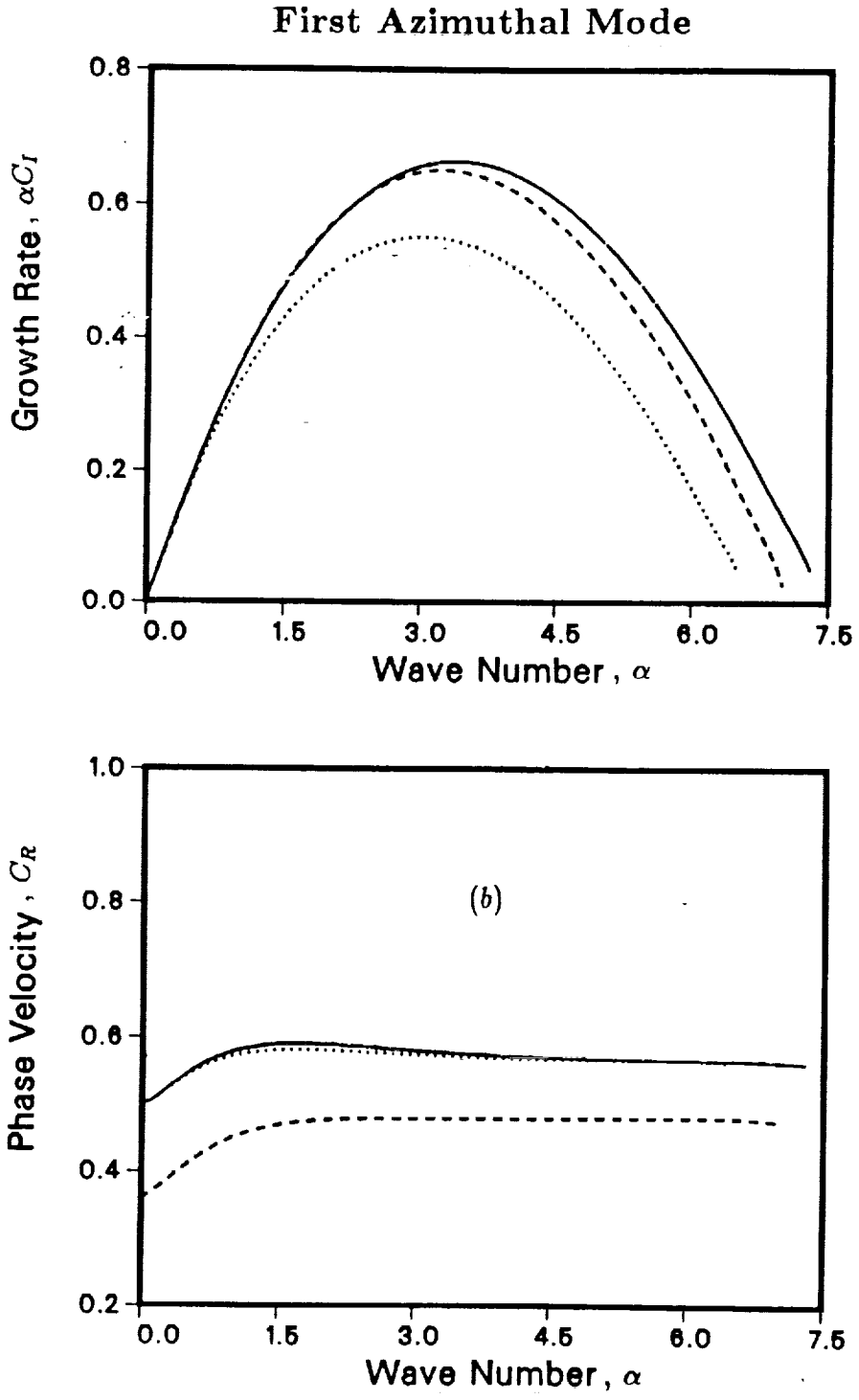

Fig. 5.8 Inviscid (a) growth rate and (b) phase velocity of the azimuthal modes $\beta = 1$ and $\theta = 1/15$ for various M_j and T_j. $M_j = 0$, $T_* = 1$ (solid lines). $M_j = 0.8$, $T_* = 1$ (dot). $M_j = 0$, $T_* = 2$ (dash).

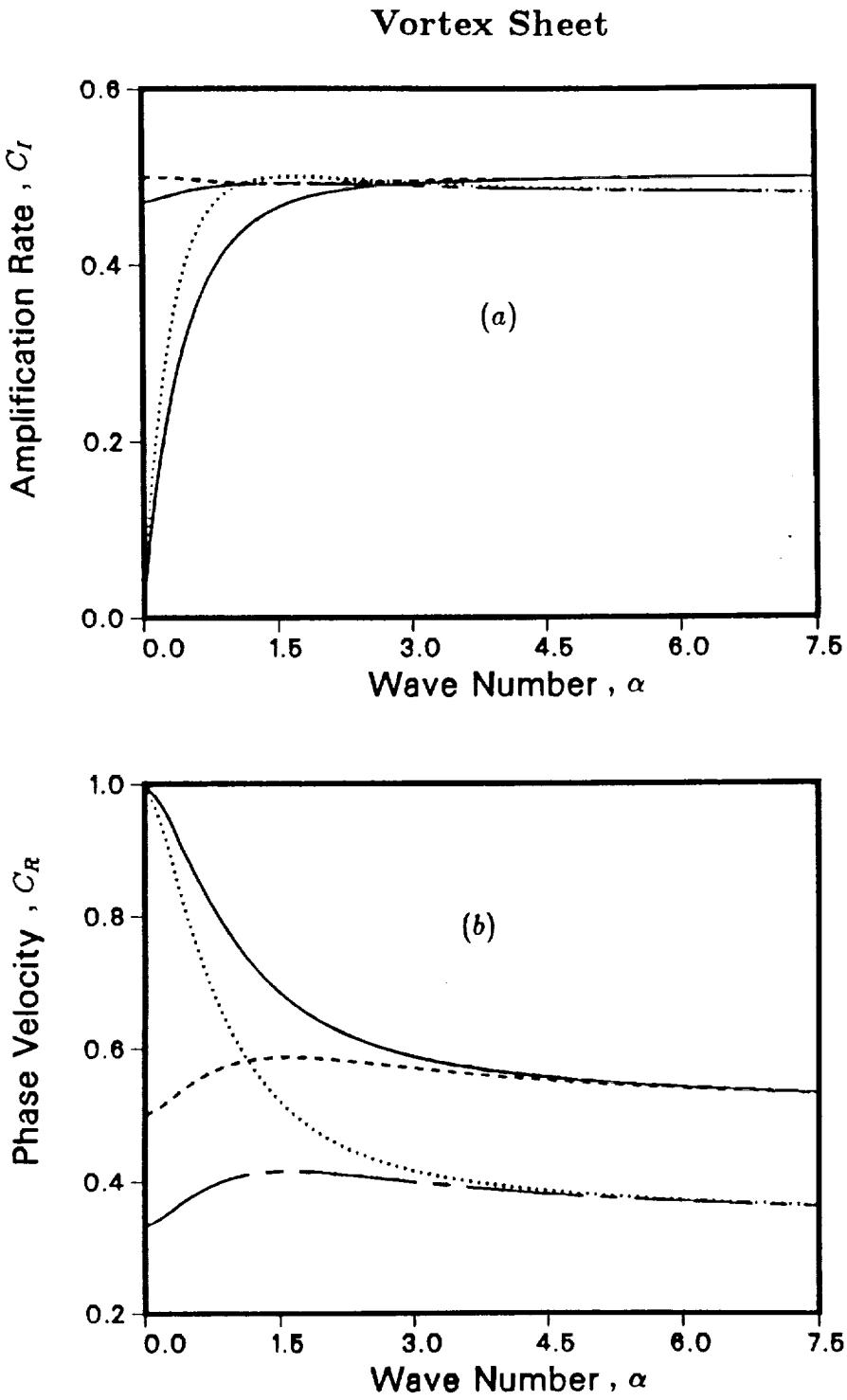

Fig. 5.9 (a) Amplification rate (C_I) and (b) phase velocity (C_R) of a vortex sheet for $\beta = 0$ and $\beta = 1$ modes. $\beta = 0$, $T_* = 1$ (solid lines). $\beta = 0$, $T_* = 2$ (dot). $\beta = 1$, $T_* = 1$ (dash). $\beta = 1$, $T_* = 2$ (chaindash). $M_j = M_a = 0$.

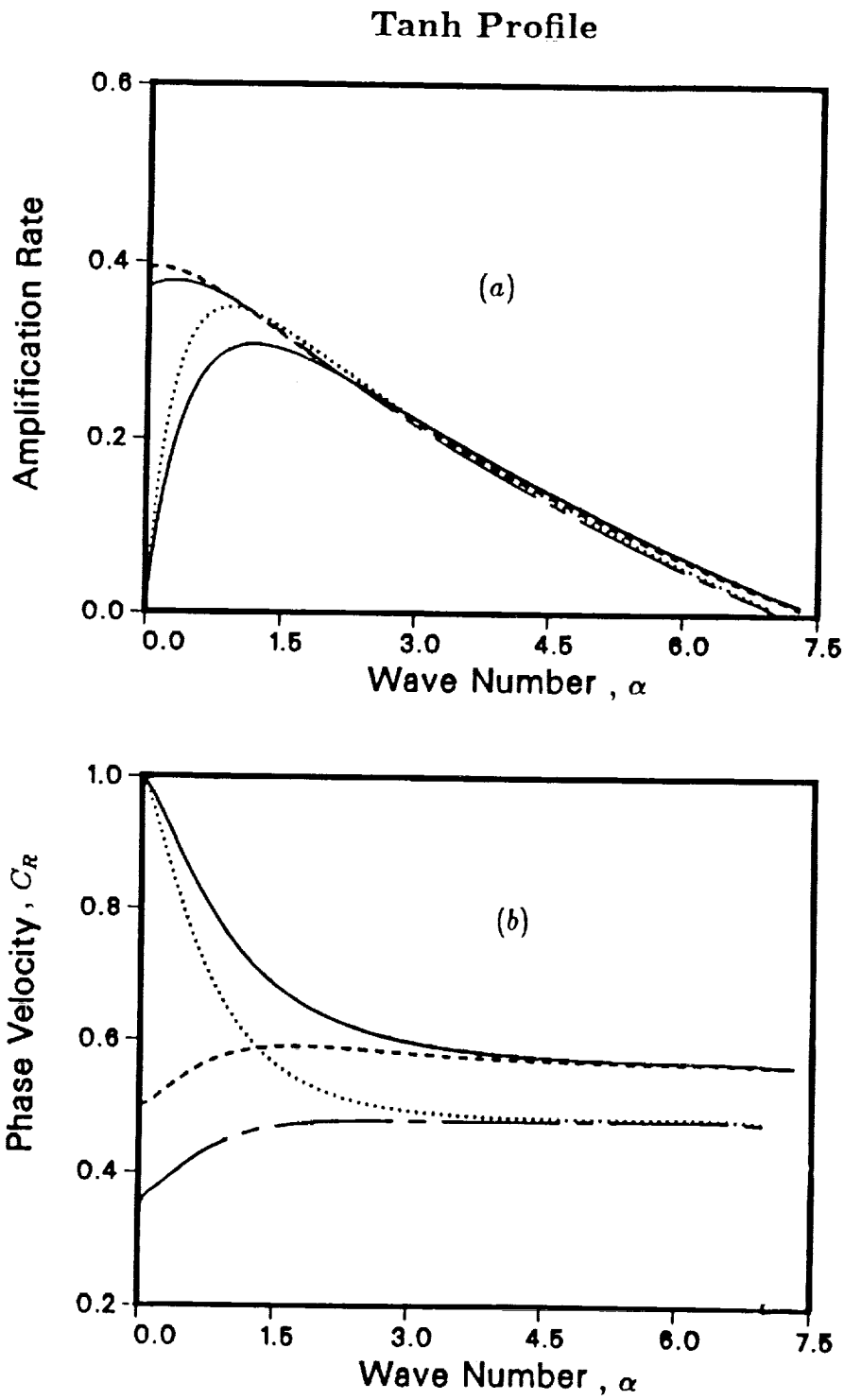

Fig. 5.10 Inviscid (a) growth rate and (b) phase velocity of the azimuthal modes $\beta = 0$ and $\beta = 1$ for $\theta = 1/15$ and $M_j = 0$. $\beta = 0$, $T_* = 1$ (solid lines). $\beta = 0$, $T_* = 2$ (dot). $\beta = 1$, $T_* = 1$ (dash). $\beta = 1$, $T_* = 2$ (chaindash). $M_j = M_a = 0$.

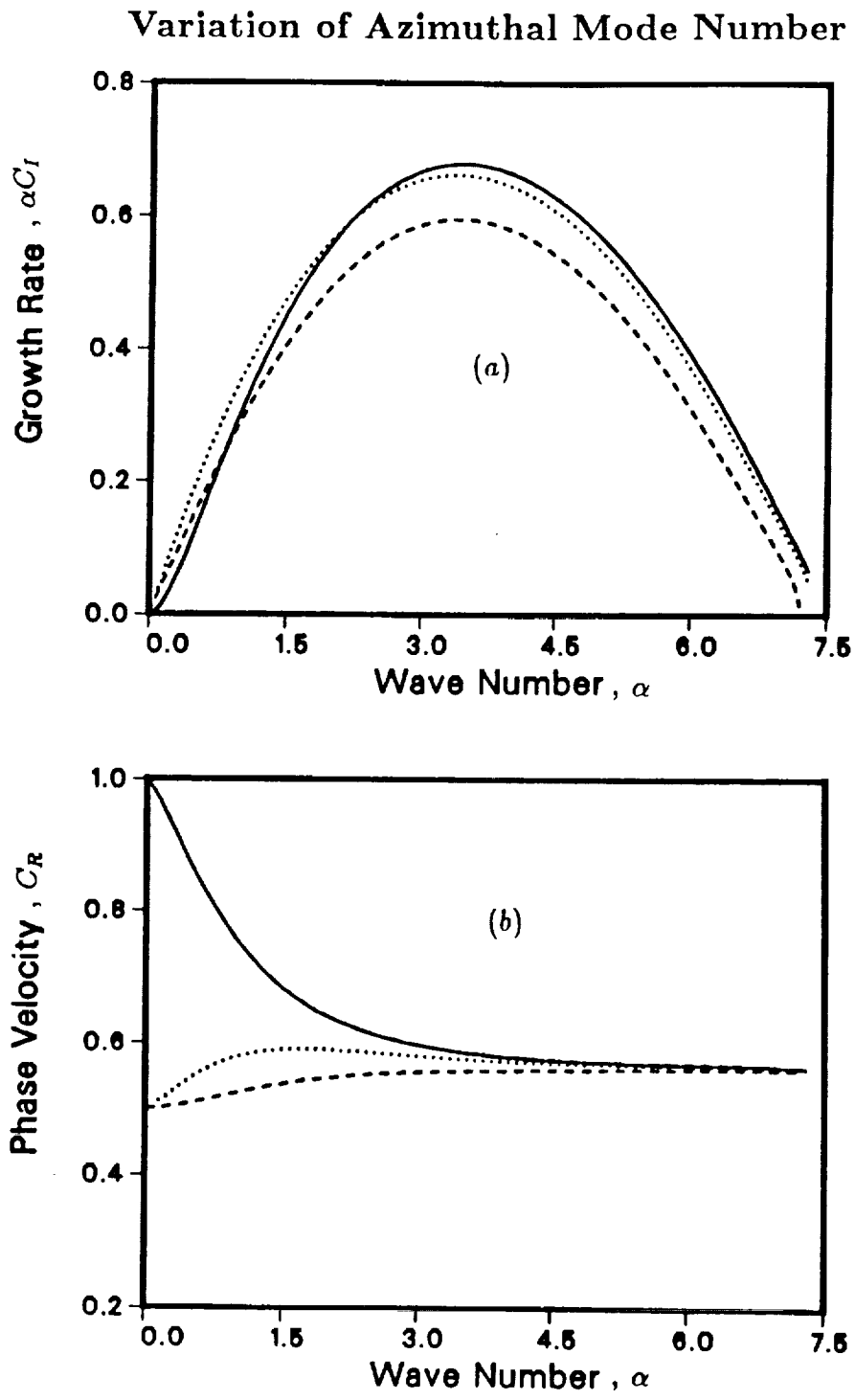

Fig. 5.11 Inviscid (a) growth rate and (b) phase velocity of the azimuthal modes $\beta = 0$ (solid lines), $\beta = 1$ (dot), and $\beta = 2$ (dash). Calculations are for $\theta = 1/15$, $M_j = 0$, $T_* = 1$.

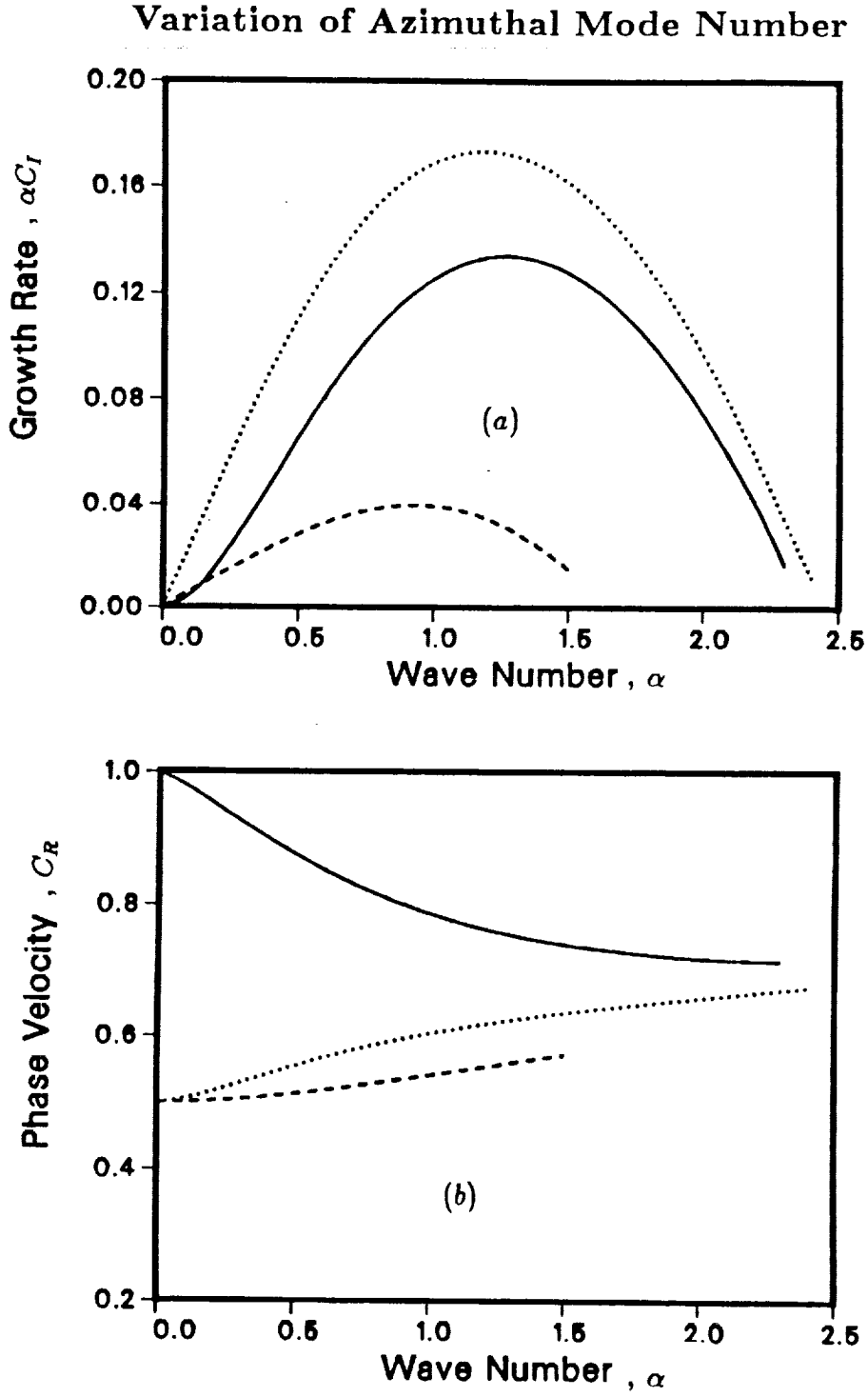

Fig. 5.12 Inviscid (a) growth rate and (b) phase velocity of the azimuthal modes $\beta = 0$ (solid lines), $\beta = 1$ (dot), and $\beta = 2$ (dash). Calculations are for $\theta = 1/5$, $M_j = 0$, $T_* = 1$.

Chapter 6

SUBHARMONIC INSTABILITY MODES

As discussed in Chapter 3, a principal effect of excitation is to generate a primary wave which grows in amplitude, and then reaches a finite amplitude (i.e., saturation) as it propagates downstream. In turbulent flows, this primary wave is usually called a coherent structure. An objective of this work is to investigate, via a secondary instability theory, the conditions under which this primary wave can destabilize a subharmonic mode. Since subharmonic disturbances generate vortex pairing (and vice-versa), in a physical sense, the present chapter focuses on the conditions, as a function of Mach number, temperature ratio etc, which enhance, or at least influence, vortex pairing. This process of merging (or pairing or amalgamation), is generally believed to be an important mechanism in the spreading of jet flows.

Although secondary instability theory in round jets is presently still new, its predictive capabilities are, for the most part, undisputed in incompressible planar mixing layers and boundary layer flows. We now digress momentarily to review some of these known results, and outline some distinct features of round jets that are absent in mixing layers and boundary layers.

By using a secondary instability analysis, Kelly (1967) argued that the sequential merging of vortices in planar mixing layers can be attributed to the subharmonic instability modes in a periodic base flow. These modes, which absorb energy from the mean flow via the catalytic role of a periodic fundamental mode, predominate in the flow at approximately the location where vortex pairing occurs. Ho & Huang (1982) also demonstrated

that after each pairing of coherent structures, the peak frequency of the energy spectrum was halved, and the merging process was found to be at the location where the sub-harmonic modes become the dominant instability modes. Their findings reinforced the predictive capability of a secondary instability theory.

Further, Herbert (1983, 1984, 1985) demonstrated that a secondary instability analysis can unravel some of the fundamental routes to transition in incompressible wall-bounded flows. In a particular route, he has shown that the essential flow physics associated with the formation of staggered lambda vortices in boundary layers, although seemingly formidable, can be revealed by a linear secondary instability theory. It may be remarked that boundary layer flows are fundamentally different from shear flows. This difference is marked by the presence of a solid wall which constitutes an additional viscous no-slip condition on the velocity perturbations. Consequently, the growth of an instability mode is induced by viscosity, and hence, the growth rate is small. This means that when the viscosity is turned off in wall-bounded boundary layer flows, there are no instability modes. In contrast, the instability modes in shear flows are predominantly inviscid, and the growth rates are generally large; at least in the sense that the amplitude of the fundamental changes by a significant amount in one period or wavelength.

Jets and planar mixing layers belong to the same class of flows, which are characterized by the existence of a generalized inflection point in the parallel flow profiles. However, the former have a few distinct features that are absent in the latter. The qualities that discriminate jets from mixing layers are:

1. The radius of a jet nozzle constitutes a length scale, which is used in our normalization, in addition to the shear layer thickness. Thus the shear layer thickness becomes a bona-fide parameter for a jet; this quantity can be scaled out for a mixing layer.

2. The vortex stretching term, which represents the extension or contraction of vorticity lines by the strain rate of the flow, is nonzero for azimuthal disturbances.

Because of (1) above, the symmetry of the base vorticity about the critical point of a jet is broken, and, as a result, the waves are dispersive so that waves with different wavenumbers are convected with the flow at different speeds. Furthermore, the criterion for the existence of an inflectional mode is now a function of the mean flow and the mode number, β, of the instability mode (Batchelor & Gill 1962). In contrast, the necessary and sufficient condition for the existence of an instability mode in a planar mixing layer depends on the base flow alone.

We will employ a generalization of the current incompressible secondary instability theories to gain a better understanding of the mechanisms governing the amalgamation of coherent structures in compressible round jets. High speed jets, whether for heating or for nonzero Mach number, introduce density perturbations. These result in quadratic and cubic interactions between the density perturbations and other types of perturbations. This cubic interaction results in considerable algebra in the secondary instability analysis, and therefore necessitate some simplifications which we will now discuss.

Recall that a deficiency of linear stability analysis is that it cannot determine a unique amplitude A. In this work, the amplitude A is a small arbitrary prescribed quantity which corresponds to the maximum amplitude of the streamwise velocity perturbation. A consequence of this normalization is that if all other types of perturbations are at most the same order as A, then the quadratic interaction between $\mathbf{F}_1$ and $\mathbf{F}_2$ will play a more important role than the cubic interaction between $\mathbf{F}_1$ and itself and $\mathbf{F}_2$. This is because, for small A, the quadratic interaction is of order $A\varepsilon$ while the cubic interaction is of order $A^2\varepsilon$. There are, however, possible situations where this definition of A might cause inconsistencies with our analysis. These happen in strongly heated jets where the parallel stability analysis provides a density eigenfunction that is much greater than the streamwise velocity eigenfunction. As a result, the magnitude of the density perturbation ($A\rho_1$) will no longer be small compared to the unperturbed density (ρ_0). This will invalidate the

present stability analysis where the amplitudes of all types of perturbations are assumed to be small compared to the mean flow. Nevertheless, these possibilities can be avoided by normalizing A so that it corresponds to the maximum amplitude of the density perturbation. This implies that when A is small, the amplitude of all types of perturbations will be small too. Therefore, in this work, we shall focus on the cases where A^2 and higher order terms can be neglected. The preceding remark is consistent with our representation of the flow arising from the finite-amplitude growth of the primary disturbance associated with the parallel base flow. Formally, this flow [say, $\breve{u}$] may be expanded as

$$\breve{u}(x,r,t) = u_0(r) + A^2 u_0^1 + \cdots + A\left\{u_1(r) + A^2 u_1^1(r) + \cdots\right\}\exp(i\alpha_1 x) + \left\{A^2 u_2^1 + \cdots\right\}\exp(2i\alpha_1) + \cdots + c.c \tag{6.1}$$

where the superscript 1 denotes a correction due to the nonlinear self-interactions of the primary wave, and the finite amplitude A can, in principle, be obtained from the so-called Landau's equation (Jarrah 1989). Since the periodic base flow we have modeled (i.e., $u_0 + (Au_1\exp(i\alpha_1 x) + c.c.)$) is formally valid to $O(A)$, on the basis of the expansion (6.1), any quantity involving A^2 and higher order terms in the secondary stability analysis should be truncated. Further, as noted by Kelly, we also assume that the terms of $O(A)$ and higher in (6.1) do not eliminate the generalized inflection point associated with the parallel mean flow, as otherwise, the perturbation analysis will be invalid.

Fully developed coherent structures (or roughly, vortices) can be viewed as manifestations of a primary instability wave that propagates and grows in the downstream direction. Although the quantitative experimental data on the vortex-pairing scenario in round jets is presently still very scant, the evidence of the pairing phenomenon can be seen in the experimental work of Wille (1963) and Reynolds (1988). In our study , the merging of coherent structures is idealized as being composed of two externally excited disturbances: an axisymmetric fundamental wave and its subharmonic. The fundamental wave is chosen to be axisymmetric for two reasons. First, the axisymmetric geometry of a jet nozzle tends

to accentuate an axisymmetric wave near the nozzle. Secondly, the resonance condition on mode numbers, which has been established in Chapter 3, can be satisfied exactly for a subharmonic mode with an arbitrary mode number. Further, the merging of two ring-like coherent structures is idealized as the resonant interaction between two axisymmetric waves. And, any appearance of helical motions can be attributed to a helical subharmonic resonanting with its axisymmetric fundamental. This idealized model, which assumes that other frequencies and fine scale motions play a minor role in the overall flow physics describing the merging of coherent structures, provides a blueprint for future studies and comparisons.

To recap, the assumptions used in the secondary instability analysis are:

1. The magnitude of the subharmonic disturbance is sufficiently small to allow linearization about the primary wave and the parallel base flow.

2. The mean flow profiles are kept unchanged and the mode shape (i.e., the cross-space structure) of the primary wave is given by a linear theory even though the amplitude of this wave may be quite large (say, $A = 0.10$). Some justification of this assumption lies in the work of Petersen & Samet (1988).

3. We shall assume that A is a *prescribed* constant, although in experiments we find that during and after saturation, while the subharmonic is growing, A is a slow function of x. In our temporal theory, this translates into $A = A(t)$; we ignore this slow dependence on time.

A consequence of these assumptions is that the stability characteristics of the fundamental mode can be approximated by the linear modes of parallel flow analysis. It may be reiterated that the disturbances are normalized such that A is the amplitude corresponding to the maximum of the streamwise velocity perturbation of the primary wave, and we consider a disturbance to be an infinite wave train that is spatially periodic but temporally

growing.

6.1 Resonance Conditions

In the method of multiple scales, we considered two small amplitude waves of arbitrary wavenumbers and growth rates evolving temporally in a parallel shear flow. The lowest order nonlinear interaction can occur only through quadratic wave interactions. In a perturbation scheme, the flow field at this order may be thought of as the response of a linear oscillator to a small forcing function comprised of the quadratic wave (or, oscillation) interaction terms. The response of the oscillator to this small forcing function is small unless there is a resonant wave interaction. This happens when the growth rate, mode number and wavenumber of a forced wave, generated by the forcing term, are the same as that of an instability wave of the parallel flow. A consequence of the quadratic wave interactions is an enhancement of the transfer of energy from the mean shear flow to the forced wave, which after a sufficient period of time, grows to an amplitude that is comparable in size to a primary mode associated with the roll-up of a coherent structure. Recall that in order to have resonant wave interactions, the two unstable wave modes must fulfill the following resonance conditions:

$$|\alpha_1| C_I(|\alpha_1|, |\beta_1|) + |\alpha_2| C_I(|\alpha_2|, |\beta_2|) = |\alpha_2 + \alpha_1| C_I(|\alpha_2 + \alpha_1|, |\beta_1 + \beta_2|) \tag{3.16}$$

$$\alpha_2 C_R(|\alpha_1|, |\beta_1|) + \alpha_2 C_R(|\alpha_2|, |\beta_2|) = (\alpha_2 + \alpha_1) C_R(|\alpha_2 + \alpha_1|, |\beta_1 + \beta_2|) \tag{3.17}$$

where the α's and β's can be positive or negative, and are so far arbitrary. These conditions, upon close examination, can be satisfied by selecting all of the following restrictions:

(6.1) The wavelength of the subharmonic disturbance is twice that of the primary (or, fundamental) wave [i.e, $\alpha_1 = -2\alpha_2$].

(6.2) The sum of the azimuthal mode numbers of the fundamental and its subharmonic is equal to the azimuthal mode number of the subharmonic alone.

(6.3) The phase velocity of the fundamental equals that of the subharmonic.

(6.4) The sum of the growth rates of the fundamental and the subharmonic is the same as the growth rate of the subharmonic alone.

The condition (6.2) can be satisfied exactly by taking the fundamental to be axisymmetric, while the subharmonic can be axisymmetric or helical. The condition (6.3) requires the waves to be nondispersive and this can only occur when the jet momentum thickness is small (i.e., near the jet nozzle). In round jets, where the waves are dispersive, this condition is met only approximately. In contrast, the phase velocities in planar mixing layers are independent of the wavenumbers and hence guarantee this condition exactly. For the tanh velocity profile, the matching of phase velocity can be approximately satisfied in two different ways. The first way represents a near neutral fundamental mode interacting with a near maximally amplified subharmonic, while the second way involves a near maximally amplified fundamental interacting with a subharmonic whose growth rate lies between zero for $\alpha = 0$ and the most amplified value. For clarity, we called these two ways *route I* and *route II* to subharmonic instabilities, respectively. *Route I* is physically more meaningful since a fundamental wave attains a finite-amplitude saturation when it is within the vicinity of a neutral point. As revealed in Figure (6.1), an axisymmetric subharmonic can interact with the fundamental via *route I*, while the matching of phase velocities between a helical subharmonic and the fundamental can occur through either *route I* or *route II*; note that the fundamental is axisymmetric. In Figure (6.1), the subscripts f and s denote

the phase velocities of the fundamental and the subharmonic, respectively; symbolically, *route I* is represented by an interaction between I_f and I_s, while *route II* is represented by an interaction between II_f and II_s.

The condition (6.4) can approximately be fulfilled by choosing an almost maximally amplified subharmonic and a fundamental wave that is near neutral. Strictly speaking, this condition will preclude *route II*, although sometimes this condition is abandoned altogether under the assumption that growth rates are generally "small". It is worth noting that the wave resonant interactions in the bulk of Kelly's work (1967) on planar mixing layers in achieved via *route II*. A consequence of this choice is that the condition on the growth rate is <u>not</u> met. The effect on the secondary subharmonic modes for not imposing the condition (6.4) will be examined in round jets in subsequent sections.

In summary, in order for <u>all</u> the resonance conditions to be satisfied simultaneously, the fundamental must be a near neutral axisymmetric mode, while the subharmonic can have an arbitrary azimuthal mode number and is nearly maximally amplified.

6.2 Comparison of Approaches

In view of the absence of any previous studies on the secondary instabilities of subsonic heated round jets, two distinct yet complementary approaches are used. One of these is a perturbation method and the other is a generalization of normal mode approach to a periodic base flow. Typical results from the two approaches for $\theta = 1/15$ and various jet parameters are compared in this section. In Figures (6.2) - (6.4), the solid lines represent the method of multiple scales, while the open circles indicate the normal mode analysis. In the normal mode analysis, the |relative frequency| $= |\hat{\sigma}_{2I}|$ — the absolute value of the imaginary part of $\hat{\sigma}_2$ defined in (3.45)— refers to the frequency of the subharmonic in a frame of reference that moves with the phase velocity of the fundamental wave. When

this |relative frequency| is zero, the relative phase velocity in the streamwise direction between the fundamental and its subharmonic becomes zero.

In Figures (6.2 a-b), the growth rate of the secondary wave (i.e., the real part of $\hat{\sigma}_2 = \hat{\sigma}_{2R}$) and its |relative frequency|, as a function of the amplitude, A, of a near maximally amplified fundamental mode are plotted. These figures represent the case where the phase velocity approximately satisfies the resonance condition (6.3), whereas the growth rates do not adequately fulfill condition (6.4). A couple of interesting observations can be extracted from these figures. First, the normal mode analysis produces a "dominant" subharmonic mode whose growth rate increases at a rate proportional to the amplitude A of the fundamental and a second mode which suffers a decay as A increases. In the perturbation method, we focus on the subharmonic whose growth rate increases with A. The growth rate of the dominant mode is increased by about 3% when A changes from 0 to 0.02. At a larger value of A, the decaying mode is physically insignificant relative to the dominant mode and, it will not be pursued here. Secondly, when A ranges from 0 to 0.02, the growth rate of the dominant subharmonic mode agrees well with that obtained from the method of multiple scales. Finally, the phase velocity of the subharmonic wave remains synchronized with its fundamental when A becomes finite. Note that in all of these calculations, A is still very small; because of the presence of the (periodic) primary wave, the subharmonic possesses a growth rate which is larger than what it would have in the parallel base flow.

The previous results are extended to larger amplitudes, A, in Figure (6.3). In comparing the two approaches, it can be seen that when A is less than 0.03, they are in agreement. However, when A increases from 0.03 to 0.1, the perturbation method overestimates the growth rate. We conjecture that this disagreement arises from the inaccuracy of the low order perturbation method for large A, which is presumably caused by the limited accuracy of the truncated asymptotic expansion (3.21) - (3.24). An obvious suggestion is

to introduce a second slow time scale $T_2 = \delta^2 t$ in order to absorb the parabolic dependence of the growth rate on A for large A. Rather than extending the analytical approach in this way, we chose to explore the normal mode method whose range of validity is somewhat larger than that of the asymptotic method and which also provides an independent check. Once the primary wave attains a finite amplitude, the secondary instability of the jet, as manifested by the growth rate of the subharmonic, increases. We believe that this instability will result in the pairing of the vortex rings associated with the primary wave.

Figures (6.4 a-b) show the growth rate and the |relative frequency| as a function of the amplitude of a near neutral fundamental mode for a heated jet. It can be observed that when A increases from 0 to 0.02, the growth rate of the subharmonic mode is augmented by about 7%. Further, for this range of A, the two approaches are in good agreement, and the phase velocity of the subharmonic mode matches that of the fundamental.

It is worth noting that the periodic flow destabilizes the subharmonic mode of Figure (6.4) more dramatically than that of Figure (6.2). This can be attributed to the fact that the results in Figure (6.2) do not adequately fulfill the growth rate restriction (6.4). These results are rather typical of our calculations, and therefore, we can conclude that in order to achieve optimum enhancement of a subharmonic instability mode, its wavenumber, phase velocity and growth rate must satisfy the resonance conditions simultaneously.

Additionally, in subsequent sections of this chapter, it will be found that in order to compare these approaches, it is essential that the phase velocity of the primary subharmonic disturbance matches (or, almost matches) the fundamental. This is because when the linear waves are nondispersive, there is no mechanism in the low order perturbation analysis to guarantee the destabilization of a subharmonic mode by the periodic flow by means of phase-locking with the fundamental.

6.3 Compressibility Effect

In this section, the influence of M_j on the secondary subharmonic instability in an unheated compressible jet is presented. It should be remembered that as the jet Mach number changes, the shape of the primary mode also changes. Therefore, both this change in the primary waves as well the explicit dependence of the secondary wave on M_j will alter the instabilities of the subharmonic. [For reference, compressibility *stabilizes* the primary eigenmodes]. The axial wavenumbers of the subharmonic and the fundamental are chosen to correspond to a near maximally amplified wavenumber and a near neutral wavenumber, respectively. In accordance with the discussion in the previous section, only the "dominant" subharmonic is shown.

A typical influence of M_j on the growth rate and the |relative frequency| of subharmonic instability modes ($\beta_2 = 0$) and ($\beta_2 = 1$) in the presence of a finite amplitude primary mode is exhibited in Figure (6.5). With reference to Figure (6.5b), an interesting feature is that when the waves are (initially at A =0) slightly dispersive, a finite threshold (fundamental) amplitude A_{th} is required for the matching of phase velocities to be established. After this matching is established, the dominant subharmonic mode always travels with the speed of the fundamental, and the growth rate of the subharmonic mode increases substantially as A increases (see Figure 6.5a). This threshold amplitude generally decreases as the difference (at $A = 0$) between the phase velocities of the fundamental and subharmonic decrease. This observation is important because it implies that for small amplitudes of A which are less than the threshold value, the low order perturbation series (3.21), which assumes that the matching of phase velocities is *independent* of A, might not be able to correctly predict the growth rate of the secondary disturbance when the primary waves are dispersive. This is sensible, on physical grounds, since the matching of phase velocity means that the two waves travel in unison. Therefore, there is a possibility for the effective transfer of energy from the mean flow to the subharmonic mode via the catalytic role of

the finite-amplitude primary wave; this is because there is no "phase cancellation" by the motion of the subharmonic relative to the fundamental.

In order to have a representative idea of the effect of compressibility, it is sensible to use the total increment of the growth rate of a subharmonic mode from parallel flow analysis due to the effect of the primary wave. Let $\aleph$ represent this increment when A changes from 0 to 0.1. Conveniently, some of the more important results pertaining to Figure (6.5) can be tabulated as below:

β_2	M_j	A_{th}	$\aleph$
0	0.1	0.011	0.236
0	0.8	0.004	0.204
1	0.1	0.006	0.205
1	0.8	0.011	0.180

The above calculations are for Re = 5000, $\theta = 1/15$, $T_* = 1$, and $\beta_1 = 0$. The value of A_{th} is only an estimated one because we did not have enough runs in the neighborhood of A_{th}. For an incompressible jet, when the amplitude A changes from 0 to about 0.1, the growth rates of the $\beta_2 = 0$ and $\beta_2 = 1$ are augmented by 0.236 and 0.205, respectively. This is about a 40 % increase over their values at $A = 0$ and suggests that subharmonic instabilities play a major role in the development of a jet flow. Furthermore, when A is greater than the threshold value, compressibility has a moderate stabilizing effect on secondary subharmonic instability modes so that vortex pairing, which results from subharmonic instability, is expected to be less important in compressible flows. For example, for the $\beta_2 = 0$, the increment, $\aleph$, is reduced from 0.236 to 0.204 due to compressibility.

6.4 Heating Effect

In this section, the influence of T_* on the secondary subharmonic growth rates in a heated ($T_* > 1$) and low Mach number ($M_j = 0$) jet is discussed. The comparison between heated and unheated flows is again rather subjective since the primary eigenmodes also depend on T_*. As noted in Chapter 5, heating is found to have a slight stabilizing effect on primary modes with axial wavenumbers larger than the most amplified wavenumber. As before, the axial wavenumbers of the subharmonic and the fundamental are chosen to correspond to a near maximally amplified wavenumber and a near neutral wavenumber, respectively (i.e., via *Route I*).

Figure (6.6) shows the influence of T_* on the growth rate and the |relative frequency| of subharmonic instability modes ($\beta_2 = 0$ and $\beta_2 = 1$) as a function of the amplitude A of the fundamental mode. In this figure, $\theta = 1/15$, $M_j = 0.1$, and $\beta_1 = 0$ are used. Again, for clarity, $\aleph$ refers to the increment in the growth rate of the subharmonic mode when A changes from 0 to 0.1, and A_{th} represents an approximate threshold amplitude for the onset of a secondary subharmonic instability mode. The more significant information pertaining to Figure (6.6) can be tabulated as below:

β_2	T_*	A_{th}	$\aleph$
0	1	0.011	0.236
0	2	0.014	0.206
1	1	0.006	0.205
1	2	0.001	0.122

Several interesting features can be seen in this figure, using the above table as an aid. First, the growth rate of subharmonic instability modes in a heated jet, again, increases as A increases. Secondly, while heating slightly suppresses the growth rate of an axisymmetric secondary mode (by about 15%), it *decreases* the growth rate of $\beta = 1$ mode considerably (by about 40%). This leads us to believe that heating tends to inhibit

vortex-pairing in round jets, and this inhibition is substantially more pronounced for the first azimuthal subharmonic mode with $\beta = 1$. Finally, heating increases the threshold amplitude required for the onset of a secondary subharmonic with $\beta = 0$, but it reduces the corresponding threshold amplitude for $\beta = 1$ mode. To conclude, vortex pairing in a heated, incompressible jet is likely to be an axisymmetric phenomenon.

6.5 Shear Layer Thickness Effect

We recall that jet instability is caused by the induction of the vorticity, which is contained within a narrow region in jet shear layers. The physical mechanism for an amplified disturbance can be explained in terms of a vortex sheet in a homogeneous incompressible fluid (Drazin & Reid). According to the Biot-Savart law, each vortex in an inviscid fluid is carried with the fluid and induces a circulating flow proportional to the strength of the vortex line. Specifically, the velocity induced at any point by the vortices will amplify the sinusoidal displacement of a vortex sheet.

In a given parallel velocity profile, the mean vorticity is inversely proportional to the thickness of the shear layer. This vorticity of the steady mean flow can be interpreted as a source term from which energy is transferred to the unsteady perturbation vorticity. This point can be illustrated by considering a two-dimensional incompressible inviscid fluid with a steady mean vorticity Ω_0 and an unsteady small perturbation vorticity Ω'. The equations governing the dynamics of the total vorticity and the perturbation vorticity are, respectively,

$$\frac{D}{Dt}(\Omega_0 + \Omega') = 0 \tag{6.2}$$

$$(\frac{\partial}{\partial t} + u_0\frac{\partial}{\partial x})\Omega' = -v\frac{d\Omega_0}{dr} \tag{6.3}$$

where

$$\frac{D}{Dt} = \frac{\partial}{\partial t} + \mathbf{v} \cdot \nabla,$$

and u_0 and v are the mean flow velocity and the radial perturbation velocity, respectively. These equations reveal that while the total vorticity of a material element carried with the fluid is conserved, the perturbation vorticity, which is being convected by the mean flow u_0, changes along the mean flow because of the "source term" $-vd\Omega_0/dr$.

Although in secondary instability analysis, the presence of a finite-amplitude fundamental mode will restructure the vorticity distribution, the growth rate of a subharmonic mode is, nevertheless, expected to increase as θ becomes smaller. This growth is revealed in Figure (6.7), which is plotted for Re = 5000, $M_j = 0.1$, $T_* = 1$, $\beta_1 = 0$ and two different values of θ: $\theta = 1/30$ and $\theta = 1/15$. It may be noted that the flow is taken to be unheated ($T_* = 1$) and almost incompressible ($M_j = 0.1$) in order to isolate the effect of the parameter θ, which appears explicitly in the velocity profile. It is shown that, when A changes from 0 to 0.1, the total increment, $\aleph$, of the growth rates of the axisymmetric subharmonic modes for $\theta = 1/30$ are approximately twice that for $\theta = 1/15$. These results indicate that although the presence of a primary wave redistributes the vorticity of the parallel flow, the growth rate of a secondary subharmonic mode is seen to increase proportionally to $1/\theta$, just as in the primary stability analysis. This implies that if vortex pairing is a resonant interaction between these structures and a small amplitude subharmonic mode, the former exerts the greatest influence in reinforcing the latter when the shear layer thickness is small (i.e., near the jet nozzle). This means that each successive coalescence of a coherent vortex structures not only makes the primary wave more dispersive because of the larger shear layer thickness, but also makes it less conducive to pairing.

In Figure (6.7), it may also be noted that the solid lines represent the case where the resonance condition on the growth rate (6.4) is not met, and subsequently, the increase in the subharmonic growth rate is less pronounced than in the case where the condition

(6.4) is fulfilled.

6.6 Mode Number Effect

In this section, we will discuss the influence of the finite amplitude primary axisymmetric mode on the growth rate and the |relative frequency| of a subharmonic mode for various mode numbers. In Chapter 5, we found that the tanh velocity profile with small values of θ, which characterize the mean flow close to jet exit, is unstable to a large number of azimuthal modes. When θ increases, the $\beta = 1$ mode increasingly becomes the dominant instability mode. Further, it is found that the periodic flow is most unstable to subharmonic disturbances whose phase velocity is the same as that of the fundamental. This matching of the phase velocity only occurs when the jet momentum thickness is sufficiently small, since otherwise, the wave speed cannot be matched because of dispersiveness. The value $\theta = 1/15$ is chosen because at this value of θ, not only can resonant wave interactions occur, but also the streamwise location implied by this value is sufficiently far from the jet nozzle to ensure that a finite-amplitude saturation of the fundamental mode can be attained. Some evidence of this particular value of θ can be found in the work of Cohen (1986).

In Figures (6.8) and (6.9), the subharmonic growth rate and the |relative frequency| for various azimuthal numbers are plotted as a function of the amplitude of the fundamental mode. The results in these figures are based on Re = 5000, $\theta = 1/15$, $\beta_1 = 0$, $T_* = 1$, $M_j = 0.1$, $\alpha_2 = 3.66$, $\alpha_1 = 7.32$. These figures show that for a low Mach number jet, the overall increment of the subharmonic growth rate of the azimuthal modes $\beta = 0$, 1 and 2 increase as A increases. The secondary growth rates of $\beta = 0$ and $\beta = 1$ are of comparable size, while the corresponding quantity for $\beta = 2$ is relatively small. It is rather surprising to note that the threshold amplitude A_{th} of $\beta = 3$ mode is rather high, and the

phase-locking phenomenon is never established for $\beta = 4$ mode. The secondary growth rate of $\beta = 3$ is in fact smaller than the growth rate obtained from parallel flow analysis. These results are of interest because they indicate that the approximate fulfillment of the resonance condition on the phase velocity does not automatically lead to an increase in the (temporal) growth rate of a subharmonic mode. Physically, the suppression of the growth rate of the subharmonic, and hence the vortex-pairing, means the energy is pumped from the subharmonic to the mean flow. It would be interesting to see whether these observations could be verified experimentally or by full numerical simulations.

These results suggest that in order to achieve maximum mixing enhancement in round jets via the amalgamation of coherent structures, it is most effective to excite a subharmonic mode with $\beta = 0$ or $\beta = 1$ modes.

6.7 Influence of A on the Eigenfunction of Subharmonic Modes

In the previous sections, the secondary growth rate and the |relative frequency| in the presence of a base flow consisting of a parallel mean flow and a finite-amplitude fundamental mode are discussed. This section considers the influence of the fundamental mode on the eigenfunctions of the subharmonic. For clarity, the eigenfunctions of the fundamental and its subharmonic are written, respectively, as

$$\mathbf{f}_1 = |\mathbf{f}_1| \exp i(\theta_1) \tag{6.4}$$

$$\mathbf{f}_{2,1} = |\mathbf{f}_{2,1}| \exp i(\theta_{2,1}) \tag{6.5}$$

$$\mathbf{f}_{2,-1} = |\mathbf{f}_{2,-1}| \exp i(\theta_{2,-1}) \tag{6.6}$$

where the amplitudes $|\mathbf{f}_1|$, $|\mathbf{f}_{2,1}|$ and $|\mathbf{f}_{2,-1}|$ as well as the phases θ_1, $\theta_{2,1}$ and $\theta_{2,-1}$ are functions of the radial variable r.

For a real $\hat{\sigma}_2$, the substitution of (6.4) - (6.6) into (3.39) and (3.45) yields

$$\mathbf{F}_1 = 2A|\mathbf{f}_1|\cos(\alpha_1 x + \theta_1) \tag{6.7}$$

$$\mathbf{F}_2 = 2\varepsilon \exp(\hat{\sigma}_2 t)\{|\mathbf{f}_{2,1}|\cos(\alpha_2 x + \beta_2 \phi + \theta_{2,1}) + |\mathbf{f}_{2,-1}|\cos(\alpha_2 x - \beta_2 \phi + \theta_{2,-1})\} \tag{6.8}$$

Recall that when $\hat{\sigma}_2$ is purely real, the |relative frequency| is zero. Further, the eigenfunctions are normalized in such a manner that A and ε becomes the maximum amplitudes of the streamwise velocity perturbations.

In Figures (6.10) - (6.11), the amplitude $|\mathbf{f}_{2,1}|$ and the phase $\theta_{2,1}$ as a function of the radial variable, r, are plotted for three different values of A: $A = 0.0$, $A = 0.05$ and $A = 0.1$. [For reference, the corresponding growth rate and |relative frequency| are plotted in Figures (6.2) - (6.3).] As discussed before, these figures characterize the case where the resonance condition on phase velocity (6.3) is approximately met, whereas the resonance condition on the growth rate is not satisfied. Except for small changes in the amplitudes of the radial and azimuthal velocity components as A becomes larger, the secondary eigenfunctions are generally unaffected by the size of A. This lends credibility to the fact that the mode shape of the secondary instability wave or that of the primary during saturation is given reasonably well by the parallel flow results.

Figures (6.12) - (6.13) show the amplitude and the phase of a near maximally amplified subharmonic disturbance ($\beta = 1$) for an unheated low Mach number jet. The jet parameters are identical with the previous case. [For reference, the corresponding growth rate and "relative frequency" are plotted in Figure (6.4).] These figures represent the case where the resonance conditions on phase velocity (6.3) and growth rate (6.4) are adequately satisfied. Again, with the exception of a slight decrease of the eigenfunction amplitudes in the vicinity of the critical layer as A increases, the amplitude functions of the secondary subharmonic modes are minimally affected by the magnitude of A.

In summary, we conclude that while the finite-amplitude fundamental mode can sub-

stantially enhance the growth rate of its subharmonic, it has only a small to moderate effect on the mode shape of the subharmonic.

Routes of Resonant Interactions: I & II

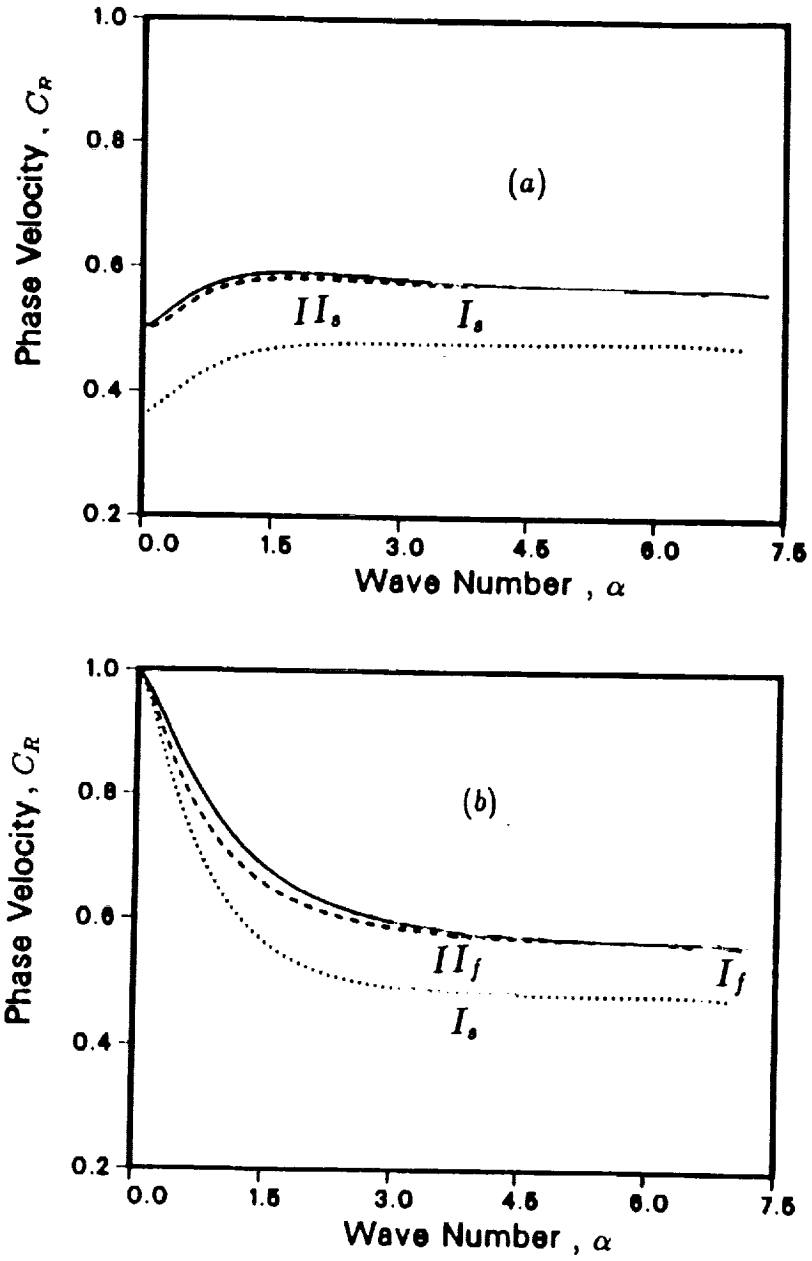

Fig. 6.1 Inviscid phase velocity for various mean profiles at $\theta = 1/15$.
Solid lines: $M_j = 0.0$, $T_* = 1$. Dot: $M_j = 0.0$, $T_* = 2$. Dash: $M_j = 0.8$, $T_* = 1$.
(a) Helical mode: $\beta = 1$. (b) Axisymmetric mode: $\beta = 0$.

Comparison of Approaches: Incompressible, Isothermal Jet

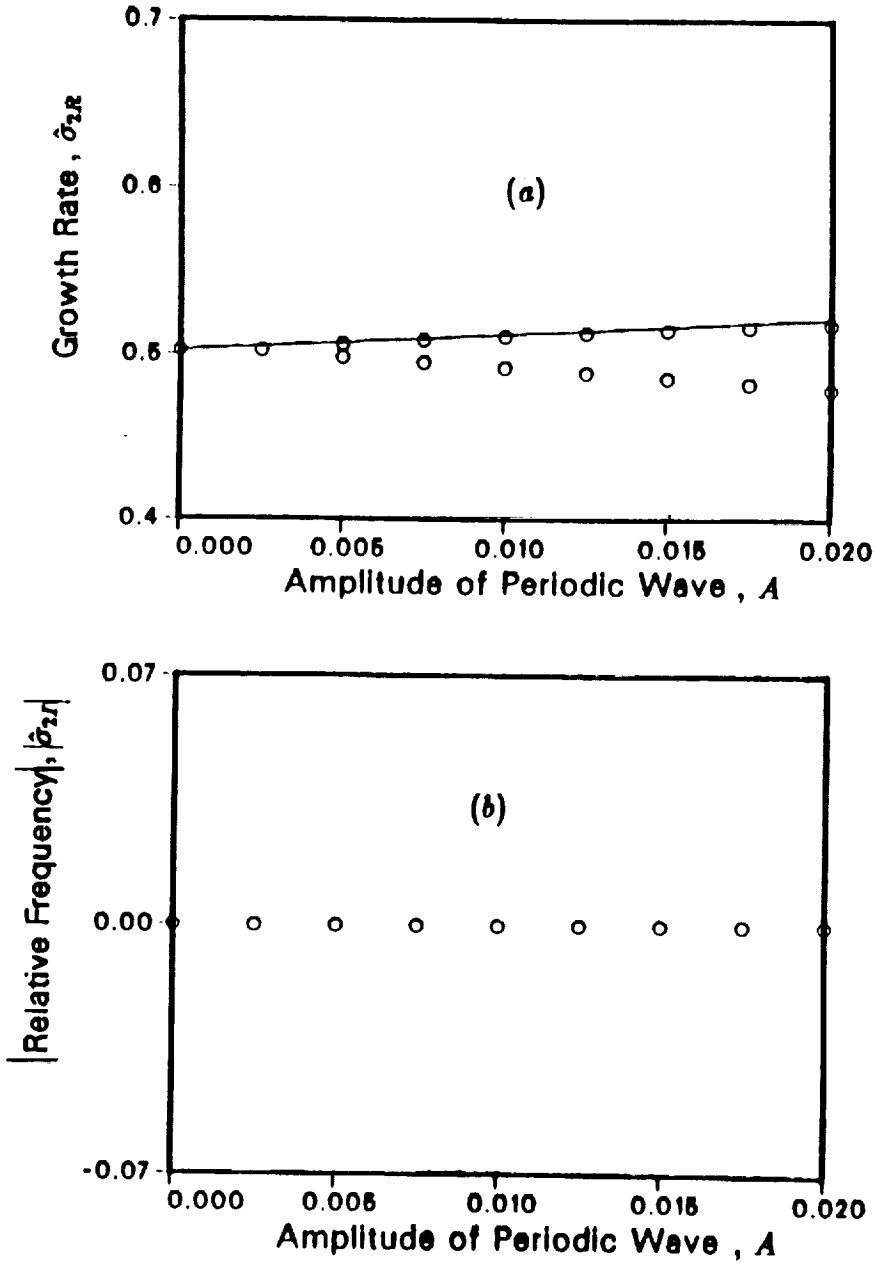

Fig. 6.2 (a) Growth rate and (b) |relative frequency| as a function of the amplitude of the periodic wave with a near maximally amplified wavenumber. Calculations are for $Re = 5000, \theta = 1/15, M_j = 0.1, T_* = 1, \beta_1 = 0, \alpha_2 = 1.7, \beta_2 = 1$.
Solid lines: multiple scales. Circles: normal mode analysis.

Comparison of Approaches: Incompressible, Isothermal Jet

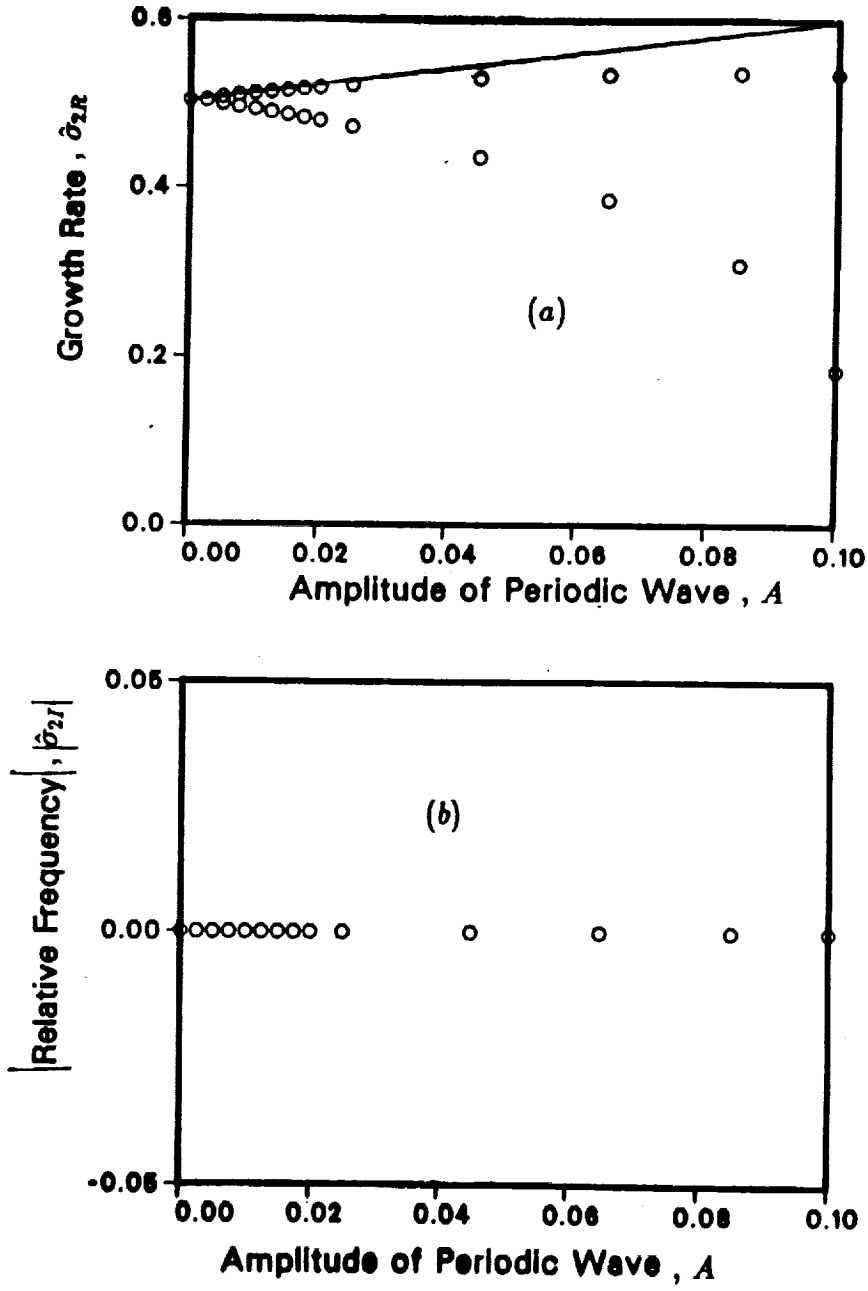

Fig. 6.3 (a) Growth rate and (b) |relative frequency| as a function of the amplitude of the periodic wave with a near maximally amplified wavenumber. Calculations are for $Re = 5000, \theta = 1/15, M_j = 0.1, T_* = 1, \beta_1 = 0$, $\alpha_2 = 1.7, \beta_2 = 1$.
Solid lines: multiple scales. Circles: normal mode analysis.

Comparison of Approaches: Incompressible, Hot Jet

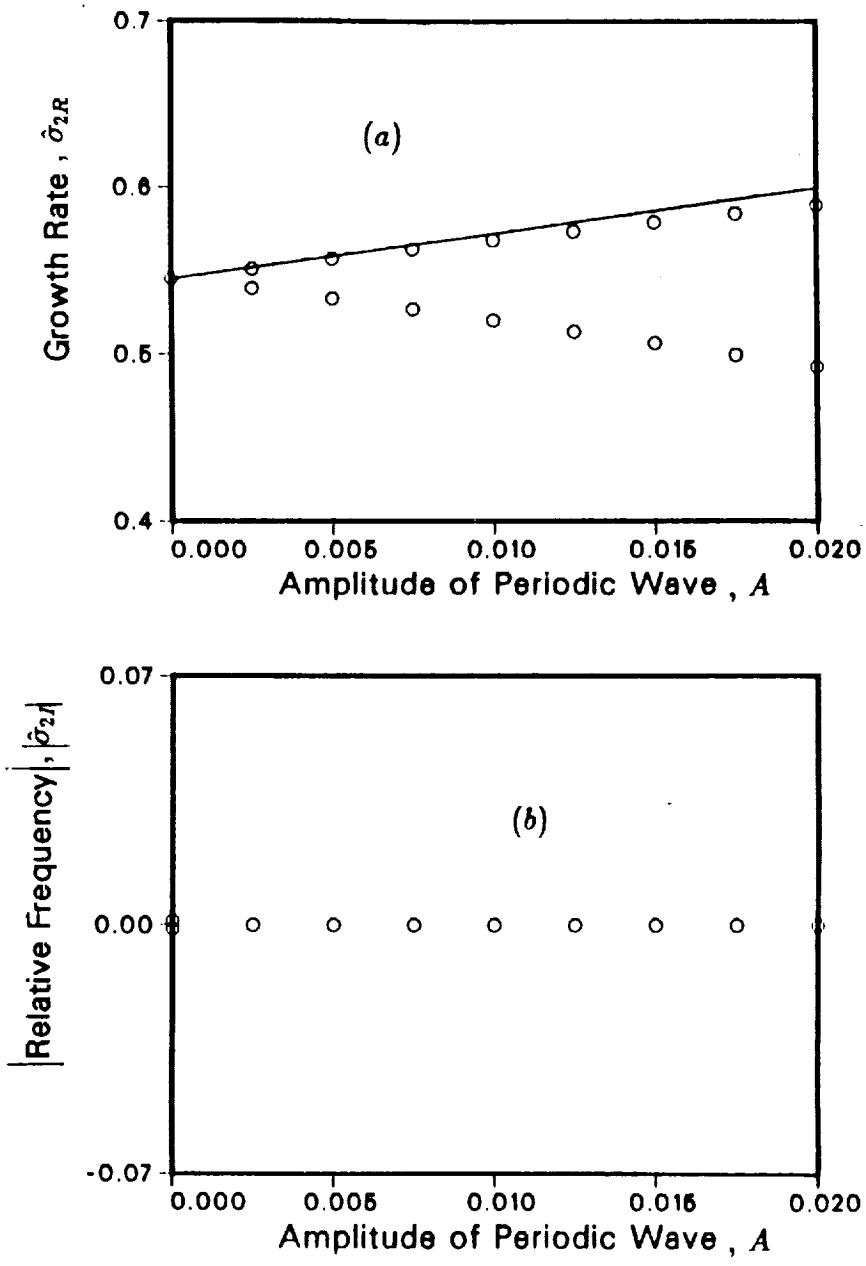

Fig. 6.4 (a) Growth rate and (b) |relative frequency| as a function of the amplitude of the periodic wave with a near neutral wavenumber. Calculations are for $Re = 500, \theta = 1/15, M_j = 0.1, T_* = 2, \beta_1 = 0, \alpha_2 = 3.2, \beta_2 = 1$.
Solid lines: multiple scales. Circles: normal mode analysis.

Compressibility Effect: Isothermal jet

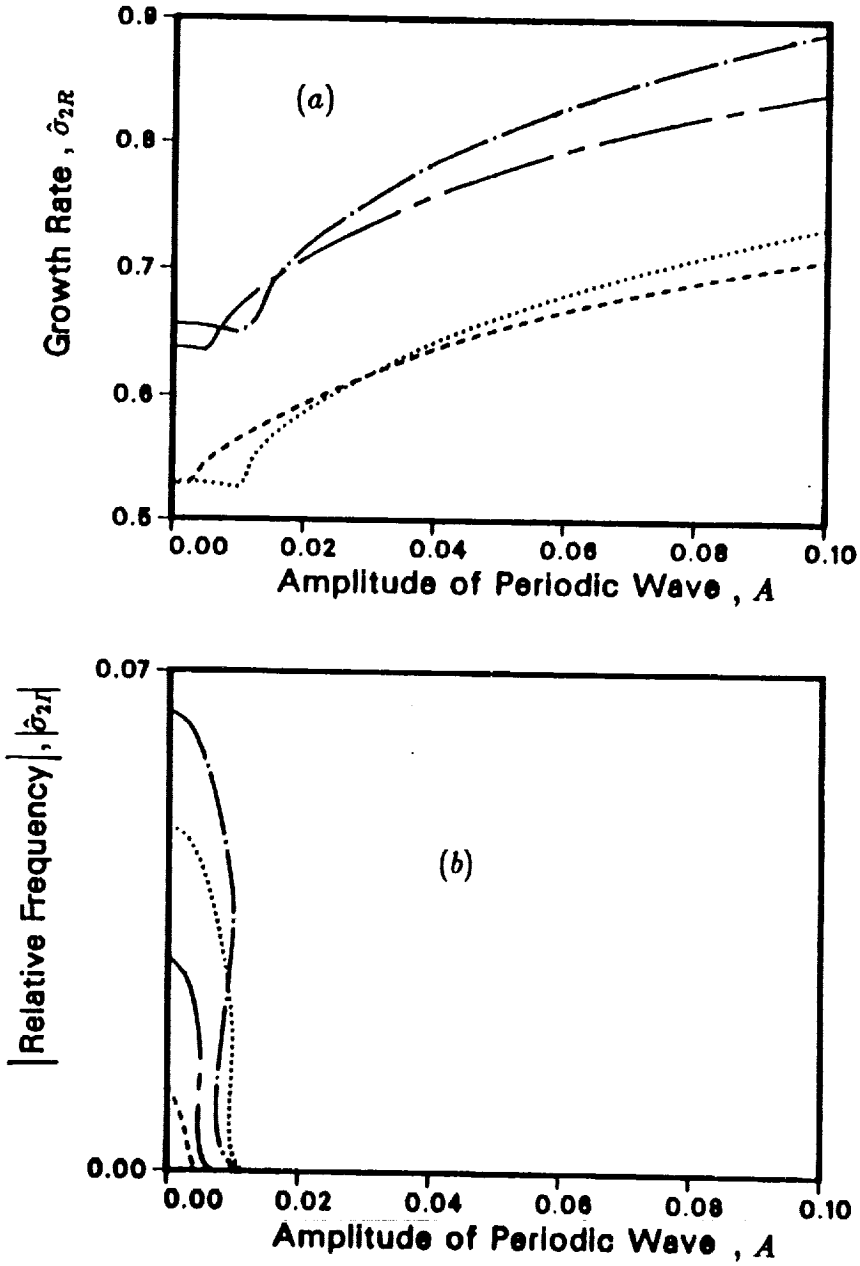

Fig. 6.5 (a) Growth rate and (b) |relative frequency| as a function of the amplitude of the periodic wave with a near neutral wavenumber. Calculations, using normal analysis, are for $Re = 5000, \theta = 1/15, T_* = 1, \beta_1 = 0$. Dot: $\alpha_2 = 3.275, \beta_2 = 0, M_j = 0.8$. Dash: $\alpha_2 = 3.275, \beta_2 = 1, M_j = 0.8$. Chaindot: $\alpha_2 = 3.66, \beta_2 = 0, M_j = 0.1$. Chaindash: $\alpha_2 = 3.66, \beta_2 = 1, M_j = 0.1$.

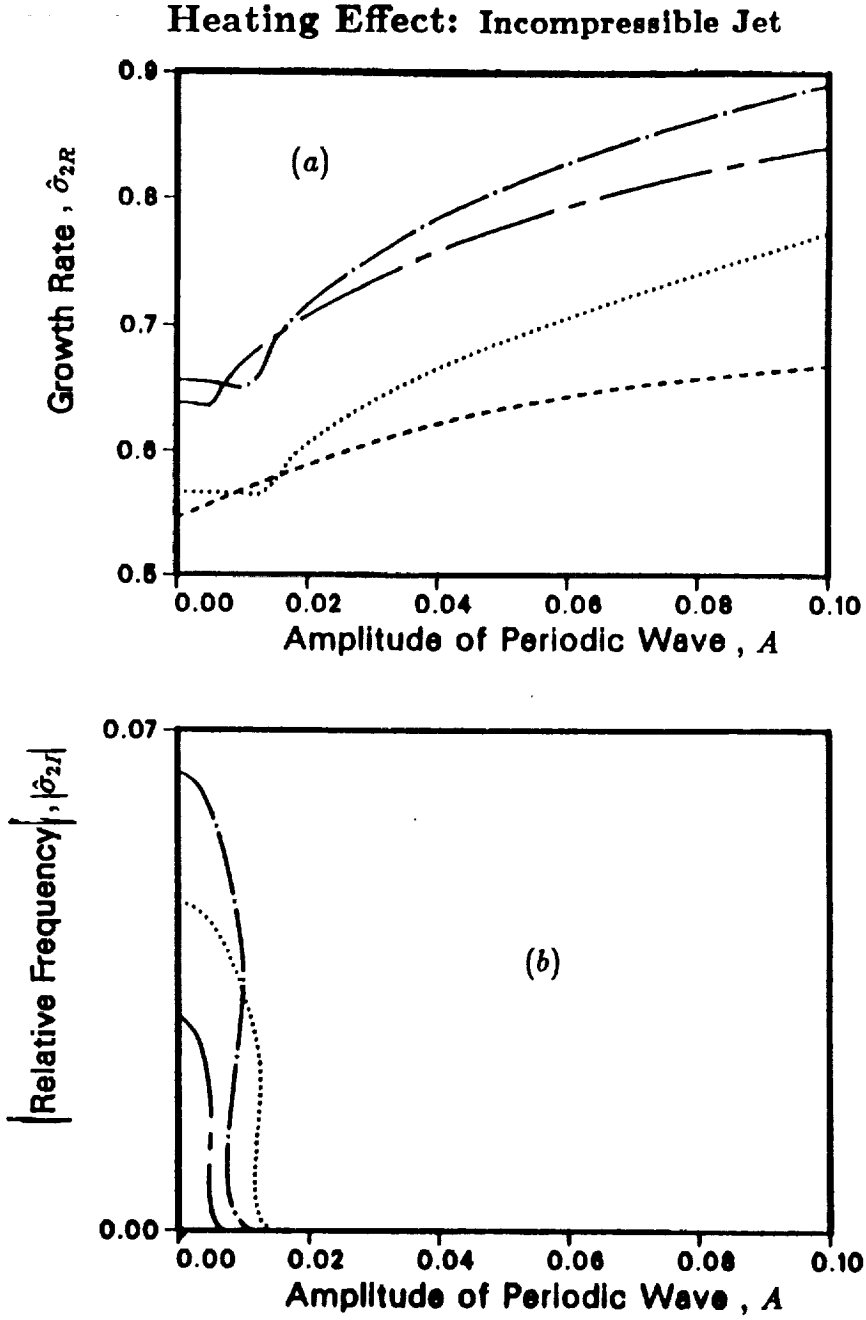

Fig. 6.6 (a) Growth rate and (b) |relative frequency| as a function of the amplitude of the periodic wave with a near neutral wavenumber. Calculations, using normal analysis, are for $\theta = 1/15, M_j = 0.1, \beta_1 = 0$.Dot: $Re = 500, \alpha_2 = 3.2, \beta_2 = 0, T_* = 2$. Dash: $Re = 500, \alpha_2 = 3.2, \beta_2 = 1, T_* = 2$. Chaindot: $Re = 5000, \alpha_2 = 3.66$, $\beta_2 = 0, T_* = 1$. Chaindash: $Re = 5000, \alpha_2 = 3.66, \beta_2 = 1, T_* = 1$.

Shear Layer Thickness Effect: Incompressible, Cold Jet

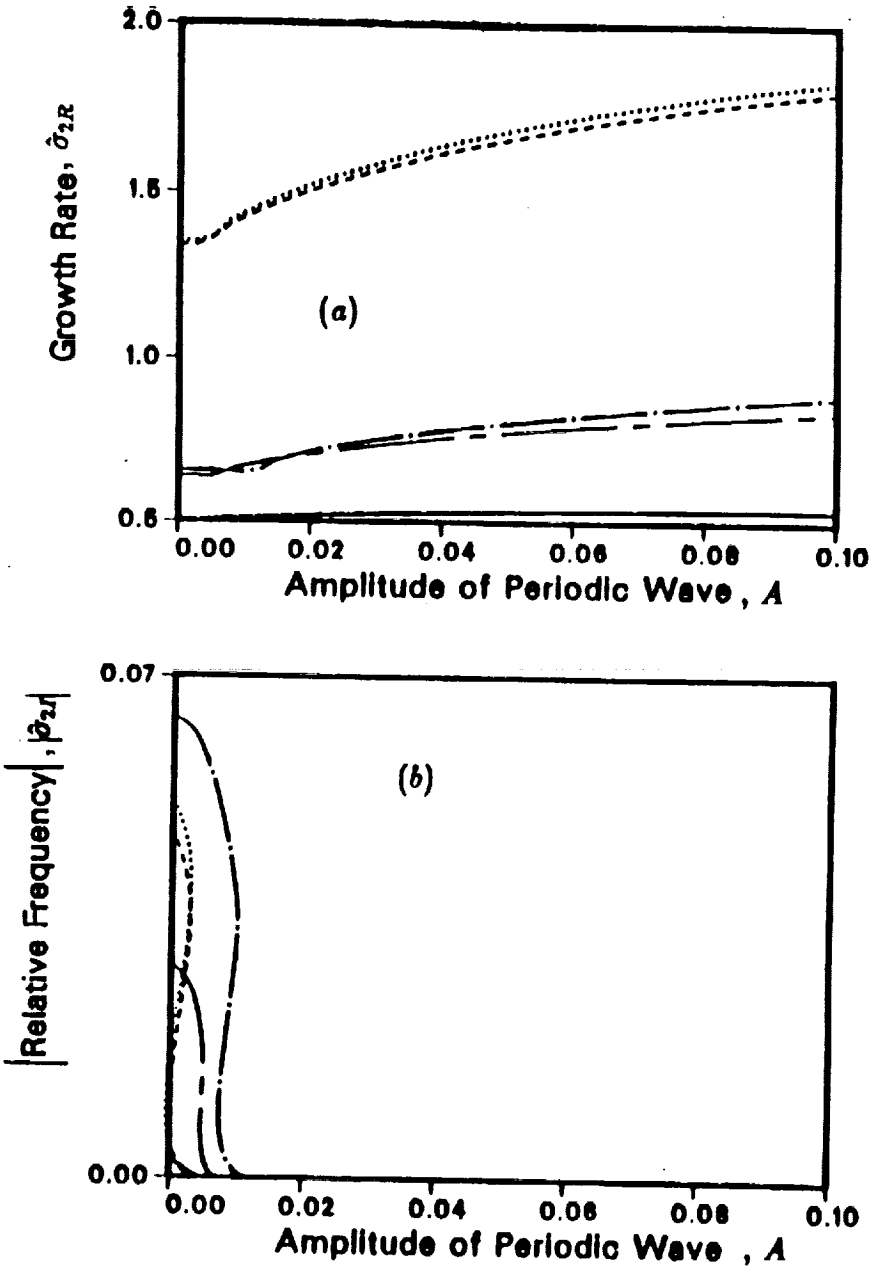

Fig. 6.7 (a) Growth rate and (b) |relative frequency| as a function of the amplitude of the periodic wave with a near neutral wavenumber. Calculations, using normal analysis, are for $Re = 5000$, $M_j = 0.1, T_* = 1, \beta_1 = 0$. Dot: $\alpha_2 = 7.3, \beta_2 = 0$, $\theta = 1/30$. Dash: $\alpha_2 = 7.3, \beta_2 = 1, \theta = 1/30$. Chaindot: $\alpha_2 = 3.66, \beta_2 = 0, \theta = 1/15$. Chaindash: $\alpha_2 = 3.66, \beta_2 = 1, \theta = 1/15$. Solid lines: $\alpha_2 = 1.7, \beta_2 = 1, \theta = 1/15$.

Mode Number Effect: Incompressible, Isothermal Jet

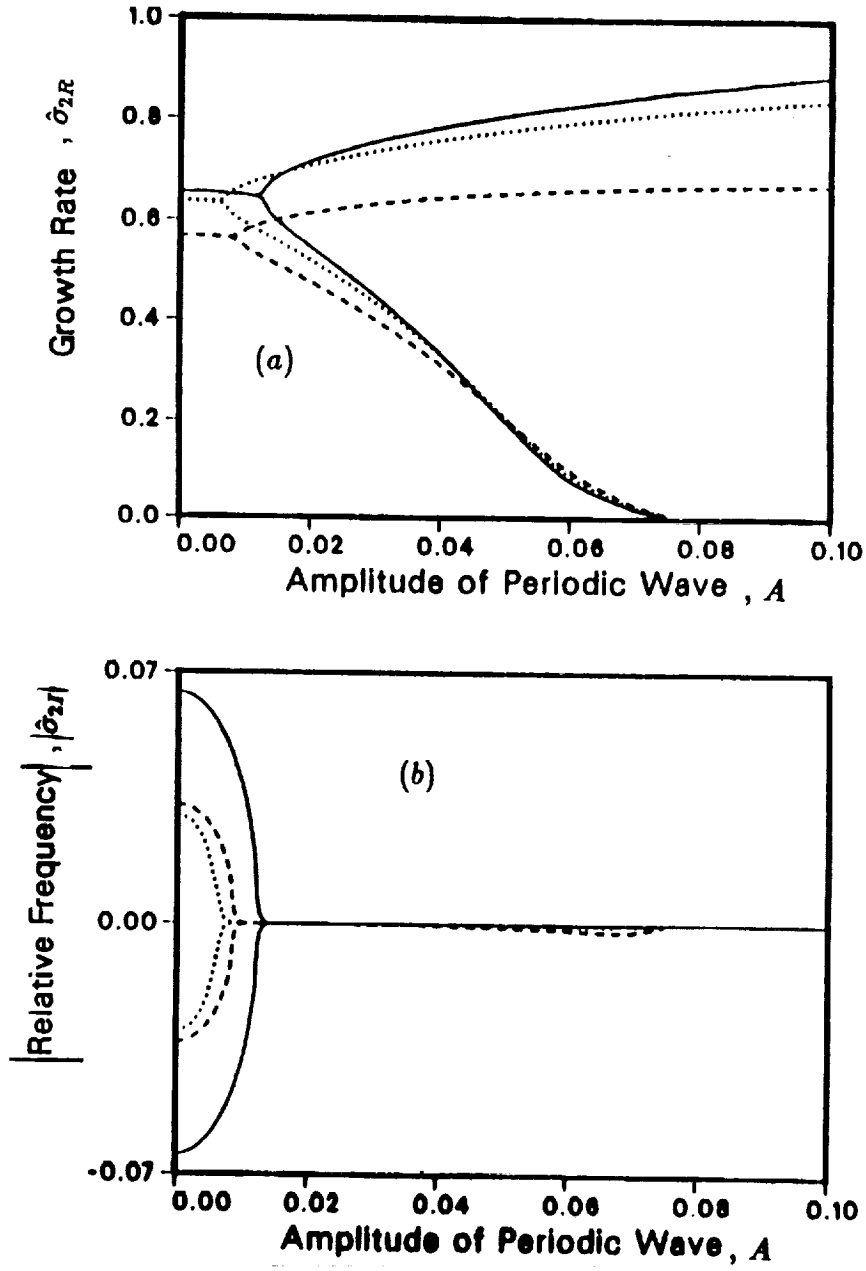

Fig. 6.8 (a) Growth rate and (b) |relative frequency| as a function of the (unrestrited) amplitude of the periodic wave with a near neutral wavenumber. Calculations, using normal analysis, are for $Re = 5000$, $\theta = 1/15, M_j = 0.1, T_* = 1, \beta_1 = 0$, $\alpha_2 = 3.66$. Solid lines: $\beta_2 = 0$. Dot: $\beta_2 = 1$. Dash: $\beta_2 = 2$.

Mode Number Effect: Incompressible, Isothermal Jet

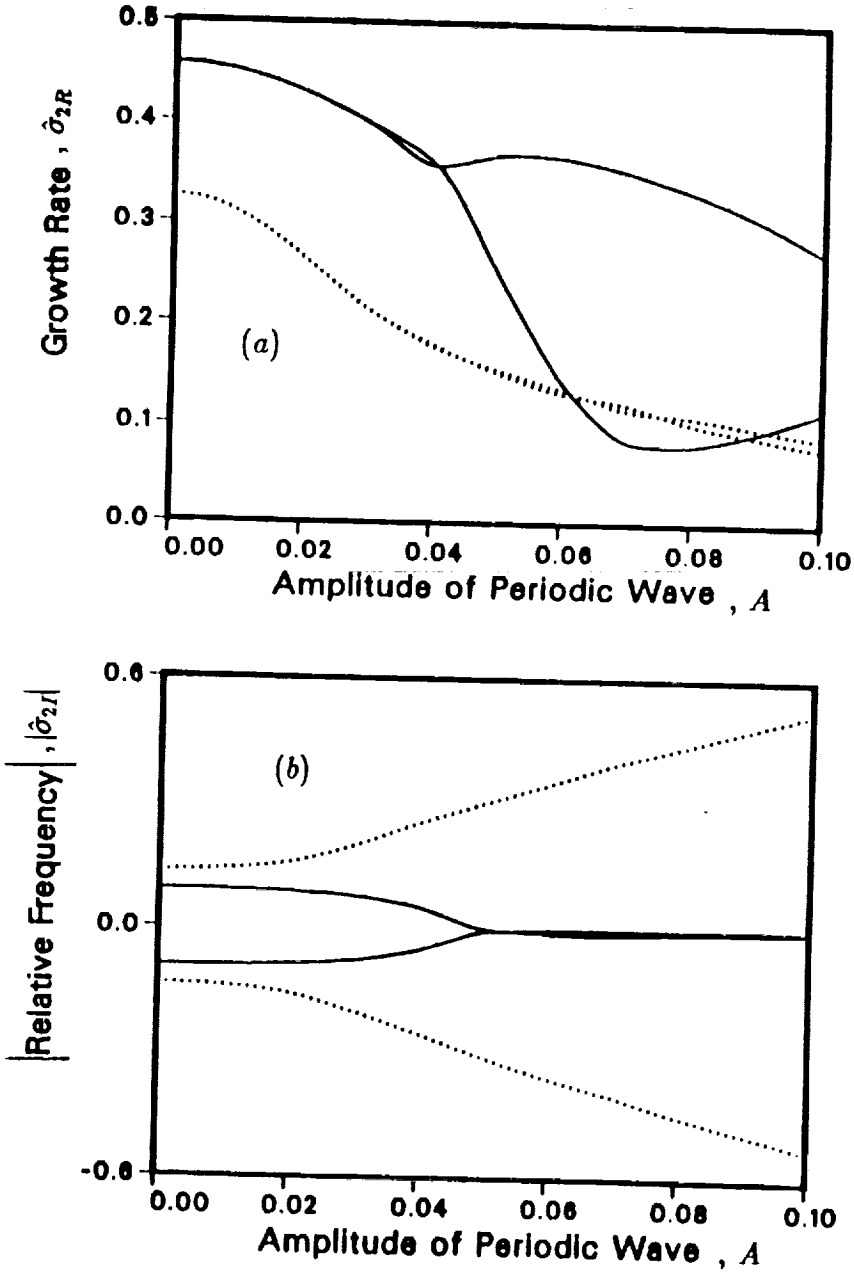

Fig. 6.9 (a) Growth rate and (b) |relative frequency| as a function of the (unrestricted) amplitude of the periodic wave with a near neutral wavenumber. Calculations, using normal analysis, are for $Re = 5000, \theta = 1/15$, $M_j = 0.1, T_* = 1$, $\beta_1 = 0, \alpha_2 = 3.66$. Solid lines: $\beta_2 = 3$. Dot: $\beta_2 = 4$.

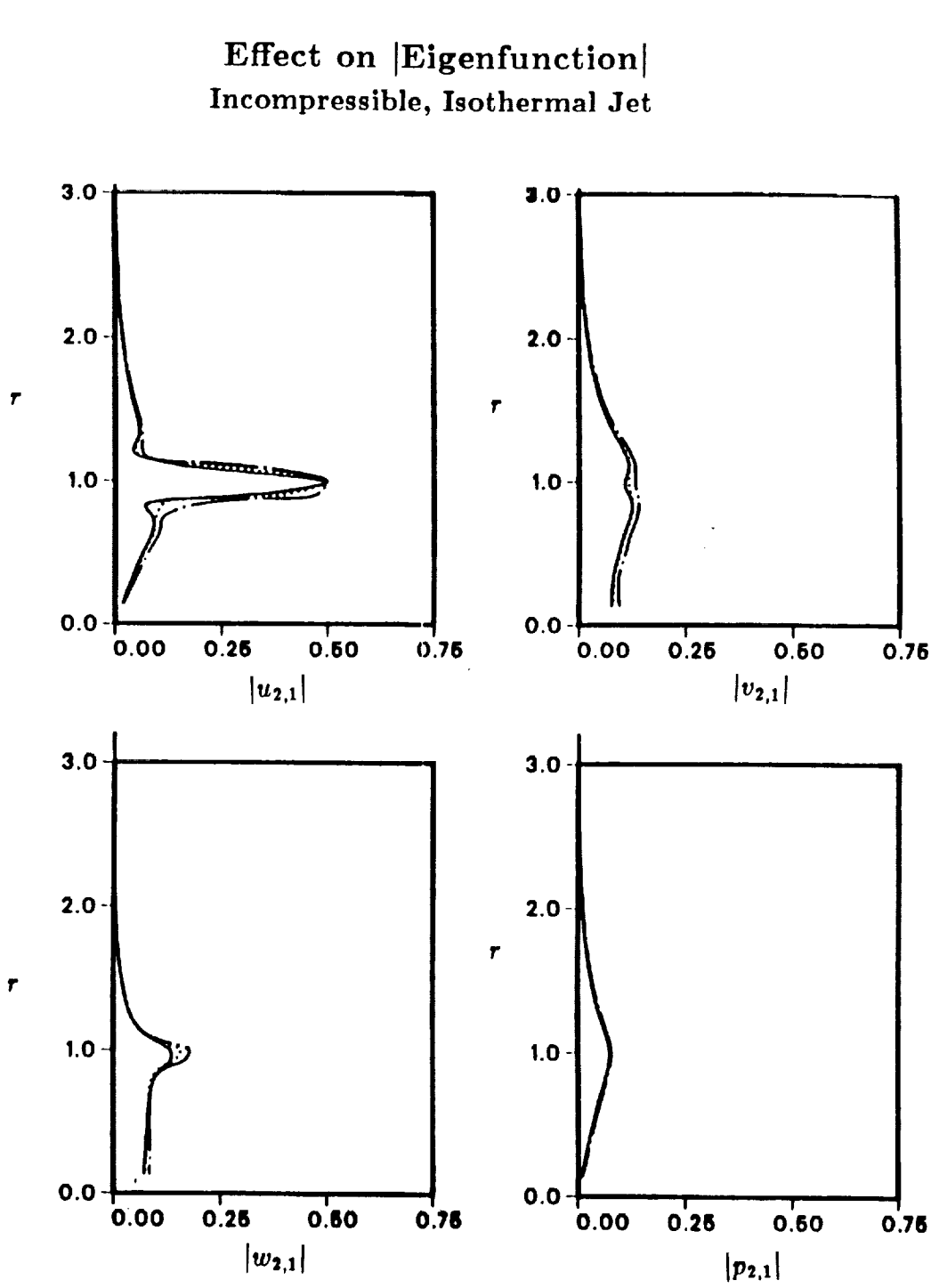

Fig. 6.10 Distributions of the |eigenfunction| of a subharmonic disturbance as a function of the radial variable r. Calculations are for $Re = 5000, T_* = 1.0, M_j = 0.1$, $\theta = 1/15, \beta_1 = 0, \alpha_2 = 1.7, \beta_2 = 1$. Solid lines: $A = 0$. Dot: $A = 0.05$. Chaindot: $A = 0.1$.

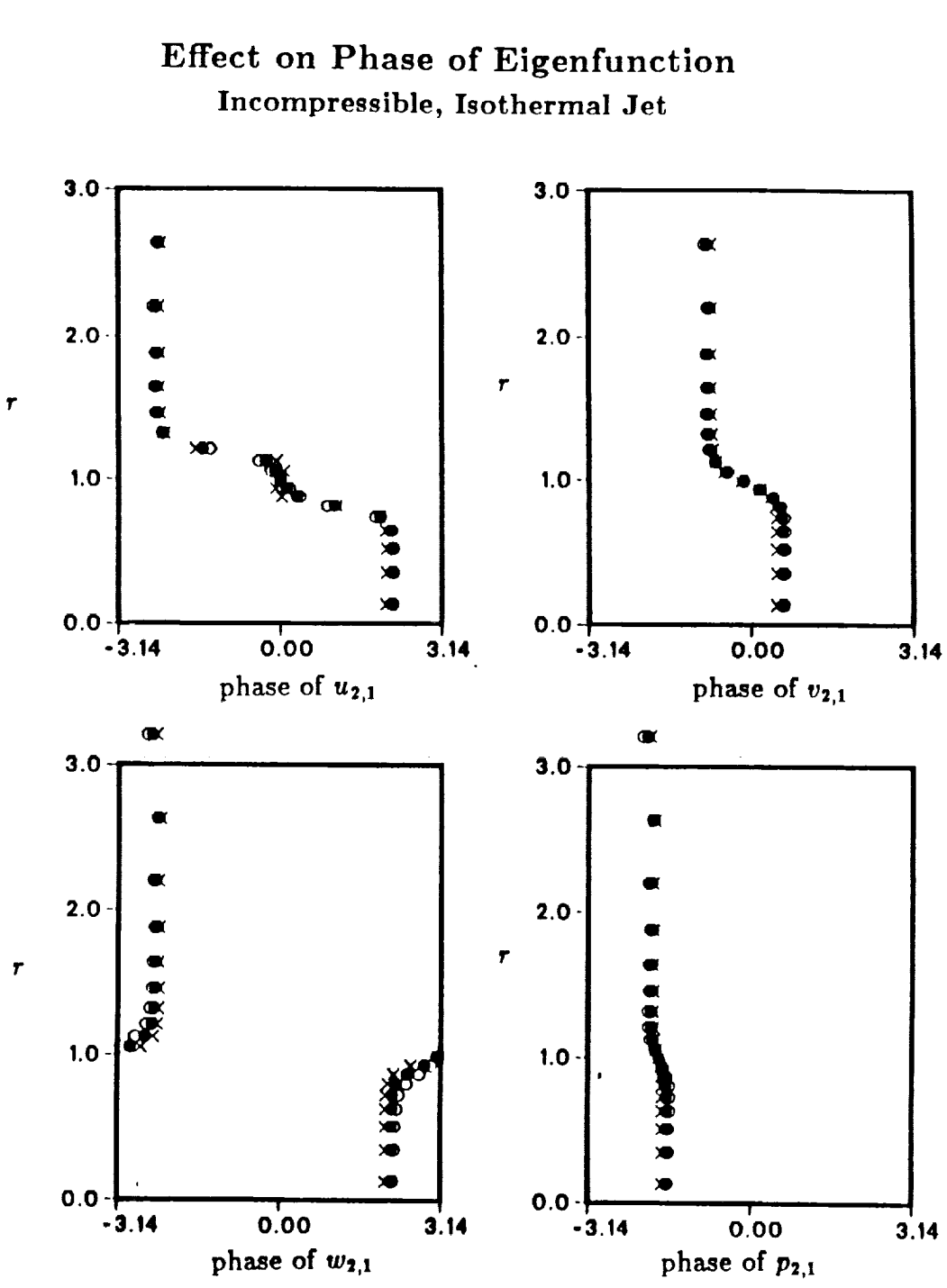

Fig. 6.11 Distributions of the phase of a subharmonic disturbance as a function of the radial variable r. Calculations are for $Re = 5000, T_* = 1.0, M_j = 0.1$, $\theta = 1/15, \beta_1 = 0, \alpha_2 = 1.7, \beta_2 = 1$. $\times$: $A = 0$. $\bullet$: $A = 0.05$. $\circ$: $A = 0.1$.

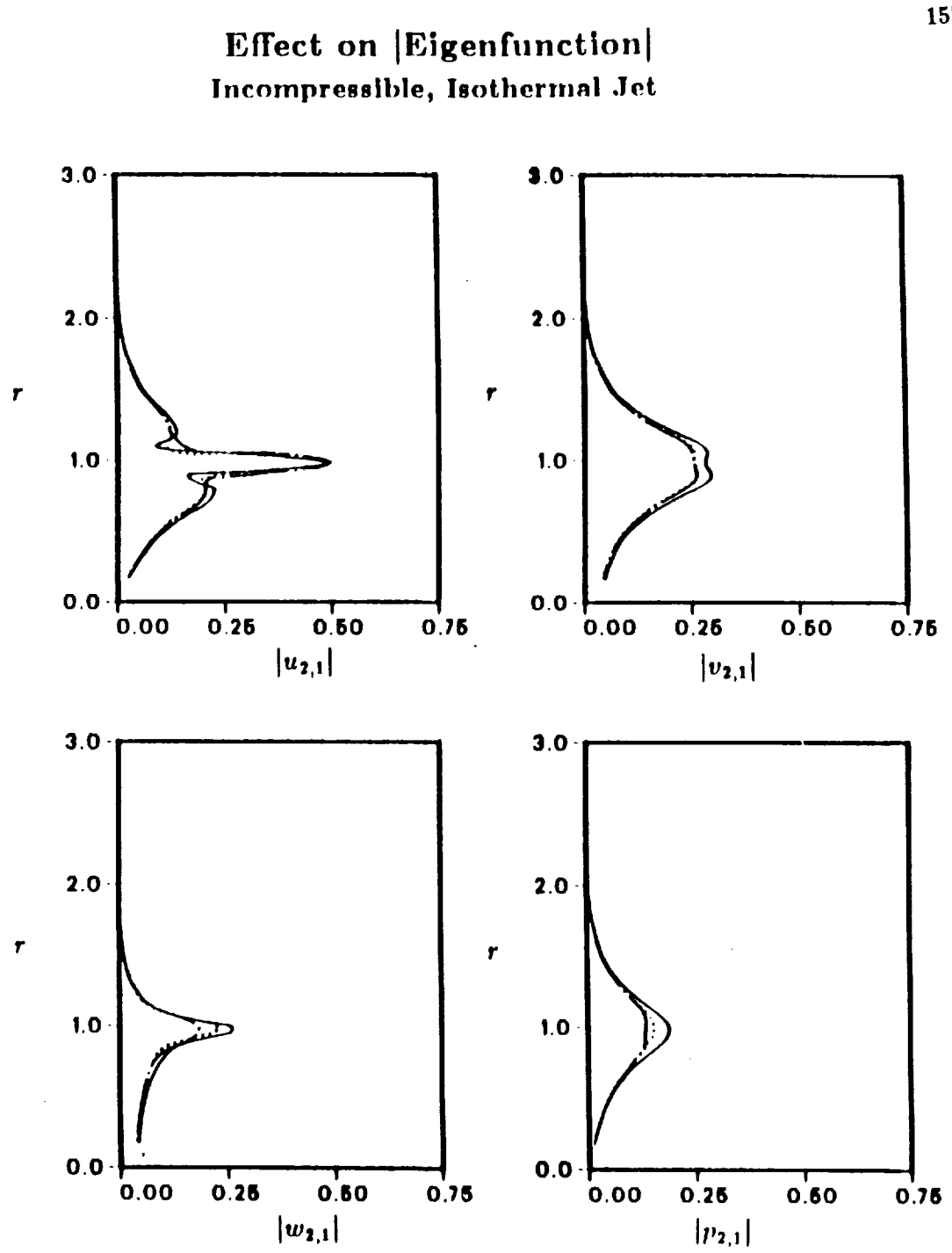

Fig. 6.12 Distributions of the |eigenfunction| of a near maximally amplified subharmonic disturbance as a function of the radial variable r. Calculations are for $Re = 5000, T_* = 1.0, M_j = 0.1, \theta = 1/15, \beta_1 = 0, \alpha_2 = 3.66, \beta_2 = 1$.
Solid lines: $A = 0$. Dot: $A = 0.05$. chaindot: $A = 0.1$.

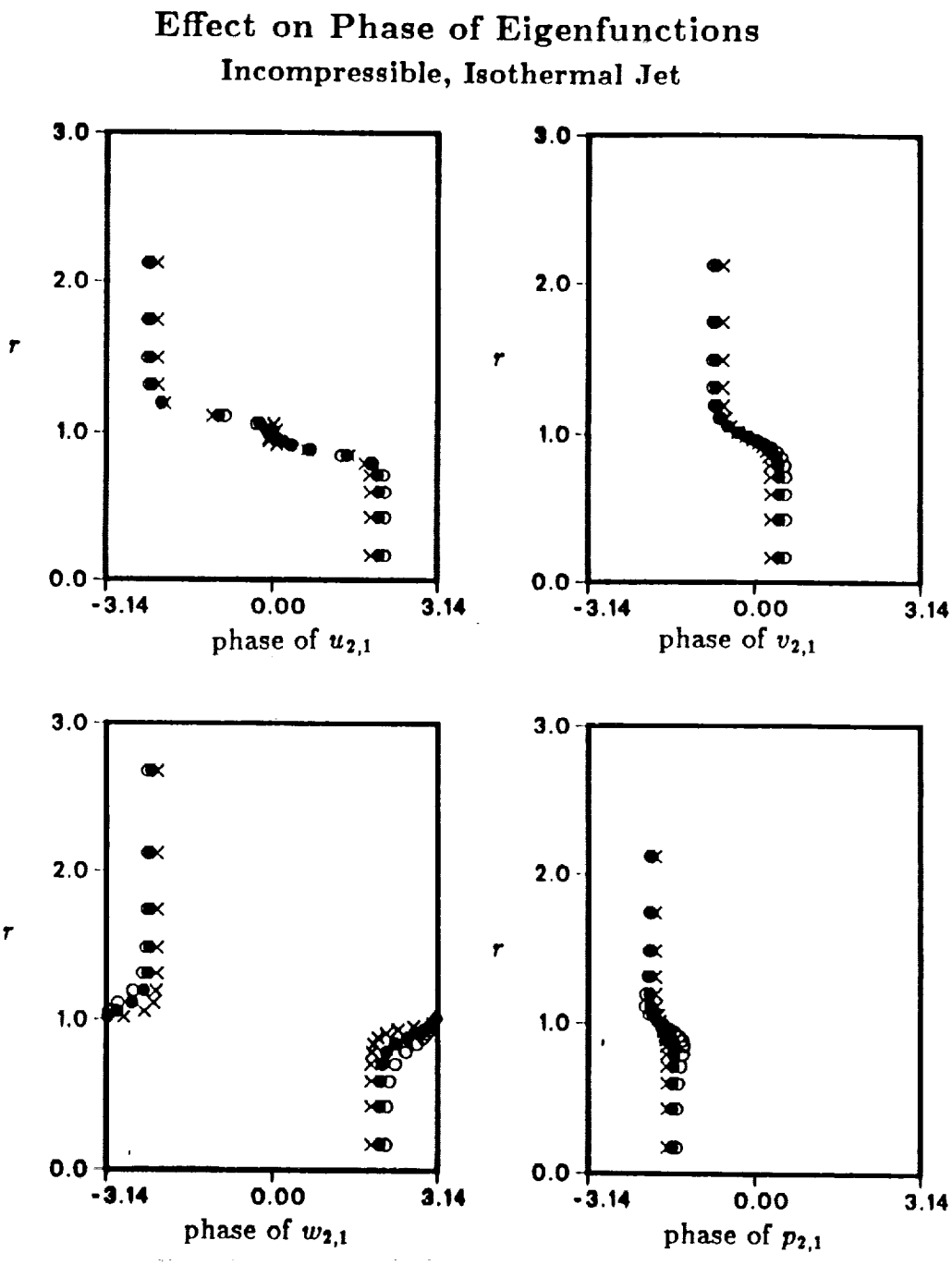

Fig. 6.13 Distributions of the phase of a near maximally amplified subharmonic disturbance as a function of the radial variable r. Calculations are for $Re = 5000, T_* = 1.0, M_j = 0.1, \theta = 1/15, \beta_1 = 0, \alpha_2 = 3.66, \beta_2 = 1$. $\times$: $A = 0$. $\bullet$: $A = 0.05$. $\circ$: $A = 0.1$.

Chapter 7

SUMMARY & CONCLUSIONS

This research concerns the (temporal) instabilities and resonances of the shear layer generated by a subsonic heated jet emanating from an axisymmetric nozzle. When the shear layer is excited by a harmonically oscillating disturbance of a suitable frequency (or wavenumber), an instability wave develops in the flow. For clarity, this instability wave is termed a primary wave or fundamental wave. In the initial stages of development — where the amplitude of the disturbance relative to the mean flow is small — the stability characteristics (e.g., growth rate, phase velocity and mode shape) of the primary wave are described quite accurately by linear instability theory. We begin our research with the systematic investigation of the linear instability characteristics of a small disturbance superimposed on a prescribed parallel mean flow approximated by the hyperbolic tangent function. By generalizing Howard's semi-circle theorem to compressible round jets, we have shown that compressibility reduces the range of unstable wavenumbers and has a ***stabilizing*** effect. The role of subsonic Mach number, M_j, in affecting jet instability properties is numerically examined for the tanh velocity profile with $\theta = 1/15$. We have concentrated our research on this value of θ because it provides a good representation of the velocity profile at a downstream location where the shear layer is sufficiently thin to ensure that resonance interactions between two waves (i.e., fundamental and subharmonic) can occur. Hence, subsequent discussions, unless otherwise indicated, pertain only to these mean profiles with $\theta = 1/15$.

Calculations show that the most unstable temporal growth rates of a (2-d) axisymmet-

ric mode and a (3-d) first helical mode (i.e., $\beta = 1$)in an incompressible flow are approximately equally dominant, and compressibility (in the subsonic range) *reduces* the growth rates of the axisymmetric mode and the helical mode by approximately 19% and 17%, respectively. Compressibility also decreases slightly the phase velocities of those instability modes whose wavenumbers are smaller than the maximally amplified wavenumber, and has no apparent effect on the phase velocities of those with higher wavenumbers. In order to single out the effect of heating, the stability characteristics of the tanh profile with a temperature ratio $T_* = 2$ — but with Mach number $M_j = 0$ — are numerically examined. The results indicate that while the phase velocity is rather insensitive to Mach number, it is, except for very long axisymmetric waves, substantially decreased by heating. Heating also appears to reduce the range of unstable wavenumber and to slightly *decrease* the growth rate of the most amplified wavenumber. The stability behavior of an instability wave which has a large wavelength relative to the radius of the jet nozzle is compared to that obtained from a heated vortex sheet analysis. The results indicate that the phase velocities of long waves (i.e., $\alpha \to 0$) — irrespective of the azimuthal mode number — in a tanh velocity profile agreed well with those obtained from the vortex sheet. For the corresponding growth rates, this agreement is found only in axisymmetric modes but not in helical modes. In fact, the disagreement becomes progressively worse as the helical mode number and the shear layer thickness is increased.

When the primary wave propagates downstream, its amplitude will — as a result of the exponential growth rate predicted by the linear instability theory — quickly grow to an appreciable size. Because of the mean flow divergence (caused by viscous spreading) and nonlinear effects, this wave eventually reaches a finite-amplitude equilibrium state (i.e., saturation) at some downstream location. We approximate the nearly periodic flow which arises from the saturation of the primary disturbance by a parallel mean flow of the hyperbolic-tangent type and a periodic component whose phase velocity, wavenumber,

mode number and mode shape are the same as those associated with the primary wave. The principal task of this research is to determine the resonances and instabilities of this periodic flow. The conditions for resonant interaction between two arbitrary instability modes are derived. The resonant interaction between two modes allows an effective mechanism for the transfer of energy from the mean flow to an instability mode. In order to satisfy the resonance conditions, we have shown that the wavenumbers and the mode numbers of the two unstable modes, a primary and a secondary, must be restricted to the following choices:

1. The primary mode is axisymmetric and has an axial wavenumber close to a neutral wavenumber.

2. The secondary wave, which can have an arbitrary mode number, is almost the maximally amplified *subharmonic* wave; the wavelength of the subharmonic is twice that of the primary wave.

A key result from the resonant conditions indicates that resonant interaction between two modes can occur only when the jet momentum thickness is sufficiently small since, otherwise, the wave speeds cannot be matched because of dispersiveness. When the resonance conditions are met, a subharmonic mode interacts strongly with the primary to produce an instability mode whose wavenumber and mode number is the sum of the wavenumbers and mode numbers of the two interacting waves. If the subharmonic mode is axisymmetric, it will interact with the fundamental to reproduce itself. The interaction involving a helical mode with mode number β will, however, produce a mode with mode number $-\beta$, and vice versa. Therefore, whenever an interaction involves a subharmonic mode which is helical, we shall assume that the secondary disturbance is comprised of a pair of helical waves whose propagating angles are equal and opposite. As a result, the secondary disturbance, whether axisymmetric or helical, when interacting with an axisymmetric primary wave will reproduce itself and therefore increase its growth rate. We have obtained this

(modified) growth rate of the subharmonic as a function of the amplitude of the primary wave — for different jet Mach numbers and jet temperatures — using two independent methods: the method of multiple scales and a generalization of the normal mode analysis in a spatially periodic base flow.

We found that when the resonance conditions are met almost exactly and when the amplitude A of the primary mode is less than 3 % of the mean flow, the two approaches are in good agreement. However, as A increases from 3 % to 10%, the perturbation method appears to progressively over-estimate the subharmonic growth rate. It is also shown that when the amplitude of the primary increases from 0 to 2%, the growth rate of the subharmonic mode is *augmented* by about 7%. This leads us to believe that the secondary instability — as manifested by the increase of the growth rate of the subharmonic — will enhance the pairing of the vortex rings associated with the primary wave. Our results indicate that the secondary (subharmonic) growth rates for a (3-d) instability wave with azimuthal number $\beta = 1$ and a (2-d) axisymmetric wave are equally dominant, while those associated with higher spinning numbers are relatively insignificant. Furthermore, compressibility has a *moderate stabilizing* effect on the secondary instability modes (whether axisymmetric or helical) so that vortex pairing, which results from subharmonic instability, is expected to be less pronounced in compressible flows.

In order to have a representative idea of the effects of compressibility and heating, we use the total increment, denoted by $\aleph$, of the growth rate of a subharmonic mode when the amplitude of the primary wave changes from 0 to 10%. Compressibility reduces the increment, $\aleph$, of an axisymmetric mode and a helical ($\beta = 1$) mode by about 15% and 12%, respectively. While heating seems to *suppress moderately* the increment, $\aleph$, of the secondary growth rate of an axisymmetric mode (by about 15%), it *reduces* the corresponding increment of the $\beta = 1$ mode significantly (by about 40%). This leads us to conjecture that heating tends to inhibit vortex-pairing in an axisymmetric jet, and

this inhibition is most pronounced for the $\beta = 1$ mode; we infer that vortex-paring in a heated, incompressible jet is most likely to be a (2-d) axisymmetric phenomenon. Our calculations also show that the mode shapes of the subharmonic instability modes are generally unaffected by the presence of the (finite) amplitude primary wave. Finally, when we calculated secondary instability for other values of θ, we found that the growth rate of the subharmonic mode increased in proportion to $1/\theta$. This implies that vortex-paring is more likely to occur near the jet nozzle. (of course, we also have the requirement of phase speed matching which is most perfect for small θ).

In summary, the principal effect of excitation is to generate a saturated large-scale structure whose vortices may merge because of subharmonic (secondary) instabilities. Since the secondary growth rates of the subharmonic instability modes — which are at least partially responsible for jet spreading and mixing — are suppressed by heating and compressibility, we conjecture that it will be more difficult to control vortex-mergings in a subsonic heated jet than in a low speed cold jet.

APPENDIX A

The Primary Stability Equations

The stability equations for the evolution of linear disturbances superimposed on a parallel mean flow are of the form

$$\mathbf{A}_b \mathbf{f}_b = 0 \tag{2.31}$$

where $\mathbf{A}_b$ is a 5×5 matrix whose elements, a_{ij}, are

$$a_{11} = \frac{1}{Re}\left(\partial_r^2 + \frac{1}{r}\partial_r + \frac{\partial_\phi^2}{r^2} + \partial_x^2\right) - \rho_0 \partial_x u_0 - \partial_t$$

$$a_{12} = -\rho_0 u_0'$$

$$a_{13} = 0$$

$$a_{14} = -\partial_x$$

$$a_{15} = 0$$

$$a_{21} = 0$$

$$a_{22} = a_{11} - \frac{1}{Rer^2}$$

$$a_{23} = \frac{-2\partial_\phi}{Rer^2}$$

$$a_{24} = -\partial_r$$

$$a_{25} = 0$$

$$a_{31} = 0$$

$$a_{32} = -a_{23}$$

$$a_{33} = a_{22}$$

$$a_{34} = \frac{-\partial_\phi}{r}$$

$$a_{35} = 0$$

$$a_{41} = -\gamma p_0 \partial_x$$

$$a_{42} = -\gamma p_0 (\frac{1}{r} + \partial_r)$$

$$a_{43} = \frac{-\gamma p_0 \partial_\phi}{r}$$

$$a_{44} = -\partial_x u_0 - \frac{\gamma}{PrRe}\left(\frac{\rho_0''}{\rho_0^2} - 2\frac{\rho_0'^2}{\rho_0^3} + \frac{\rho_0'}{\rho_0^2 r} - \frac{\partial_x^2}{\rho_0} - \frac{\partial_\phi^2}{r^2\rho_0}\right) - \frac{\gamma}{PrRe}\left(\frac{2\rho_0'}{\rho_0^2} - \frac{1}{\rho_0 r}\right)\partial_r + \frac{\gamma}{PrRe\rho_0}\partial_r^2 - \partial_t$$

$$a_{45} = -\frac{\gamma p_0}{PrRe}\left(\frac{\rho_0''}{\rho_0^3} + \frac{\rho_0'}{r\rho_0^3} + \frac{\partial_x^2}{\rho_0^2} + \frac{\partial_\phi^2}{\rho_0^2 r^2}\right) - \frac{\gamma p_0}{PrRe}\left(\frac{1}{\rho_0^2 r} - \frac{4\rho_0'}{\rho_0^3}\right)\partial_r - \frac{\gamma p_0}{PrRe\rho_0^2}\partial_r^2$$

$$a_{51} = -\rho_0 \partial_x$$

$$a_{52} = -\rho_0' - \rho_0(\frac{1}{r} + \partial_r)$$

$$a_{53} = \frac{-\rho_0 \partial_\phi}{r}$$

$$a_{54} = 0$$

$$a_{55} = -u_0 \partial_x - \partial_t$$

where

$$\partial_r^n = \frac{\partial^n}{\partial r^n}$$

$$\partial_x^n = \frac{\partial^n}{\partial x^n}$$

$$\partial_\phi^n = \frac{\partial^\phi}{\partial \phi^n}$$

$$\partial_t = \frac{\partial}{\partial t},$$

the primes denote differentiation with respect to r, and the subscript 0 refers to the parallel base flow.

APPENDIX B

Stability Equations for the Primary Eigenmodes

The elements of $\mathbf{A}_1$ and $\mathbf{B}_1$ in equation (2.33) are

$$a_{11} = \frac{1}{Re}\left(D^2 + \frac{1}{r}D - \frac{\beta^2}{r^2} - \alpha^2\right) - \rho_0 i\alpha u_0$$

$$a_{12} = -\rho_0 u_0'$$

$$a_{13} = 0$$

$$a_{14} = -i\alpha$$

$$a_{15} = 0$$

$$a_{21} = 0$$

$$a_{22} = a_{11} - \frac{1}{Rer^2}$$

$$a_{23} = \frac{-2i\beta}{Rer^2}$$

$$a_{24} = -D$$

$$a_{25} = 0$$

$$a_{31} = 0$$

$$a_{32} = -a_{23}$$

$$a_{33} = a_{22}$$

$$a_{34} = \frac{-i\beta}{r}$$

$$a_{35} = 0$$

$$a_{41} = -\gamma p_0 i\alpha$$

$$a_{42} = -\gamma p_0 (\frac{1}{r} + D)$$

$$a_{43} = \frac{-\gamma p_0 i\beta}{r}$$

$$a_{44} = -i\alpha u_0 - \frac{\gamma}{PrRe}\left(\frac{\rho_0''}{\rho_0^2} - 2\frac{\rho_0'^2}{\rho_0^3} + \frac{\rho_0'}{\rho_0^2 r} + \frac{\alpha^2}{\rho_0} + \frac{\beta^2}{r^2\rho_0}\right) - \frac{\gamma}{PrRe}\left(\frac{2\rho_0'}{\rho_0^2} - \frac{1}{\rho_0 r}\right) D + \frac{\gamma}{PrRe\rho_0} D^2$$

$$a_{45} = -\frac{\gamma p_0}{PrRe}\left(\frac{\rho_0''}{\rho_0^3} + \frac{\rho_0'}{r\rho_0^3} - \frac{\alpha^2}{\rho_0^2} - \frac{\beta^2}{\rho_0^2 r^2}\right) - \frac{\gamma p_0}{PrRe}\left(\frac{1}{\rho_0^2 r} - \frac{4\rho_0'}{\rho_0^3}\right) D - \frac{\gamma p_0}{PrRe\rho_0^2} D^2$$

$$a_{51} = -\rho_0 i\alpha$$

$$a_{52} = -\rho_0' - \rho_0 (\frac{1}{r} + D)$$

$$a_{53} = \frac{-\rho_0 i\beta}{r}$$

$$a_{54} = 0$$

$$a_{55} = -u_0 i\alpha$$

$$b_{11} = \rho_0$$

$$b_{22} = \rho_0$$

$$b_{33} = \rho_0$$

$$b_{44} = 1$$

$$b_{55} = 1$$

$$b_{jk} = 0 \quad \text{for j} \neq \text{k}$$

where

$$D^n = \frac{d^n}{dr^n}$$

and the primes denote differentiation with respect to r.

APPENDIX C

Governing Equations for the Secondary Disturbance

Perturbation Method

The governing equation for the secondary (subharmonic) disturbance — obtained at $O(\delta\varepsilon)$ — is of the form

$$\mathbf{L}_{12}(\mathbf{F})_{12} = E_+\mathbf{R}_+ + E_-\mathbf{R}_- + c.c. \tag{3.4}$$

where

$$\mathbf{R}_+ = [F_u, F_v, F_w, F_p, F_\rho]^T,$$

$$\mathbf{R}_- = [F_{u-}, F_{v-}, F_{w-}, F_{p-}, F_{\rho-}]^T,$$

and the components of $\mathbf{R}_+$ and $\mathbf{R}_-$ are found to be:

$$\begin{aligned}
F_u &= -\{\rho_0[v_2u_1' + v_1u_2' + i\beta_1u_1\tfrac{w_2}{r} \\
&\quad + i\beta_2u_2\tfrac{w_1}{r} + i\alpha_1u_2u_1 + i\alpha_2u_1u_2] + u_0'(v_2\rho_1 + v_1\rho_2) \\
&\quad + u_0(\rho_2 i\alpha_1u_1 + \rho_1 i\alpha_2u_2) + \rho_1\sigma_2u_2 + \rho_2u_1\sigma_1\} \\
F_v &= -\{\rho_0[v_2v_1' + v_1v_2' + i\alpha_1u_2v_1 \\
&\quad + i\alpha_2u_1v_2 + i\beta_1\tfrac{v_1w_2}{r} + \tfrac{i\beta_2}{r}v_2w_1 - \tfrac{2w_2w_1}{r}] \\
&\quad + u_0(\rho_2 i\alpha_1v_1 + \rho_1 i\alpha_2v_2) + \rho_1\sigma_2v_2 + \rho_2v_1\sigma_1\} \\
F_w &= -\{\rho_0[v_2w_1' + v_1w_2' + i\alpha_1u_2w_1 + i\alpha_2u_1w_2 \\
&\quad + i\beta_1\tfrac{w_1w_2}{r} + i\beta_2\tfrac{w_1w_2}{r} + \tfrac{w_2v_1}{r} + \tfrac{w_1v_2}{r}] \\
&\quad + u_0(\rho_2 i\alpha_1w_1 + \rho_1 i\alpha_2w_2) + \rho_2\sigma_1w_1 + \rho_1\sigma_2w_2\} \\
F_p &= -\{v_2p_1' + v_1p_2' + u_2i\alpha_1p_1 + u_1p_2i\alpha_2 \\
&\quad + \tfrac{w_2}{r}p_1i\beta_1 + \tfrac{w_1}{r}p_2i\beta_2 + \gamma p_2(\tfrac{v_1}{r} + v_1' + \\
&\quad \tfrac{1}{r}w_1i\beta_1 + u_1i\alpha_1) + \gamma p_1(\tfrac{v_2}{r} + v_2' + \tfrac{1}{r}w_2i\beta_2 + u_2i\alpha_2)\}
\end{aligned}$$

$$
\begin{aligned}
F_\rho &= -\{\rho_1 i\beta_1 w_2/r + \rho_2 i\beta_2 w_1/r + \rho_1 v_2' + \rho_1 w_2 i\beta_2/r \\
&\quad +\rho_2 w_1 i\beta_1/r + (\rho_1' + \rho_1/r)v_2 + \rho_2 v_1' + (\rho_2' + \rho_2/r)v_1 \\
&\quad +\rho_1 i\alpha_2 u_2 + u_2 i\alpha_1 \rho_1 + \rho_2 i\alpha_1 u_1 \\
&\quad +\rho_2 i\alpha_2 u_1\}
\end{aligned}
$$

$$
\begin{aligned}
F_{u-} &= -\{\rho_0[\tilde{v}_2 u_1' + v_1 \tilde{u}_2' + i\beta_1 u_1 \tfrac{\tilde{w}_2}{r} \\
&\quad -i\beta_2 \tilde{u}_2 \tfrac{w_1}{r} + i\alpha_1 \tilde{u}_2 u_1 - i\alpha_2 u_1 \tilde{u}_2] + u_0'(\tilde{v}_2\rho_1 + v_1\tilde{\rho}_2) \\
&\quad +u_0(\tilde{\rho}_2 i\alpha_1 u_1 - \rho_1 i\alpha_2 \tilde{u}_2) + \rho_1 \tilde{\sigma}_2 \tilde{u}_2 + \tilde{\rho}_2 u_1 \sigma_1\}
\end{aligned}
$$

$$
\begin{aligned}
F_{v-} &= -\{\rho_0[\tilde{v}_2 v_1' + v_1 \tilde{v}_2' + i\alpha_1 \tilde{u}_2 v_1 \\
&\quad -i\alpha_2 u_1 \tilde{v}_2 + i\beta_1 \tfrac{v_1 \tilde{w}_2}{r} - \tfrac{i\beta_2}{r}\tilde{v}_2 w_1 - \tfrac{2\tilde{w}_2 w_1}{r}] \\
&\quad +u_0(\tilde{\rho}_2 i\alpha_1 v_1 - \rho_1 i\alpha_2 \tilde{v}_2) + \rho_1 \tilde{\sigma}_2 \tilde{v}_2 + \tilde{\rho}_2 v_1 \sigma_1\}
\end{aligned}
$$

$$
\begin{aligned}
F_{w-} &= -\{\rho_0[\tilde{v}_2 w_1' + v_1 \tilde{w}_2' + i\alpha_1 \tilde{u}_2 w_1 - i\alpha_2 u_1 \tilde{w}_2 \\
&\quad +i\beta_1 \tfrac{w_1 \tilde{w}_2}{r} - i\beta_2 \tfrac{w_1 \tilde{w}_2}{r} + \tfrac{\tilde{w}_2 v_1}{r} + \tfrac{w_1 \tilde{v}_2}{r}] \\
&\quad +u_0(\tilde{\rho}_2 i\alpha_1 w_1 - \rho_1 i\alpha_2 \tilde{w}_2) + \tilde{\rho}_2 \sigma_1 w_1 + \rho_1 \tilde{\sigma}_2 \tilde{w}_2\}
\end{aligned}
$$

$$
\begin{aligned}
F_{p-} &= -\{\tilde{v}_2 p_1' + v_1 \tilde{p}_2' + \tilde{u}_2 i\alpha_1 p_1 - u_1 \tilde{p}_2 i\alpha_2 \\
&\quad +\tfrac{\tilde{w}_2}{r} p_1 i\beta_1 - \tfrac{w_1}{r}\tilde{p}_2 i\beta_2 + \gamma\tilde{p}_2(\tfrac{v_1}{r} + v_1' + \\
&\quad \tfrac{1}{r} w_1 i\beta_1 + u_1 i\alpha_1) + \gamma p_1(\tfrac{\tilde{v}_2}{r} + \tilde{v}_2' - \tfrac{1}{r}\tilde{w}_2 i\beta_2 - \tilde{u}_2 i\alpha_2)\}
\end{aligned}
$$

$$
\begin{aligned}
F_{\rho-} &= -\{\rho_1 i\beta_1 \tilde{w}_2/r - \tilde{\rho}_2 i\beta_2 w_1/r + \rho_1 \tilde{v}_2' - \rho_1 \tilde{w}_2 i\beta_2/r \\
&\quad +\tilde{\rho}_2 w_1 i\beta_1/r + (\rho_1' + \rho_1/r)\tilde{v}_2 + \tilde{\rho}_2 v_1' + (\tilde{\rho}_2' + \tilde{\rho}_2/r)v_1 \\
&\quad -\rho_1 i\alpha_2 \tilde{u}_2 + \tilde{u}_2 i\alpha_1 \rho_1 + \tilde{\rho}_2 i\alpha_1 u_1 - \tilde{\rho}_2 i\alpha_2 u_1\}
\end{aligned}
$$

In the above equations, the primes denote differentiation with respect to r, and the tilde represents the complex conjugate of a quantity.

APPENDIX D

Amplitude Equation Derived from Viscous Analysis

Here we consider the solvability condition for a system of ODE's. The approach here follows closely from Nayfeh (1980). In analyzing the stability problem of a compressible and viscous jets, the lowest inhomogeneous problem occurs at order $\delta\epsilon$. This problem governs the quadratic interaction between two linear waves: $\mathbf{F}_1$ and $\mathbf{F}_2$. The appropriate governing equations for the case where the interaction between $\mathbf{F}_1$ and $\mathbf{F}_2$ reinforces $\mathbf{F}_2$ are

$$(\S - \sigma_2\rho_0)u_{12} - \rho_0 u_0' v_{12} - i\alpha_2 p_{12} = R_u^v \qquad (D.1)$$

$$(\S - \sigma_2\rho_0 - \frac{1}{Rer^2})v_{12} - \frac{2i\beta_2}{Rer^2}w_{12} - Dp_{12} = R_v^v \qquad (D.2)$$

$$\frac{2i\beta_2}{Rer^2}v_{12} + (\S - \sigma_2\rho_0 - \frac{1}{Rer^2})w_{12} - \frac{i\beta_2}{r}p_{12} = R_w^v \qquad (D.3)$$

$$-\gamma p_0 i\alpha_2 u_{12} - \gamma p_0(\frac{1}{r} + D)v_{12} - \frac{\gamma p_0 i\beta_2}{r}w_{12} + (-i\alpha u_0 - \sigma_2)p_{12} = R_p^v \qquad (D.4)$$

where

$$\S = \frac{1}{Re}\left(D^2 + \frac{1}{r}D - \frac{\beta_2^2}{r^2} - \alpha_2^2\right) - \rho_0 i\alpha_2 u_0$$

$$R_u^v = \left\{\rho_0(\frac{\partial B}{\partial t_1} + u_0\frac{\partial B}{\partial x_1})u_2 + p_2\frac{\partial B}{\partial x_1} - \frac{2}{Re}(i\alpha_2\frac{\partial B}{\partial x_1} + \frac{i\beta_2}{r^2}\frac{\partial B}{\partial \phi_1})u_2\right\} - \tilde{B}\hat{F}_{u-}$$

$$R_v^v = \left\{\rho_0(\frac{\partial B}{\partial t_1} + u_0\frac{\partial B}{\partial x_1})v_2 - \frac{2}{Re}(i\alpha_2\frac{\partial B}{\partial x_1} + \frac{i\beta_2}{r^2}\frac{\partial B}{\partial \phi_1})v_2\right\} - \tilde{B}\hat{F}_{v-}$$

$$R_w^v = \left\{\rho_0(\frac{\partial B}{\partial t_1} + u_0\frac{\partial B}{\partial x_1})w_2 - \frac{2}{r^2 Re}\frac{\partial B}{\partial \phi_1}v_2 - \frac{2}{Re}(i\alpha_2\frac{\partial B}{\partial x_1} + \frac{i\beta_2}{r^2}\frac{\partial B}{\partial \phi_1})w_2 + \frac{\partial B}{r\partial \phi_1}p_2\right\} - \tilde{B}\hat{F}_{w-}$$

$$R_p^v = \left\{p_2(\frac{\partial B}{\partial t_1} + u_0\frac{\partial B}{\partial x_1}) + \gamma p_0(\frac{w_2}{r}\frac{\partial B}{\partial \phi_1} + u_2\frac{\partial B}{\partial x_1})\right\} - \tilde{B}\hat{F}_{p-}$$

where $\hat{F}_{u-}, \hat{F}_{v-}, \hat{F}_{w-}$ and $\hat{F}_{p-}$ are given in Appendix E.

The boundary conditions at $r = 0$ are

$$u_{12}(0) = p_{12}(0) = v'_{12}(0) = w'_{12}(0) \quad \text{for } \beta_2 = \ odd \tag{D.5}$$

$$u'_{12}(0) = p'_{12}(0) = v_{12}(0) = w_{12}(0) \quad \text{for } \beta \neq \ odd \tag{D.6}$$

and at $r \to \infty$, the disturbances vanish. The inhomogeneous problem has a solution provided that a solvability condition is satisfied. To determine this condition, we multiply $D.1$ by $r\xi_1$, $D.2$ by $r\xi_2$, $D.3$ by $r\xi_3$ and $D.4$ by $r\xi_4$. After adding the resulting equations and integrating the results by parts, we obtain

$$\begin{aligned}&\int_0^\infty \{\mathrm{L}_1\}u_{12} + \{\mathrm{L}_2\}v_{12} + \{\mathrm{L}_3\}w_{12} + \{\mathrm{L}_4\}p_{12}\ dr + \{Boundary\ Terms\}_0^\infty \\ &= \int_0^\infty r(\mathbf{R}\cdot\mathbf{\Xi})dr\end{aligned} \tag{D.7}$$

where

$$\mathbf{R} = (R_u^v, R_v^v, R_w^v, R_p^v)$$

$$\mathbf{\Xi} = (\xi_1, \xi_2, \xi_3, \xi_4)$$

The adjoint equations are defined by setting each of the coefficients of u_{12}, v_{12}, w_{12} and p_{12} in the integrands of $D.7$ equals to zero. They are

$$(\S - \sigma_2\rho_0)\xi_1 - i\alpha_2\gamma p_0\xi_4 = 0 \tag{D.8}$$

$$-\rho_0 u'_0\xi_1 + (\S - \sigma_2\rho_0 - \frac{1}{Rer^2})\xi_2 + \frac{2i\beta_2}{Rer^2}\xi_3 + \gamma p_0 D\xi_4 = 0 \tag{D.9}$$

$$-\frac{2i\beta_2}{Rer^2}\xi_2 + (\S - \sigma_2\rho_0 - \frac{1}{Rer^2})\xi_3 - \frac{i\beta_2}{r}\gamma p_0\xi_4 = 0 \qquad (D.10)$$

$$-i\alpha_2\xi_1 + (\frac{1}{r} + D)\xi_2 - \frac{i\beta_2}{r}\xi_3 - (i\alpha_2 u_0 + \sigma_2)\xi_4 = 0 \qquad (D.11)$$

To determine the boundary conditions on the $\xi's$, we set the *boundary terms* in $D.7 = 0$, and after invoking the homogeneous boundary conditions (D.5) and (D.6), the adjoint boundary conditions are found to be

$$\xi_1(0) = \xi_4(0) = \xi_2'(0) = \xi_3'(0) = 0 \quad \text{for } \beta_2 = odd \qquad (D.12)$$

$$\xi_1'(0) = \xi_4'(0) = \xi_2(0) = \xi_3(0) = 0 \quad \text{for } \beta_2 \neq odd \qquad (D.13)$$

It may be noted that if we replace ξ_1 by u_{12}, ξ_2 by $-v_{12}$, ξ_3 by w_{12} and $\gamma p_0\xi_4$ by p_{12} in (D.8) - (D.12), the asymptotic equations where contant flows prevail are identical with (D.1) - (D.4). Comparing the adjoint problem with the original homogeneous problem, we find that although their boundary conditions are identical, the differential equations are different, and hence, the homogeneous problem is not self-adjoint. The solvability condition, which obtained from equation (D.7), is given as

$$\int_0^\infty r\mathbf{R}\cdot\mathbf{\Xi}dr = 0 \qquad (D.14)$$

The above equation can be simplified to

$$q_1^v\frac{\partial B^v}{\partial t_1} + q_2^v\frac{\partial B^v}{\partial x_1} + q_3^v\frac{\partial B^v}{\partial \phi_1} + q_4^v\tilde{B}^v = 0. \qquad (D.15)$$

$$q_1^v = \int_0^\infty r\rho_0\left\{u_2\xi_1 + v_2\xi_2 + w_2\xi_3 + \frac{p_2\xi_4}{\rho_0}\right\}dr$$

$$q_4^v = \int_0^\infty -r\left\{\hat{F}_{u-}\xi_1 + \hat{F}_{v-}\xi_2 + \hat{F}_{w-}\xi_3 + \hat{F}_{p-}\xi_4\right\}dr$$

where the superscript v indicates that a quantity is obtained from the viscous analysis, and the tilde denotes the complex conjugate. Here q_1^v, q_2^v and q_3^v arise from the dependence of the $\mathbf{F_2}$ on the slow scales, q_4^v contains the particular set of interactions between $\mathbf{F_1}$ and $\mathbf{F_2}$ that reproduces $\mathbf{F_2}$, while q_2^v, q_3^v are included in the above equation to allow the resonance to be developed spatially; their explicit expressions are not given here because our analysis is based on temporal theory.

Again, as in equation (3.32), the same exponential dependence of B^v on the slow scales is assumed, i.e.,

$$B^v \sim \exp(\lambda_1^v x_1 + \lambda_2^v t_1 + \lambda_3^v \phi_1) \qquad (D.16)$$

The above equation, together with $(D.15)$ and its complex conjugate, yields

$$|q_1^v|^2\lambda_1^{v2}+|q_2^v|^2\lambda_2^{v2}+|q_3^v|^2\lambda_3^{v2}+(2\tilde{q}_1^v q_2^v)_R\lambda_1^v\lambda_2^v+(2\tilde{q}_1^v q_3^v)_R\lambda_2^v\lambda_3^v+(2\tilde{q}_2^v q_3^v)_R\lambda_1^v\lambda_3^v = |q_4^v|^2 \quad (D.17)$$

The λ^v's are in general complex and $(\ \cdot\ )_R$ denotes the real part of a complex number. We consider a subharmonic disturbance with fixed wavenumber and it is allowed to grow only in time, (D.17) can then be simplified to

$$\lambda_2^v = \pm\frac{|q_4^v|}{|q_1^v|}. \qquad (D.18)$$

The physical interpretation of λ_2^v has been discussed in Chapter 3, and will not be repeated here.

APPENDIX E

Resonant Wave Interactions Terms

The governing equation for the linearized disturbance equation for pressure — obtained at $O(\delta\varepsilon)$ — is of the form

$$L(p_{12}) = \frac{d^2p_{12}}{dr^2} + \left[\frac{1}{r} - \frac{2u_0'}{u_0 - C_2} - \frac{\rho_0'}{\rho_0}\right]\frac{dp_{12}}{dr} + \left[\alpha_2^2(u_0 - C_2)^2\rho_0 M_j^2 - \frac{\beta_2^2}{r^2} - \alpha_2^2\right]p_{12} = rhs \tag{3.29}$$

where

$$rhs = h_1\frac{\partial B}{\partial t_1} + h_2\frac{\partial B}{\partial x_1} + h_3\frac{\partial B}{\partial \phi_1} + h_{12}\tilde{B} \tag{3.30}$$

$$h_{12} = i\alpha_2\hat{F}_{u-} + [\frac{1}{r} - \frac{2u_0'}{u_0 - C_2} - \frac{\rho_0'}{\rho_0} + \frac{d}{dr}]\hat{F}_{v-} + i\beta_2\hat{F}_{w-}/r - i\alpha_2(u_0 - C_2)\rho_0 M_j^2\hat{F}_{p-}$$

In the above equations, all variables, except for $\hat{F}_{u-}$, $\hat{F}_{v-}$, $\hat{F}_{w-}$ and $\hat{F}_{p-}$, have been defined in Chapter 3. The undefined variables are

$$\begin{aligned}
\hat{F}_{u-} &= -\{\rho_0[v_{-2}u_1' + v_1u_{-2}' + i\beta_1u_1\tfrac{w_{-2}}{r} \\
&\quad + i\beta_2u_{-2}\tfrac{w_1}{r} + i\alpha_1u_{-2}u_1 - i\alpha_2u_1u_{-2}] + u_0'(v_{-2}\rho_1 + v_1\rho_{-2}) \\
&\quad + u_0(\rho_{-2}i\alpha_1u_1 - \rho_1i\alpha_2u_{-2}) + \rho_1\sigma_2u_{-2} + \rho_{-2}u_1\sigma_1\} \\
\hat{F}_{v-} &= -\{\rho_0[v_{-2}v_1' + v_1v_{-2}' + i\alpha_1u_{-2}v_1 \\
&\quad - i\alpha_2u_1v_{-2} + i\beta_1\tfrac{v_1w_{-2}}{r} + \tfrac{i\beta_2}{r}v_{-2}w_1 - \tfrac{2w_{-2}w_1}{r}] \\
&\quad + u_0(\rho_{-2}i\alpha_1v_1 - \rho_1i\alpha_2v_{-2}) + \rho_1\sigma_2v_{-2} + \rho_{-2}v_1\sigma_1\}
\end{aligned}$$

$$\begin{aligned}
\hat{F}_{w-} &= -\{\rho_0[v_{-2}w_1' + v_1 w_{-2}' + i\alpha_1 u_{-2} w_1 - i\alpha_2 u_1 w_{-2} \\
&\quad + i\beta_1 \tfrac{w_1 w_{-2}}{r} + i\beta_2 \tfrac{w_1 w_{-2}}{r} + \tfrac{w_{-2} v_1}{r} + \tfrac{w_1 v_{-2}}{r}] \\
&\quad + u_0(\rho_{-2} i\alpha_1 w_1 - \rho_1 i\alpha_2 w_{-2}) + \rho_{-2}\sigma_1 w_1 + \rho_1 \sigma_2 w_{-2}\} \\
\hat{F}_{p-} &= -\{v_{-2}p_1' + v_1 p_{-2}' + u_{-2} i\alpha_1 p_1 - u_1 p_{-2} i\alpha_2 \\
&\quad + \tfrac{w_{-2}}{r} p_1 i\beta_1 + \tfrac{w_1}{r} p_{-2} i\beta_2 + \gamma p_{-2}(\tfrac{v_1}{r} + v_1' + \\
&\quad \tfrac{1}{r} w_1 i\beta_1 + u_1 i\alpha_1) + \gamma p_1(\tfrac{v_{-2}}{r} + v_{-2}' + \tfrac{1}{r} w_{-2} i\beta_2 - u_{-2} i\alpha_2)\}
\end{aligned}$$

In accordance with the discussion in Chapter 3.2, the eigenfunctions $u_{-2}, v_{-2}, w_{-2}, p_{-2}$ and ρ_{-2} are for an unstable mode with a wavenumber $-\alpha_2$ and a mode number β_2.

APPENDIX F

Secondary Instability Equations Using Normal Mode Analysis

The shape function of the subharmonic disturbance **g** is written as

$$\mathbf{g} = (u_2, u_{-2}, v_2, v_{-2}, w_2, w_{-2}, p_2, p_{-2}, \rho_2, \rho_{-2})^T \tag{3.47}$$

The stability of subharmonic disturbance superimposed on a periodic flow consisting of a finite amplitude primary wave and a parallel mean flow is governed by the following set of 10 coupled linear ODE's:

$$\S u_2 - \rho_0 u_0' v_2 - i\alpha_2 p_2 - A\hat{F}_{u-} = \hat{\sigma}_2(\rho_0 u_2 + A\rho_1 u_{-2}) \tag{F.1}$$

$$(\S - \frac{1}{Re r^2})v_2 - \frac{2i\beta_2}{Re r^2} w_2 - Dp_2 - A\hat{F}_{v-} = \hat{\sigma}_2(\rho_0 v_2 + A\rho_1 v_{-2}) \tag{F.3}$$

$$\frac{2i\beta_2}{Re r^2} v_2 + (\S - \hat{\sigma}_2\rho_0 - \frac{1}{Re r^2})w_2 - \frac{i\beta_2}{r} p_2 - A\hat{F}_{w-} = \hat{\sigma}_2(\rho_0 w_2 + A\rho_1 w_{-2}) \tag{F.5}$$

$$-\gamma p_0 i\alpha_2 u_2 - \gamma p_0(\frac{1}{r} + D)v_2 - \frac{\gamma p_0 i\beta_2}{r} w_2 + a_{44}p_2 + a_{45}\rho_2 - A(\hat{F}_{p-} + \psi_{con}) = \hat{\sigma}_2(p_2 + A\rho_1/\rho_0) \tag{F.7}$$

$$-\rho_0 i\alpha_2 u_2 - \rho_0' v_2 - \rho_0(\frac{1}{r} + D)v_2 - \frac{\rho_0 i\beta_2}{r} w_2 - u_0 i\alpha_2 \rho_2 - A\hat{F}_{\rho-} = \hat{\sigma}_2\rho_2 \tag{F.9}$$

where

$$\S = \frac{1}{Re}\left(D^2 + \frac{1}{r}D - \frac{\beta_2^2}{r^2} - \alpha_2^2\right) - \rho_0 i\alpha_2 u_0,$$

After replacing the subscript 2 of the components of the shape function g by -2 (and -2 by 2) and by substituting the coefficients (with the exception of $i\beta_2$) by their complex conjugates in equations (F.1), (F.3), (F.5), (F.7), and (F.9), equations (F.2), (F.4), (F.6), (F.8), and (F.10) are obtained, respectively.

In equations (F.1) - (F.10), the prime denotes a differentiation with respect to r, u_0 refers to the mean velocity in a moving frame of reference, a_{44} and a_{45} are given in Appendix B, $\hat{F}_{u-}, \hat{F}_{v-}, \hat{F}_{w-}, \hat{F}_{p-}$ and $\hat{F}_{\rho-}$ are given in Appendix E, and ψ_{con}, which arises from the quadratic interactions in the conduction term of the energy equation, is found to be

$$\psi_{con} = -\sum_{j=1}^{7} \psi_j \qquad (F.11)$$

where

$$\psi_1 = -\frac{\rho_1\alpha_2^2\rho_{-2}}{\rho_0^3} - \frac{p_1\alpha_2^2\rho_{-2}}{\rho_0^2} - \frac{4p_0\alpha_1\alpha_2\rho_1\rho_{-2}}{\rho_0^3} + \frac{2\alpha_1\alpha_2 p_1\rho_{-22}}{\rho_0^2} + \frac{p_0\rho_1\rho''_{-2}}{\rho_0^3} + \frac{p_1\rho''_{-2}}{\rho_0^2}$$

$$\psi_2 = \frac{p_0\rho_1\rho'_{-2}}{(r\rho_0^3)} - \frac{4p_1\rho'_0\rho'_{-2}}{\rho_0^3} + \frac{p_1\rho_{-2}}{(r\rho_0^2)} + \frac{2p'_1\rho'_{-2}}{\rho_0^2} - \frac{p_0\rho_1\beta_2^2\rho_{-2}}{(r^2\rho_0^3)} - \frac{4p_0\rho'_1\rho'_{-2}}{\rho_0^3}$$

$$\psi_3 = -\frac{p_1\beta_2^2\rho_{-2}}{(r^2\rho_0^2)} - \frac{4p_0\rho_1\rho_{-2}\beta_2\beta_1}{(r^2\rho_0^3)} + \frac{2\beta_1\beta_2\rho_{-2}p_1}{(r^2\rho_0^2)} - \frac{p_0\alpha_1^2\rho_1\rho_{-2}}{\rho_0^3}$$

$$\psi_4 = \frac{p_0\rho''_1\rho_{-2}}{\rho_0^3} + \frac{p_0\rho'_1\rho_{-2}}{(r\rho_0^3)} - \frac{p_0\beta_2^2\rho_1\rho_{-2}}{(r^2\rho_0^3)} + \frac{p_1\rho''_0\rho_{-2}}{\rho_0^3} + \frac{p_1\rho'_0\rho_{-2}}{(r\rho_0^3)} + \frac{2p'_1\rho'_0\rho_{-2}}{(\rho_0^3)} - \frac{2p'_1\rho_{-2}}{(r\rho_0^2)} + \frac{2\beta_1^2p_1\rho_{-2}}{(r^2\rho_0^2)}$$

$$\psi_5 = \frac{2\alpha_1^2p_1\rho_{-2}}{\rho_0^2} - \frac{2p''_1\rho_{-2}}{\rho_0^2} - \frac{p_{-2}\alpha_1^2\rho_1}{\rho_0^2} + \frac{2p_{-2}\rho_1\alpha_1\alpha_2}{\rho_0^2} + \frac{p_{-2}\rho''_1}{\rho_0^2} - \frac{4p_{-2}\rho'_0\rho'_1}{\rho_0^3} + \frac{p_{-2}\rho'_1}{(r\rho_0^2)} + \frac{2p'_{-2}\rho'_1}{\rho_0^2}$$

$$\psi_6 = -\frac{p_{-2}\rho''_1\beta_1^2}{(r^2\rho_0^2)} + \frac{2\beta_2\beta_1p_{-2}\rho_1}{(r^2\rho_0^2)} + \frac{p_{-2}\rho''_0\rho_1}{\rho_0^3} + \frac{p_{-2}\rho'_0\rho_1}{(r\rho_0^3)} + \frac{2p'_2\rho'_0\rho_1}{\rho_0^3} - \frac{2p_{-2}\rho_1}{(r\rho_0^2)} + \frac{2\beta_2^2p_{-2}\rho_1}{(r^2\rho_0^2)}$$

$$\psi_7 = \frac{2\alpha_2^2p_{-2}\rho_1}{\rho_0^2} - \frac{2p''_{-2}\rho_1}{\rho_0^2}$$

The appropriate boundary conditions at $r \to 0$ are

$$u_2(0) = p_2(0) = \rho_2(0) = v'_2(0) = w'_2(0) \quad \text{for } \beta_2 = \ odd \qquad (F.12)$$

$$u'_2(0) = p'_2(0) = \rho'_2(0) = v_2(0) = w_2(0) \quad \text{for } \beta \neq \ odd \qquad (F.13)$$

$$u_{-2}(0) = p_{-2}(0) = \rho_{-2}(0) = v'_{-2}(0) = w'_{-2}(0) \quad \text{for } \beta_2 = \ odd \qquad (F.14)$$

$$u'_{-2}(0) = p'_{-2}(0) = \rho'_{-2}(0) = v_{-2}(0) = w_{-2}(0) \quad \text{for } \beta \neq \ odd \qquad (F.15)$$

and at $r \to \infty$, the subharmonic disturbances vanish.

REFERENCES

[1] Abramowitz, M. & Stegun, I. A. 1972, *Handbook of Mathematical Functions with Formulas, Graphs, and Mathematical Tables* (gov. Printing Office, Washington, D.C.).

[2] Ahuja, K. K., J. Lepicovsky and W. H. Brown 1986, "Some Unsolved questions on Hot-Jet Mixing Control" AIAA Paper 86-1956.

[3] Ahuja, K. K., J. Lepicovsky, C. K. W. Tam, P. J. Morris and R. H. Burrin 1982, "Tone-Excited Jet," NASA Contractor Report 3538.

[4] Anderson, D. A., J. C. Tannehill and R. H. Pletcher 1984, *Computational Fluid Mechanics and Heat Transfer*, McGraw-Hill, New York, pp 247-251.

[5] Balsa, T. F. 1987, "On the Spatial Instability of Piecewise Linear Free Shear Layers," *J. Fluid Mech.*, Vol. 174, pp. 553-563.

[6] Balsa, T. F. 1988, "On the Receptivity of Free Shear Layers to Two-Dimensional External Excitation," submitted to *J. Fluid Mech.*, Vol. 187, pp. 155-177.

[7] Batchelor, G. K. 1967, *An Introduction to Fluid Dynamics*, Cambridge University Press, Cambridge.

[8] Batchelor, G. K. and A. E. Gill 1962, "Analysis of the Stability of Axisymmetric Jets," *J. Fluid Mech.*, Vol. 14, pp. 529-551.

[9] Bender, C. M. and S. A. Orszag 1978, *Advanced Mathematical Methods For Scientists and Engineers*, McGraw-Hill, New York.

[10] Betchov, R. and W. O. Criminale 1967, *Stability of Parallel Flows*, Academic Press, New York.

[11] Betchov, R. and A. Szewczyk 1963, "Stability of a Shear Layer Between Parallel Streams," *Phys. Fluids*, Vol. 6, No. 10, pp. 1391-1396.

[12] Bird R., W. E. Steward and E. N. Lightfoot 1960, *Transport Phenomena*, John Wiley and Sons, New york.

[13] Blumen, W. 1970, " Shear Layer instability of an inviscid compressible fluid," *J. Fluid Mech.*, Vol. 40, pp. 769-781.

[14] Boyd, J. P. 1978b, "Spectral and Pseudospectral Methods for Eigenvalue and Non-separable Boundary Value Problems," *Mon. Weather Rev.*, Vol. 106, pp. 1192-1203.

[15] Bretherton, F. P. 1964, "Resonant Interactions Between Waves. The Case of Discrete Oscillations," *J. Fluid Mech.*, Vol. 20, pp. 457-479.

[16] Brown, G. L. and A. Roshko 1974, "On Density Effects and Large Structure in Turbulent Mixing Layers," *J. Fluid Mech.*, Vol. 64, pp. 775-816.

[17] Canuto, C., M. Y. Hussaini, A. Quarteroni and T. A. Zang 1987, Jr., *Spectral Methods in Fluid Dynamics*, Springer Series in Computational Physics.

[18] Chan, Y. Y. 1974, "Spatial Waves in Turbulent Jets," *The Physics of Fluids*, Vol. 17, No. 1, pp. 46-53.

[19] Cohen, J. 1986, "Instabilities in Turbulent Free Shear Flows," Ph.D. Thesis, Department of Aerospace and Mechanical Engineering, University of Arizona, Tucson.

[20] Crighton, D. G. and Gaster, M. 1976, " Stability of slowly Diverging Jet flow," *J. Fluid Mech.*, Vol. 77, pp. 397-413.

[21] Crow, S. C. and F. H. Champagne 1971, "Orderly Structure in Jet Turbulence," *J. Fluid Mech.*, Vol. 48, pp. 547-592.

[22] Crighton, D. G. and Gaster, M. 1976, " Stability of slowly Diverging Jet flow," *J. Fluid Mech.*, Vol. 77, pp. 397-413.

[23] Drazin, P. G. and W. H. Reid 1981, *Hydrodynamic Stability*, Cambridge University Press, Cambridge.

[24] Eckart, C. 1963, " Extension of Howard's circle theorem to Adiabatic Jets," *Phys. Fluids*, Vol. 6, pp. 1042-1047.

[25] Ffowcs Williams, J. E. and A. J. Kempton 1978, "The Noise from the Large-Scale Structure of a Jet," *J. Fluid Mech.*, Vol. 84, pp. 673-694.

[26] Freymuth, P. 1966, "On Transition in a Separated Laminar Boundary Layer," *J. Fluid Mech.*, Vol. 25, pp. 683-704.

[27] Gaster, M. 1962 "A note on the relation between temporally-increasing and spatially-increasing disturbances in hydrodynamic stability," *J. Fluid Mech.*, Vol. 14, pp.222-224.

[28] Gaster, M., E. Kit and I. Wygnanski 1985 "Large Scale Structures in a Forced Turbulent Mixing Layer," *J. Fluid Mech.*, Vol. 150, pp. 23-39.

[29] George, W. D. and J. D. Hellums 1972, "Hydrodynamic Stability in Plane Poiseuille Flow with Finite Amplitude Disturbances," *J. Fluid Mech.*, Vol. 51, pp. 687-704.

[30] Gottlieb, D. and S. A. Orszag 1977, "Numerical Analysis of Spectral Methods: Theory and Applications," SIAM-CBMS, Philadelphia.

[31] Gropengiesser, H. 1969, "On the Stability of Free Shear Layers in Compressible Flows (in German)," Deutsche Luft. und Raumfahrt, FB 69-25, 123 pp. Also, NASA Tech. Translation NASA TT F-12, 786.

[32] Grosch, C. E. and H. Salwen 1978, "The Continuous Spectrum of the Orr-Sommerfeld Equation. Part 1. The Spectrum and the Eigenfunctions," *J. Fluid Mech.*, Vol. 87, pp. 33-54.

[33] Herbert, T. 1985, "Three-dimensional phenomenon in the Transitional Flat-plate Boundary Layer," AIAA Paper No. 85-0489.

[34] Herbert, T. 1984, "Analysis of the Subharmonic Route to Transition in Boundary Layers," AIAA Paper No. 84-0009.

[35] Herbert, T. 1983b, "Secondary Instability of Plane Channel Flow to Subharmonic Three-Dimensional Disturbances," *Phys. Fluids*, Vol. 26, pp. 871-874.

[36] Ho, C. M. and P. Huerre 1984, "Perturbed Free Shear Layers," *Ann. Rev. Fluid Mech.*, Vol. 16, pp. 365-424.

[37] Ho, C. M. and L. S. Huang 1982, "Subharmonics and Vortex Merging in Mixing Layer," *J. Fluid Mech.*, Vol. 119, pp. 443-473.

[38] Howard, L. N. 1961, "Note on a paper by John W. Miles," *J. Fluid Mech.*, Vol. 10, pp. 509-512.

[39] Huerre, P. and P. Monkewitz 1985, "Absolute and Convective Instabilities in Free Shear Layers," *J. Fluid Mech.*, Vol. 159, pp. 151-168.

[40] Huerre, P. 1988, "Subharmonic resonance, pairing and shredding in the mixing layer," *J. Fluid Mech.*, Vol. 188, pp. 223-252.

[41] Jarrah, Y. 1989, "Weakly Nonlinear Stability of Shear Layers and Heated Subsonic Round Jets," Ph.D. Thesis, University of Arizona.

[42] Jackson, T. L. and C. E. Grosch 1988 " Spatial Stability of a Compressible Mixing Layer," NASA Contractor Report 181671.

[43] Kelly, R. E. 1967, "On the Stability of an Inviscid Shear Layer which is Periodic in Space and Time," *J. Fluid Mech.*, Vol. 27, pp. 657-689.

[44] Ko, D. R., T. Kubato and L. Lees 1970, "Finite Disturbance Efect on the Stability of a Laminar Incompressible Wake Behind a Flat Plate," *J. Fluid Mech.*, Vol. 40, part 2, pp. 315-341.

[45] Laurien, E. and L. Kleiser 1985, "Numerical Simulation of Transition Control in Boundary Layers," *Sixth GAMM Conference on Numerical Methods in Fluid Mechanics.*

[46] Lees, L. and Lin, C. C. 1946, "Investigation of the Stability of the Laminar Boundary Layer in a Compressible Fluid," NACA TN-1115.

[47] Lin, C. C. 1955, *The Theory of Hydrodynamic Stability*, Cambridge University Press, Cambridge.

[48] Mattingly, G. E. and C. C. Chang 1974, "Unstable Waves on an Axisymmetric Jet Column," *J. Fluid Mech.*, Vol. 65, pp. 541-560.

[49] Metcalfe, R. W., S. A. Orszag, M. E. Bracket, S. Menon and J. J. Riley 1987, "Secondary Instability of a Temporally Growing Mixing Layer," *J. Fluid Mech.*, Vol. 184, pp. 207-243.

[50] Michalke, A. 1984, "Survey on Jet Instability Theory," *Prog. Aerospace Sci.*, Vol. 21, pp. 159-199.

[51] Michalke, A. 1971, "Instabilität eins Kompressiblen Ruden Friestrahls unter Berücksichtingung des Einflusses der Strahlgrenzschichtdicke," *Z. Flugwiss.*, Vol. 19, pp. 319-328, 1971, English Translation NASA Tech. Memo. 75190.

[52] Michalke, A. and G. Hermann 1982, "On the Inviscid Instability of a Circular Jet with External flow," *J. Fluid Mech.*, Vol. 114, pp. 343-359.

[53] Miles, J. H. and G. Raman 1987, "Influence of a Tripped Boundary Layer on Instability Pressure Waves in a Subsonic Cold Jet," Presented at the 40th Meeting of the Division of Fluid Dynamics of the American Physical Society in Eugene, Oregon, Nov. 23-25.

[54] Monkewitz, P. 1987, " Subharmonic resonance, pairing and shredding in the mixing layer," *J. Fluid Mech.*, Vol. 188, pp. 223-252.

[55] Monkewitz, P. and K. Sohn 1986, "Absolute instabilities in Hot Jets and their control," *AIAA Paper* 86-1882.

[56] Moore, F. K. 1964, *Theory of Laminar Flows*, Princeton University Press, Princeton.

[57] Morris, P. J. 1976, "The Spatial Viscous Instability of Axisymmetric Jets," *J. Fluid Mech.*, Vol. 77, pp. 511-529.

[58] Morris, P. J. and Tam, C. K. W. 1977, " Near and Far-Field Noise From Large-Scale Instabilities of Axisymmetric Jets," *AIAA Paper* 77-1351.

[59] Nayfeh, A. H. 1980, *Introduction to Perturbation Techniques*, Wiley, New York.

[60] Nayfeh, A. H. 1973, *Perturbation Methods*, Wiley, New York.

[61] Orszag, S. A. 1971, "Accurate Solution of the Orr-Sommerfeld Stability Equation," *J. Fluid Mech.*, Vol. 50, pp. 689-703.

[62] Orszag, S. A. and A. T. Patera 1983, "Secondary Instability of Wall-Bounded Shear Flows," *J. Fluid Mech.*, Vol. 128, pp. 347-385.

[63] Paragiri, R. 1985, "The Stability Analysis of Axisymmetric Jets," Master Report, Department of Aerospace and Mechanical Engineering, University of Arizona, Tucson.

[64] Petersen, R. A. and M. M. Samet 1988, "On the Preferred Mode of Jet Instability," *J. Fluid Mech.*, Vol. 194, pp. 153-173.

[65] Petersen, R. A. and M. M. Samet 1988, " Effects of excitation level on the stability of an axisymmetric mixing layer," *Phys. Fluids*, Vol. 31, pp. 3246-3252.

[66] Petersen, R. A. 1978, "Influence of Wave Dispersion on Vortex Pairing in a Jet," *J. Fluid Mech.*, Vol. 89, pp. 469-495.

[67] Pierrehumbert, R. T. and S. E. Widnall 1982, "The Two- and Three-Dimensional Instabilities of a Spatially Periodic Shear Layer," *J. Fluid Mech.*, Vol. 114, pp. 59-82.

[68] Plaschko, P. 1979, " Helical instabilities of slowly diverging jets," *J. Fluid Mech.*, Vol. 92, pp. 209-215.

[69] Rand, R. H. 1984, *Computer Algebra in Applied Mathematics: An Introduction to MACSYMA*, Pitman Advanced Publishing Program.

[70] Santos, German. 1987, "Studies on Secondary Instabilities," Ph.D. Thesis, Virginia Polytechnic Institute and State University, Blacksburg, Virginia.

[71] Saric, W. S. and A. S. W. Thomas 1983, "Experiments on the Subharmonic Route to Turbulence in Boundary Layers," Proc. IUTAM Symposium, Kyoto, Japan.

[72] Sato, H. 1956, "Experimental investigation on the transition of Laminar separated layer," *J. Phys. Soc. Jpn.*, Vol. 7, pp. 702-709.

[73] Schade, H. 1964, "Contribution to the Nonlinear Stability Theory of Inviscid Shear Layers," *Phys. Fluids*, Vol. 7, pp. 623-628.

[74] Schlichting, H. 1979, *Boundary-Layer Theory*, 7th Ed., McGraw-Hill Book Company, New York.

[75] Shen, S. F. 1964, "stability of Laminar lows", (in *Theory of Laminar Flows*, F. K. Moore, editor), Princeton University Press.

[76] Sohn, D. K. 1986, "Absolute Instabilities in Hot Jets," Master. Thesis, University of California, Los Angeles.

[77] Spalart, P. R. 1984, "A Spectral Method for External Viscous Flows," *Contemp. Math.*, Vol. 28, pp. 315-335.

[78] Stone, J. R. and D. J. McKinzie 1984, "Acoustic Excitation - A Promising New Means of Controlling Shear Layers," NASA TM 83772.

[79] Strange, P. J. R. and D. G. Crighton 1983, "Spinning modes on axisymmetric jets. Part 1," *J. Fluid Mech.*, Vol. 134, pp. 231-245

[80] Stuart, J. T. 1967, "On Finite Amplitude Oscillations in Laminar Mixing Layers," *J. Fluid Mech.*, Vol. 29, pp. 417-440.

[81] Tam, C. K. W. and P. J. Morris 1980, "The Radiation of Sound by the Instability Waves of a Compressible Plane Turbulent Shear Layer," *J. Fluid Mech.*, Vol. 98, pp. 349-381.

[82] Tam, C. K. W. and J. A. Jackson 1983, "On the Shock and noise of Supersonic Jets ," AIAA Paper No. 83-0703, April.

[83] Tam, C. K. W. and P. J. Morris 1985, "Tone Excited Jets, Part V: A Theoretical Model and Comparison with Experiment," *Journal Sound Vibration*, Vol. 102(1), pp. 119-151.

[84] Wille, R. 1963, " Beiträge Zur Phänomenologie der Freistrahlen," *Z. Flugwiss.*, Vol. 11, pp. 223-233.

[85] Wilkinson, J. H. 1965, *The algebraic Eigenvalue Problem*, Oxford University Press, London.

[86] Winant, C. C. and F. K. Brownand 1974, "Vortex Pairing: The Mechanism of Turbulent Mixing Layer Growth at Moderate Reynolds Number," *J. Fluid Mech.*, Vol. 63, p. 237-255.

[87] Wygnanski, I. and R. A. Petersen 1987, "Coherent Motion in Excited Free Shear Flows," AIAA Journal, Vol. 25, pp.201-213.